

Feedforward control for lightweight motion systems

Citation for published version (APA):

Ronde, M. J. C. (2014). *Feedforward control for lightweight motion systems*. [Phd Thesis 1 (Research TU/e / Graduation TU/e), Mechanical Engineering]. Technische Universiteit Eindhoven.
<https://doi.org/10.6100/IR762834>

DOI:

[10.6100/IR762834](https://doi.org/10.6100/IR762834)

Document status and date:

Published: 20/01/2014

Document Version:

Publisher's PDF, also known as Version of Record (includes final page, issue and volume numbers)

Please check the document version of this publication:

- A submitted manuscript is the version of the article upon submission and before peer-review. There can be important differences between the submitted version and the official published version of record. People interested in the research are advised to contact the author for the final version of the publication, or visit the DOI to the publisher's website.
- The final author version and the galley proof are versions of the publication after peer review.
- The final published version features the final layout of the paper including the volume, issue and page numbers.

[Link to publication](#)

General rights

Copyright and moral rights for the publications made accessible in the public portal are retained by the authors and/or other copyright owners and it is a condition of accessing publications that users recognise and abide by the legal requirements associated with these rights.

- Users may download and print one copy of any publication from the public portal for the purpose of private study or research.
- You may not further distribute the material or use it for any profit-making activity or commercial gain
- You may freely distribute the URL identifying the publication in the public portal.

If the publication is distributed under the terms of Article 25fa of the Dutch Copyright Act, indicated by the "Taverne" license above, please follow below link for the End User Agreement:

www.tue.nl/taverne

Take down policy

If you believe that this document breaches copyright please contact us at:

openaccess@tue.nl

providing details and we will investigate your claim.

The background is a solid blue color. It features several white wave patterns. A prominent, large, smooth wave arches from the left side towards the center. Below this, a series of smaller, more frequent waves run horizontally across the middle of the page. At the bottom, there are more large, smooth waves, some of which are partially obscured by the author's name.

FEEDFORWARD CONTROL FOR LIGHTWEIGHT MOTION SYSTEMS

MICHAEL RONDE

Feedforward Control for Lightweight Motion Systems

disc

The research reported in this thesis is part of the research program of the Dutch Institute of Systems and Control (DISC). The author has successfully completed the educational program of the Graduate School DISC.

This research is part of the Pieken in de Delta program and is financed by the Dutch ministry of Economic Affairs and the local governments of the south-east of the Netherlands.

Feedforward Control for Lightweight Motion Systems by Michael Ronde
Eindhoven : Technische Universiteit Eindhoven, 2014 – Proefschrift.

A catalogue record is available from the Eindhoven University of Technology Library.

ISBN: 978-90-386-3544-6

Typeset by the author with the pdfL^AT_EX documentation system.

Cover design: Oranje Vormgevers, Eindhoven, The Netherlands.

Reproduction: Ipskamp Drukkers, Enschede, The Netherlands.

Copyright © 2014 by M.J.C. Ronde. All rights reserved.

Feedforward Control for Lightweight Motion Systems

PROEFSCHRIFT

ter verkrijging van de graad van doctor aan de
Technische Universiteit Eindhoven, op gezag van de
Rector Magnificus, prof.dr.ir. C.J. van Duijn, voor een
commissie aangewezen door het College voor
Promoties in het openbaar te verdedigen
op maandag 20 januari 2014 om 16.00 uur

door

Michaël Johannes Christiaan Ronde

geboren te Dordrecht

Dit proefschrift is goedgekeurd door de promotoren en de samenstelling van de promotiecommissie is als volgt:

voorzitter:	prof.dr. L.P.H. de Goey
1 ^e promotor:	prof.dr.ir. M. Steinbuch
copromotor:	dr.ir. M.J.G. van de Molengraft
leden:	Univ.-Prof. Dipl.-Ing. G. Schitter (Vienna University of Technology)
	prof.dr.ir. J. Swevers (Katholieke Universiteit Leuven)
	prof.dr.ir. H. Butler
	prof.dr. E.A. Lomonova MSc
	dr.ir. M.F. Heertjes

to my father,
John

Contents

1	Introduction	1
1.1	Towards lightweight advanced motion systems	1
1.1.1	Production of integrated circuits	1
1.1.2	Challenges for miniaturization	3
1.1.3	Advanced motion systems	3
1.1.4	Next-generation motion systems	3
1.1.5	Control of advanced motion systems	4
1.1.6	Consequences of lightweight design	5
1.2	Problem statement	6
1.3	Feedforward control approaches	8
1.3.1	Model-based approaches	8
1.3.2	Data-based approaches	9
1.3.3	Fixed-structure feedforward control	10
1.3.4	Input shaping	11
1.3.5	Setpoint trajectory design	12
1.3.6	Indirect control and inferential control	12
1.3.7	LPV and LTV feedforward control approaches	13
1.3.8	Over-actuation and over-sensing	13
1.3.9	Feedforward control in high-speed SPM	14
1.4	Research challenges and approach	14
1.5	Research contributions	16
1.6	Outline of this thesis	17
2	Model-based feedforward for inferential motion systems	19
2.1	Introduction	20
2.2	Problem formulation	24
2.3	Feedforward for indirect control structures	25
2.3.1	Motivating example	25
2.3.2	Controller structures for inferential control	27
2.3.3	Independent feedforward design for indirect control structures	28

2.4	Lifted feedforward	30
2.5	Experimental validation	31
2.5.1	Performance variables and geometric decoupling	32
2.5.2	Setpoint trajectory	33
2.5.3	Identification and feedback design	34
2.5.4	Parametric model	35
2.5.5	Feedforward implementation aspects	37
2.5.6	Results	38
2.6	Conclusions	40
3	Feedforward for flexible systems with time-varying performance locations	45
3.1	Introduction	46
3.2	Problem formulation	48
3.3	Lifted Feedforward	49
3.4	Lifted feedforward with input weightings	50
3.5	Experiments	51
3.5.1	Identification and modeling	52
3.5.2	Feedback control design	54
3.5.3	Setpoint trajectory	54
3.5.4	Feedforward control design	54
3.5.5	Design of $W(z)$	56
3.5.6	Results	56
3.6	Conclusions	60
4	Model-based spatial feedforward control for over-actuated motion systems	61
4.1	Introduction	62
4.2	Problem formulation	64
4.2.1	Assumptions	66
4.3	Spatial feedforward	66
4.3.1	Body-mode feedforward	67
4.3.2	Design freedom	68
4.3.3	Spatial feedforward control, desired solution	68
4.4	Existence of solutions	68
4.5	Partial solutions	69
4.6	Input shaping	72
4.7	Experimental validation	74
4.7.1	Prototype lightweight motion system	74
4.7.2	Identification	75
4.7.3	Actuator- and sensor selection	76
4.7.4	Decoupling and feedback control design	79
4.7.5	MIMO stability	80

4.7.6	Setpoint trajectory	82
4.7.7	Rigid-body and spatial feedforward design	82
4.7.8	Results	84
4.8	Conclusion	86
5	Data-based spatial feedforward control for over-actuated motion systems	91
5.1	Introduction	92
5.2	Problem formulation	95
5.3	Spatial feedforward	97
5.4	Optimization	99
5.4.1	Objective function	100
5.4.2	Gauss-Newton optimization	101
5.4.3	Gradient-estimation methods	102
5.5	Experimental validation	103
5.5.1	Prototype lightweight motion system	104
5.5.2	Identification	104
5.5.3	Decoupling and feedback control design	105
5.5.4	MIMO stability	106
5.5.5	Setpoint trajectory	107
5.5.6	Data-based design	108
5.5.7	Results	108
5.6	Conclusions	114
6	Conclusions and recommendations	119
6.1	Conclusions	119
6.2	Recommendations for future research	122
6.2.1	General recommendations	122
6.2.2	Recommendations for traditionally actuated systems	123
6.2.3	Recommendations for over-actuated systems	123
	Bibliography	127
A	Inferential feedforward	141
A.1	SVD truncation	141
A.2	Equivalence of control structures	142
A.3	Parametric beam model	143
B	Zero-Vibration Input Shaper	145
C	Model-based spatial feedforward	149
C.1	Rigid-body feedforward design	149
C.2	Spatial feedforward design	149

D Data-based spatial feedforward	151
D.1 Relation between the data-based feedforward controller and a diagonal feedforward controller and feedforward decoupling	151
D.2 Convexity of the objective function	152
D.3 Selection of Λ	153
D.4 Input matrix	153
E List of symbols	155
Summary	161
Dankwoord	163
Curriculum Vitae	165

Chapter 1

Introduction

IN this chapter the research objectives are defined. The background and the problem statement of this research are introduced. Subsequently, feedforward techniques and related control methods are briefly discussed. Moreover, existing control structures for feedforward control are discussed and extended towards feedforward control of lightweight motion systems.

1.1 Towards lightweight advanced motion systems

In the semiconductor industry there is an ever increasing demand for higher production speeds of integrated circuits (ICs). Moreover, miniaturization of electronic devices and the desire for faster and more energy efficient ICs with more features requires smaller chips. The production of such chips and more specifically shrinking the dies of ICs requires higher accuracy. In 1965, Gordon Moore predicted that the amount of transistors on a chip would double every year (Moore, 1965). Ten years later, he predicted that the amount of transistors doubles between 1.5 and 2 years (Moore, 1975). This prediction proved to be accurate over the past decades (Mack, 2011). Nowadays IC manufacturers use Moore's law as a roadmap, such that Moore's law has become a self-fulfilling prophecy.

1.1.1 Production of integrated circuits

One of the fundamental steps in the fabrication of integrated circuits is photolithography (Suzuki and Smith, 2007; Mack, 2007; Levinson, 2011), in which the formation of three-dimensional relief images on a substrate is created. To this end, a light sensitive layer, i.e. photo-resist, is applied to a silicon wafer with an oxide layer. In the *exposure* step, the reticle mask containing the image is projected onto the photo-resist (see Fig. 1.1). Subsequently, the photo-resist, which has been

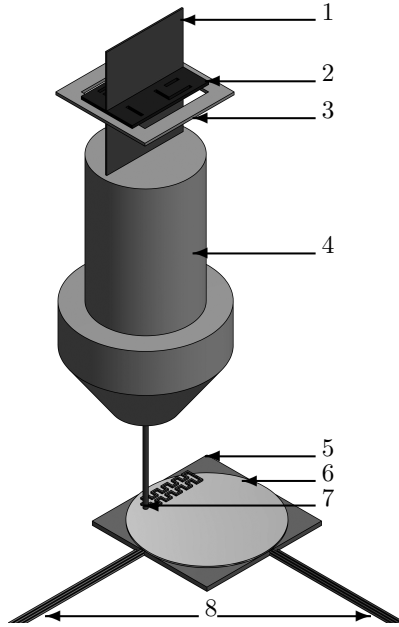


Figure 1.1: Schematic representation of a wafer-scanner. The position of the stage is typically measured at the edges of the stage, which are indicated by (8). The area to be exposed is indicated by (7). The numbers in the figure correspond to: 1) light source, 2) reticle, 3) reticle stage, 4) optical lens column, 5) wafer-stage, 6) wafer, 7) area to be exposed, 8) sensors.

exposed to light is developed and removed. This allows to etch the exposed oxide. Finally, the remaining photo-resist is removed and post-processing is applied to change the conductive properties of the silicon.

ICs are built through a sequence of such patterning steps, each creating a new layer. For proper functioning of the IC it is required that new layers are placed correctly on top of the existing structures. This lateral positioning of the different layers is called *overlay* (Levinson, 2011). During the exposure step, the wafer is positioned using a wafer-stage. The stage positioning accuracy, among others, directly influences the overlay. Moreover, errors in the positioning of the wafer-stage reduce the contrast created by the imaging process (Butler, 2011).

In the current generation of lithographic machines, i.e. wafer-scanners, the reticle stage positions the reticle in synchronization with the wafer-stage. In the previous generation, i.e. wafer-steppers, the wafer is positioned and the reticle remains at a fixed position. When the wafer arrives at the correct position, the exposure of the wafer starts. After the required amount of exposure to light, the light source is turned off and the wafer is moved to the next die. This proces,

i.e. step-expose, is repeated until the complete wafer is finished. The prescribed movement of the wafer-stage, both during exposure and when moving from one chip to the next, is called the motion profile or setpoint trajectory.

1.1.2 Challenges for miniaturization

The smallest element, which can be produced is called the *critical dimension* or the *minimum feature size*. The smallest feature that can be printed using adequate control is limited by the resolution of the optical system, which is proportional to the wavelength of the imaging light divided by the numerical aperture of the projection lens (Mack, 2007). To reduce the minimum feature size of the ICs, light sources with smaller wavelengths are used, such as Deep Ultra Violet (DUV) or Extreme Ultra Violet (EUV) lithography (Arnold, 2009; Wu and Kumar, 2009). However, using EUV light sources is not straightforward for several reasons (Talents et al., 2010). First of all, since EUV light is absorbed by air, the entire optical system must be contained in a near vacuum environment. Secondly, the use of reflective optics is required instead of optical lenses which absorb EUV radiation. Finally, a bright light source is required, since only a small percentage of the light actually reaches the wafer (Wagner and Harned, 2010), which is directly related to the production speed. Besides the resolution, the positioning accuracy during exposure is of critical importance. This positioning accuracy is required at the *performance location*, i.e. the area to be exposed. A measure for the minimum feature size is the half-pitch, see Arnold (2009). For example, 38-nm half-pitch lithography requires the positioning error to be lower than 1 nm moving average and 7 nm moving standard deviation during exposure (Butler, 2011). Therefore, accurate control is crucial to reduce the minimum feature size.

1.1.3 Advanced motion systems

Although photo-lithography is chosen as a carrier application throughout this thesis, there are many applications which suffer from very similar or even the same problems. These advanced motion systems must satisfy speed and accuracy requirements. These requirements keep increasing over and over again. The combination of high speeds and high accuracy makes these control problems very challenging. Besides wafer-scanners and -steppers, typical examples of such systems are pick-and-places machines and scanning probe microscopes, e.g. atomic force microscopes and electron microscopes.

1.1.4 Next-generation motion systems

To obtain a higher production throughput, either more aggressive motion profiles (i.e. higher acceleration) or larger wafer sizes (Mack, 2012) (i.e. higher mass) are required. Both methods will lead to larger required forces to actuate the system.

Higher bandwidths of the system are required to maintain the desired positioning accuracy due to setpoint trajectories with increased acceleration. Therefore, a system design with an increased stiffness is required, which possibly leads to more mass of the system. Moreover, miniaturization leads to higher demands on the positioning accuracy and thus the bandwidth of the system as well. These reasons lead to higher specifications on the actuators, amplifiers and cooling systems. In the rigid-body design paradigm (Soemers, 2001) this leads in an evolutionary way to systems with an increasing mass, which is expected to become infeasible in the near future due to thermal constraints.

Therefore, the next generation of advanced motion systems, e.g. wafer stages and pick-and-place machines, are likely designed to be lightweight, which results in significant internal flexibilities. The consequences will be discussed hereafter.

1.1.5 Control of advanced motion systems

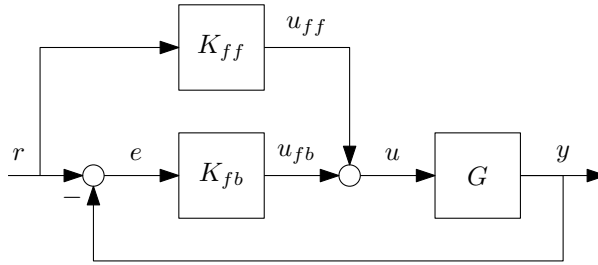


Figure 1.2: Control structure with feedback controller K_{fb} and feedforward controller K_{ff} . The signals are denoted as: setpoint trajectory r , sensor output y , tracking error e , total input u , feedback input u_{fb} and feedforward input u_{ff} .

To produce ICs with feature sizes of tens of nanometers, positioning errors of the wafer in the order of a few nanometers or even less are allowed during the exposure. Furthermore, due to the desire for high production throughput, the process time has to be minimized resulting in high accelerations. Nowadays, these accelerations are 40 m/s^2 (Butler, 2011) and will probably increase further in the near future. These high accuracy requirements in combination with high accelerations of these machines creates a challenging problem for control. To meet these challenging specifications, advanced motion systems are typically controlled using a combination of feedback- and feedforward control as shown in Fig. 1.2. Since the dynamics of such systems are highly repeatable and the largest disturbance is typically induced by the setpoint trajectory, feedforward control determines the performance to a large extend for rigid-body designed systems. For example, in Heertjes et al. (2010) feedforward control is responsible for 99.97% of the control forces and associated performances. For a general introduction to the control of

advanced motion systems see Clayton et al. (2009) and Steinbuch et al. (2010). Position control of lithographic equipment is for instance discussed in Butler (2011). In Fig. 1.2 the measured variables are controlled such that the system follows the setpoint trajectory with high accuracy. However, looking at the lithographic process in Fig. 1.1 more closely, the following observation can be made:

Observation 1. the sensors are physically non-collocated with the performance location.

For rigid-body designed systems, Observation 1 implies that the performance location can be controlled by using simple geometrical transformation, as the deformations of the system are negligible. In the next section the consequences for lightweight designed system will be explored.

1.1.6 Consequences of lightweight design

Lightweight motion systems pose several challenges for the control design:

1. flexible modes in the frequency region of interest, and
2. the relation between the measured variables and the performance variables cannot be described by a static relation due to flexibilities and non-collocated sensor- and performance-variables (see Observation 1). This implies that the performance cannot be calculated or controlled using simple geometrical transformations. Such a control problem is known as inferential control (Parrish and Brosilow, 1985), and finally
3. the input sensitivity of the system is deteriorated.

As a consequence of lightweight design, the bandwidth of the system is often limited due to the reduced stiffness, such that flexible dynamical behavior appears at lower frequencies. The limited bandwidth of the system leads to a reduced disturbance rejection. Moreover, a lower moving mass leads to reduced input disturbance rejection, which leads to higher requirements on the system bandwidth. The second consequence is that the setpoint trajectory excites the resonant part of the flexible modes, which leads to a deteriorated performance. Also, more aggressive setpoint trajectories due to increased production speeds will lead to increased excitation of the flexible modes. Therefore, it is expected that feedforward control becomes increasingly important for control of lightweight motion systems.

The second aspect relates to Observation 1. Consider for example a wafer-stage, where the position is measured at the edges of the stage, while the performance is required at the area to be exposed at the center of the stage, see Fig. 1.1. Due to the flexible dynamics, the relation between the measured- and performance variables is dynamic and cannot be calculated or controlled using a static geometric transformation such as used in rigid-body designed systems. Therefore, control methods which take this difference into account are required. Such methods are

available for feedback control, i.e. indirect (Skogestad and Postlethwaite, 2005), inferential control (Parrish and Brosilow, 1985) and (simultaneous) 2DOF inferential control (Oomen, 2010). However, feedforward control design methods for inferential systems which are independent of the existing feedback controller are not available.

The last aspect is related to the system design of lightweight motion systems, which is considered in Schneiders et al. (2003); Makarovic et al. (2004); Makarovic (2006); van der Wielen (2009). One solution to compensate for the decrease of stiffness due to lightweight construction is the use of over-actuation and over-sensing. Traditionally, one would employ as many sensors and actuators as the number of rigid-body degrees-of-freedom. In the case of over-actuation and -sensing more actuators and sensors will be used compared to traditionally designed systems, creating more design freedom in control to deal with flexibilities. This new class of over-actuated and over-sensed systems offers design freedom to develop new control methods.

Due to the fact that the bandwidth will be more limited in case of lightweight motion systems, it is expected that feedforward becomes increasingly important. Moreover, lightweight motion systems offer new challenges, such as non-collocated sensor- and performance locations, which are yet unexplored. Furthermore, many lightweight motion systems are equipped with additional actuators and sensors, which offer new design freedom to explore. Therefore, this thesis will focus on feedforward control for lightweight motion systems. The next sections will briefly discuss the research goal and approach. In the subsequent section existing feedforward methods and their relation with the problem statement will be discussed.

1.2 Problem statement

In this section the research goal and approach will be discussed. First of all, the class of motion systems is defined to limit the scope. The class of systems considered in this thesis are motion systems characterized by,

1. intrinsically multivariable behavior due to flexibilities,
2. MIMO plant, which is possibly over-actuated and/or over-sensed,
3. the sensors and actuators of the plant are considered to be fixed at a given location in the machine,
4. the sensors are typically non-collocated with the performance location, i.e. the performance location cannot be measured during normal operation; moreover, due to the photo-lithography production process the performance location may vary in time,
5. the dynamics of the physical plant are assumed to be linear and time-invariant,

6. the setpoint trajectory for the performance location r_z is assumed to be known a priori; however, the setpoint trajectory may vary due to changes in the production process, e.g. different size of ICs, different photo-reactive properties or cycles with less acceleration,
7. other external disturbances are assumed to be small or compensated otherwise, and finally
8. the plant is typically operated in feedback.

The goal of this thesis can be summarized as follows: develop feedforward control methods for lightweight advanced motion systems, which can:

1. deal with immeasurable performance location(s), and
2. exploit the use of over-actuation and over-sensing.

To achieve this, a standard two degrees-of-freedom control structure of Fig. 1.2 is extended with a performance output as shown in Fig. 1.3. In this figure, the plant to be controlled is denoted by G_i , $i \in [y, z]$, i.e. the sensor- and (immeasurable) performance output, which are typically physically non-collocated. As a consequence of internal dynamics, differences between the sensor outputs y and the performance outputs z exist, which cannot be calculated or controlled using a (static) geometric transformation.

Furthermore, static transformations T_y and $T_{u,fb}$ are included to transform the sensor- to motion-coordinates and to decouple the rigid-body dynamics of the system to allow for decoupled feedback design, respectively. The diagonal feedback controller K_{fb} is required for stabilization and disturbance suppression. For over-actuated systems it is possible to introduce a different decoupling matrix $T_{u,ff}$ in the feedforward path, since the goals of these decoupling matrices can be different. In the feedforward path it is desirable to prevent the excitation of flexible modes by making these modes uncontrollable or possibly take some energy considerations into account. For the feedback path it is undesirable to make these modes uncontrollable, since any disturbance which act in the direction of this mode cannot be dealt with. Provided that there are extra sensors or some estimation of these modes available, additional feedback loops can be employed to damp these modes or increase the stiffness in these directions of the system.

The feedforward controller K_{ff} is designed to enhance the performance. Moreover, the arrow with θ indicates the possibility to tune the parameters of the respective elements. Finally, the setpoint trajectory prefilter F is present to provide a control structure, which can handle input shaping and different setpoint for performance - and motion coordinates.

In the next section, existing feedforward solutions and their relation with the problem statement will be presented.

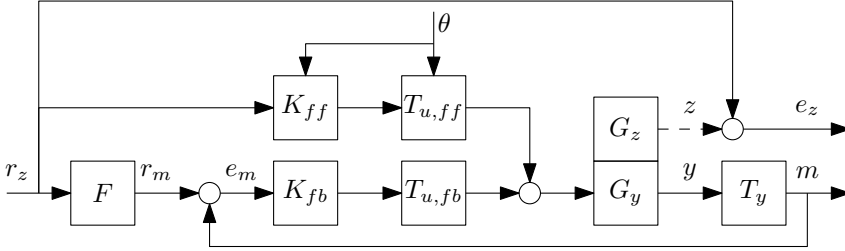


Figure 1.3: Overview of the control structure and the design of the different elements in this thesis. The blocks G_y and G_z represent the plant with sensor outputs and the plant with performance outputs, respectively. The other blocks represent the feedback controller K_{fb} , the feedforward controller K_{ff} and setpoint trajectory prefilter F , the output transformation T_y and the input transformations $T_{u,fb}$ and $T_{u,ff}$ for feedback and feedforward control, respectively. The signals are denoted as: setpoint trajectory r_z , sensor output y , motion coordinates m , tracking error e_m , performance error e_z and finally the feedforward parameter vector θ .

1.3 Feedforward control approaches

1.3.1 Model-based approaches

Perfect tracking of setpoint trajectories with only feedback control is generally not possible for all frequencies due to the Bode sensitivity integral (Freudenberg and Looze, 1985). However, with the use of a feedforward controller, i.e. an inverse dynamic model (Silverman, 1969), it may be possible to achieve perfect tracking under the assumption of solving the inverse dynamics problem. The presence of non-minimum phase (NMP) zeros (Hoagg and Bernstein, 2007) renders the inverse unstable. Due to sampled-data implementations, systems can have non-minimum phase zeros (Aström et al., 1984), even if such NMP zeros are not present in continuous time. Solutions have been proposed in terms of approximation of the NMP zeros, e.g. ZPETC (Tomizuka, 1987) and EBZPETC (Torfs et al., 1992) or preview-based approaches (Devasia et al., 1996; Hunt et al., 1996; Zou and Devasia, 1999). These inverses are noncausal, but in Sogo (2008, 2010) it is shown that these inverses approximate the continuous time inverses for a sufficiently small sample time. Furthermore, to achieve exact tracking for systems with NMP zeros an infinite preview time is required. However, the error introduced by a finite time preview can be bounded (Zou and Devasia, 1999, 2004).

In de Roover and Bosgra (2000) a (nominal and robust) learning filter is designed using a norm-based technique. Other examples for the design of a norm-based feedforward controller are \mathcal{H}_2 model matching in Zhong and Pao (2013) and \mathcal{H}_∞ feedforward design Boerlage et al. (2003).

Norm-based feedforward controllers, i.e. feedforward controllers designed using norm-based techniques such as \mathcal{H}_2 or \mathcal{H}_∞ , always result in proper and causal feedforward controllers. For strictly proper systems, having a relative degree larger than one, the slope of the inverse system has to be larger than +1. Because norm-based techniques will result in a proper controller, the resulting controller will be an approximation of the inverse.

Model uncertainty

For model-based solutions, the amount of uncertainty associated with a model is an inherent problem. In Devasia (2002) it is shown that feedforward improves the performance in case the model uncertainty is sufficiently small. However, if the model uncertainty is too large at a certain frequency, the feedforward controller may deteriorate the performance at those specific frequencies. In this case, the feedforward controller should not be used for these specific frequency (ranges). For models with low uncertainty, it is required that:

1. the system has highly reproducible behavior, and
2. the system is contained in the model set and the identification procedure does not introduce unnecessary conservatism.

The first is achieved by proper design (Soemers, 2010; Munnig Schmidt et al., 2011; Schneiders et al., 2005) and manufacturing of the system, which is typically the case for advanced motion systems. The second requirement is fulfilled using reliable (parametric) system identification techniques (Pintelon and Schoukens, 2001; Oomen et al., 2013; Oomen, 2010; Van Herpen, 2014).

1.3.2 Data-based approaches

For systems which perform the same task repeatedly after starting from the same initial conditions, Iterative Learning Control (ILC) (Moore, 1998; Longman, 2000; Bristow et al., 2006; Ahn et al., 2007) is a suitable solution for performance improvement. To achieve this performance improvement, ILC iteratively updates the control signal using data from previous experiments.

Repetitive control (RC) (Hara et al., 1988; Steinbuch, 2002; Steinbuch et al., 2007) is based on similar ideas as ILC. However, for RC identical initial conditions are not required as RC acts in feedback. Therefore, RC can affect the stability of the closed-loop system. A memory loop is employed to generate a model of the disturbance, such that according to the Internal Model Principle (Francis and Wonham, 1975), perfect disturbance rejection is possible. Typical applications of RC are rotating equipment, such as CD players. However, RC is not limited to rotating equipment, as long as the disturbance is periodic. In Merry et al. (2011) RC is applied to a metrological Atomic Force Microscope (AFM), which is used for scanning of calibration sample with a repeating structure.

Both ILC and RC have the same drawbacks, that is, the approaches are not setpoint trajectory invariant, i.e. a new learning sequence is required for every new setpoint trajectory. The setpoint trajectory varies with every different product, due to different sizes of ICs, different photo-reactive properties, different desired frequency contents or cycles with less accelerations. Feedforward control design methods, which use data from one (or more) setpoint trajectory to optimize a setpoint invariant feedforward controller are presented in the next section. Furthermore, these approaches only guarantee performance at the measured sensor locations. Therefore, these methods are not yet easily extendable to lightweight motion systems.

In van de Wijdeven and Bosgra (2007, 2008) ILC for residual vibration suppression is presented. This method only aims at suppressing the residual vibrations after a point-to-point motion by adapting the input signal during the deceleration phase. However, in the intended application the tracking errors during the point-to-point motion are important as well. In Avrachenkov and Longman (2003) ILC for over- and under-determined systems is considered. However, the additional design freedom is only employed to minimize the energy used by the input signal. An adaptive feedforward method to compensate for differences in the motor constant is presented in Butler (2013). However, for adaptive approaches certain persistence of excitation conditions are required, which puts undesired constraints on the setpoint trajectory.

1.3.3 Fixed-structure feedforward control

Fixed structure feedforward methods such as inertia or snap feedforward (Lambrechts et al., 2005; Boerlage, 2006; Steinbuch et al., 2010) make assumptions on the structure of the underlying model for feedforward control. This structure is exact for 4th-order plants, but approximate for higher-order plants. For a small number of parameters it is possible to use manual tuning. However, for a large number of parameters this becomes tedious. Therefore, some fixed structure feedforward methods combine the fixed-structure with a data based tuning, which has similarities with Iterative Feedback Tuning (Hjalmarsson, 2002). In van der Meulen et al. (2007, 2008); Tousain and van der Meulen (2009) the parameters of a fixed-structure feedforward controller are optimized based on the measured tracking errors of the previous experiment. Since this fixed structure feedforward method is based on the snap feedforward, it suffers from the same drawbacks. Snap feedforward only compensates for the deformation during motion due to the limited stiffness of the moving mass. The deterioration of the performance due to resonant behavior, which is excited by the setpoint trajectory, is not compensated for. Moreover, such methods only guarantee performance at the sensor locations.

A data-based method to optimize a MIMO FIR feedforward filter is presented in Baggen et al. (2008); Heertjes et al. (2010). This approach is extended in Bruijnen and van Dijk (2012), where a FIR setpoint prefilter is included, such

that theoretically zero errors can be obtained. Both methods result in setpoint trajectory invariant solutions and optimize the performance with respect to the actual plant. However, these approaches do not provide any means to exploit over-actuation or to deal with non-collocated sensor- and performance locations.

In van de Wijdeven and Bosgra (2010) ILC with basis functions is introduced, in which the parameters of (polynomial) basis functions are optimized, based on measurement data. Furthermore, a general framework for analysis and design, which includes the solutions in van der Meulen et al. (2007, 2008); Tousain and van der Meulen (2009), Baggen et al. (2008); Heertjes et al. (2010) and Bruijnen and van Dijk (2012), is presented. However, such solutions only provide performance guarantees at the sensor locations.

In de Gelder et al. (2006) a feedforward method is discussed which minimizes the settling time using a Linear Programming problem with Laguerre basis functions. However, issues with numerical conditioning limit the applicability to systems with a small number of in- and outputs. This makes the presented method unsuitable for systems where the interaction between multiple degrees of freedom becomes relevant, which is the case for lightweight motion systems. Also the extension towards the over-actuated (non-square) case is far from trivial given the issues with numerical conditioning.

In Heertjes and van de Molengraft (2009), the input signal from a converged ILC sequence is mapped into a FIR filter to take setpoint variation into account. The presented methods show a good robustness against variations in setpoint trajectories. However, it is not exactly clear how to choose the number of parameters. Furthermore, the method only provides performance guarantees at the sensors.

Fixed-structure methods combine the advantages of model- and data-based methods, i.e. the solution is setpoint trajectory invariant and is tuned based on experimental data resulting in a good performance. However, the current fixed structure methods do not exploit over-actuation nor do they take the difference between the sensor- and performance location into account.

1.3.4 Input shaping

Input shaping (Singh, 2010) is a common method to reduce vibrations in motion systems. The eigenfrequencies of the system are removed from the input signal by convolving the input signal with an input shaper. Input shaping aims to suppress the residual vibration after the point-to-point motion. Typical advantages of input shaping are: 1) reduced vibration, 2) independent of setpoint trajectory, 3) robust methods available. Furthermore, input shaping prevents the excitation of flexible modes, such that the performance over the complete structure improves. Moreover, positive input shapers have the property that the shaped input signals satisfy the same bounds as the original input signals (Baumgart and Pao, 2007). However, this is at the cost of extra delay, which is undesirable in the intended application. This delay can be reduced by using negative input shapers (Singhose et al., 1995;

Singh and Singhose, 2002), which provide no guarantees for the shaped input signal as a consequence. Furthermore, there is trade-off in input shaping between shaper length and parameter sensitivity (Cutforth and Pao, 2004). Therefore, an adaptive input shaping method is presented in Cutforth and Pao (2004), which can adapt the input shaping parameters. However, all input shaping approaches modify the setpoint trajectory, which is undesirable for several reasons: i) due to the loss of synchronization between the wafer- and reticle-stage, and ii) increased rise time, i.e. decreased speed.

1.3.5 Setpoint trajectory design

Fourth order setpoint trajectory design for point-to-point motion is considered in Lambrechts et al. (2005), where the setpoint trajectory satisfies a priori specified bounds on the derivatives of the setpoint trajectory. These derivatives can directly be used to compute the feedforward signal as in Boerlage (2006); Steinbuch et al. (2010), which will be used throughout this thesis.

In Fleming and Wills (2009) periodic scanning trajectories with fixed linear regions and minimal harmonic contents are designed using optimization, i.e. the setpoint prevents the excitation of the parasitic resonances. However, solutions involving setpoint trajectory redesign are considered outside the scope of this thesis, since the setpoint trajectory is determined by the intended application, e.g. due to different size of ICs, different photo-reactive properties or cycles with less acceleration,.

In de Caigny et al. (2007) the synthesis of feedforward input signal using an optimization method is presented. The method results in smooth signal, which ensures accurate tracking. However, such an approach requires a new optimization for every new setpoint trajectory. In van Loock et al. (2013) a combined approach for setpoint trajectory design and setpoint tracking is presented for differentially flat systems. A linear system is flat if, and only if, it is controllable Fliess et al. (1995, Theorem 2). This approach can include geometric constraints and constraints on the state and input. However, this method requires a new optimization for every new setpoint trajectory.

1.3.6 Indirect control and inferential control

Control of immeasurable performance variables by means of auxiliary measurements is considered in the context of indirect (Skogestad and Postlethwaite, 2005) and inferential control (Brosilow and Tong, 1978; Parrish and Brosilow, 1985; Doyle, 1998). Such control structures can be regarded as special cases of the two degrees-of-freedom (DOF) control configuration (Oomen et al., 2009, 2011; Oomen, 2010). Specifically, in Oomen et al. (2009) and Oomen (2010, Ch. 3) the identification of inferential motion systems is addressed. Moreover, Oomen et al. (2011) and Oomen (2010, Ch. 7) present a model-based inferential control design.

A multivariable inferential feedforward approach is presented in Zhang and Agustriyanto (2003), which is applied to an application in the process industry. The dominant disturbance, i.e. the disturbance with the largest effect on the performance, is immeasurable. In this thesis the tracking of setpoint trajectories is considered, which are assumed to be known a priori.

A related approach to inferential control is visual servoing (De Best, 2011; De Best et al., 2012), in which the performance variables are measured by employing camera vision. However, due the resolution and sampling frequency this is not yet suitable for advanced motion applications, such as photo-lithography.

1.3.7 LPV and LTV feedforward control approaches

As motivated in the previous section, it is typically not possible to measure at the performance location during operation. In production processes, such as lithography machines or pick-and-place machines, the performance location, i.e the location where the tool operates or the area to be illuminated is changing in time. Such systems can be modeled as linear time-varying (LTV) or linear parameter-varying (LPV) systems. Model-based feedforward approaches for LPV systems have been considered in Sato (2003, 2005, 2008) and Prempain and Postlethwaite (2008). Such solutions boil down to the solution of a large or infinite number of Linear Matrix Inequalities (LMIs), which might be computationally challenging for practical systems due to numerical issues.

1.3.8 Over-actuation and over-sensing

In Schneiders et al. (2003) an integrated design approach for over-actuated systems is presented. The freedom in actuator placement and control design is one of the advantages of over-actuation (Schneiders et al., 2004a), i.e. the actuator can be placed to optimize the controllability of the internal dynamics. In this way the controllability of the internal dynamics for feedback can be maximized, while simultaneously the controllability of the internal dynamics for feedforward can be minimized. Finally, in Schneiders et al. (2004b) a method for analysis of over-actuated systems in a modal framework is presented.

Another well-known example of over-actuated motion systems are planar motors, which are nowadays used in lithographic machines to position the wafer with respect to the lens column. Classically, a short- and long-stroke stage were combined to achieve the required positioning accuracy over the complete stroke. In this case, the long-stroke motor consists of linear motors arranged in an H-bridge configuration. Modern stages consist of a moving coil levitated planar actuator with a short-stroke stage stacked on top. Due to the presence of forcer coils and a short-stroke stage in the moving part, cables are required to deliver the required power. State of the art planar motors are moving magnet planar actuators, such as the actuators in Jansen (2007); van Lierop (2008); de Boei (2009). The advan-

tage of such actuators is the wireless operation of the moving part. Due to the position dependent behavior of such machines, control and communication of such machines is challenging. In Rovers (2013) the design of a lightweight moving magnet planar actuator is presented. For an extended overview of motor technologies see Lomonova (2010).

In Rovers et al. (2009) the static deformation of a planar actuator is presented. Moreover the deformation due to dynamic and compliant system behavior of such actuators is characterized (Rovers et al., 2013). The presented simulations show that the deformation due to the dynamic and compliant part of the system dynamics is of the same order of magnitude. A commutation method to reduce the static deformations in planar actuators is presented in Achterberg et al. (2010). In Ronde et al. (2012b) spatial feedforward for over-actuated systems is presented, where it is shown that by employing over-actuation it is possible to prevent the excitation of a flexible mode, i.e. both the compliant dynamics as well as the resonant behavior.

1.3.9 Feedforward control in high-speed SPM

A related field are Scanning Probe Microscopes (Clayton et al., 2009), which are typically driven by piezo-electric actuators over a range of several 100's of micrometers. These systems are different in the sense that no rigid-body modes are present and since in general the motion degrees-of-freedom are well decoupled SISO feedforward control is applied. Moreover, these piezo-electric actuators exhibit non-linear and/or time-varying behavior such as hysteresis, creep and drift. Examples to deal with this non-linear behavior are hysteresis compensation (Merry, 2009; Merry et al., 2009) and non-linear feedforward for friction compensation (Rijlaarsdam, 2012; Rijlaarsdam et al., 2012).

1.4 Research challenges and approach

From the perspective of system design, two types of systems can be considered: 1) traditional actuated systems, and 2) over-actuated systems. For which the research challenges will be formulated.

1. Feedforward control design methods for traditional actuated, inferential, lightweight motion systems.

In order to deal with the difference between the sensor measurements and the actual performance variables control methods are required which explicitly take the difference in dynamic behavior into account. Moreover, for lightweight systems feedforward control becomes increasingly important. From Section 1.3.6 it is clear that feedback solutions for inferential perfor-

mance variables exist. Moreover, simultaneous designs of the feedback controller and feedforward controller exist. However, methods for independent design of the feedforward controller are unavailable. Moreover, the existing frameworks do not provide any means to deal with the time-varying nature of the performance location. This leads to the following research challenges:

- (a) develop a feedforward control design framework for inferential, lightweight motion systems, which is independent of the feedback controller, and
- (b) develop a framework to explicitly deal with the time-varying nature of immeasurable performance locations

2. Feedforward control design methods for over-actuated and/or over-sensed lightweight motion systems.

The next generation of motion system is designed to be relatively lightweight. These system are possibly employed with additional actuators and sensors, called over-actuation and over-sensing. Planar motors, such as Rovers (2013), are a well known examples of over-actuated system. From Section 1.3.8 it is clear that over-actuated and over-sensed systems have additional design freedom for actuator placement and control design. However, the current feedforward techniques are either unable to deal with non-square control problems or do not exploit the additional design freedom. This leads to the following research challenges:

- (a) develop a feedforward control design method, which exploits the additional design freedom from over-actuation, and
- (b) develop a control framework allows to employ the additional design freedom to achieve different goals for feedback control and feedforward control, and finally,
- (c) develop a data-based feedforward control design method, which exploits over-actuation and over-sensing.

Both the model-based and fixed-structure feedforward approach will be explored in this thesis, because the setpoint trajectories in the intended application are known in advance. However, due to changes in the production process, e.g. different size of the chips, different photo-reactive properties or cycles with less accelerations, the setpoint trajectory may be changing. Data-based approaches, such as ILC and RC, require a new learning sequence for every new setpoint trajectory, which is undesirable in the intended application. Input shaping approaches lead to performance over the complete structure, i.e. the flexible dynamics are not excited. However, such approaches modify the setpoint, which is undesirable due to the loss of synchronization between the wafer- and reticle-stage.

1.5 Research contributions

This section will discuss the research contributions of each chapter in this thesis. Firstly, in Chapter 2 feedforward design methods for lightweight motion systems with physically non-collocated measurement and performance locations are investigated. To address **research challenge 1a**, the standard two degrees-of-freedom control configuration of Fig. 1.2 is extended with a model of the performance output of the plant as shown in Fig. 1.3. The scientific contribution described in this chapter is,

Contribution 1. the analysis of inferential motion systems. First of all, it is shown that different setpoint trajectories are required for the sensor- and performance outputs. Secondly, the general two degrees-of-freedom control configuration for inferential control is extended to facilitate the design of the feedforward controller independent from the feedback control design.

Secondly, to address **research challenge 1b** the framework of Chapter 2 is extended towards systems with time-varying performance locations. Therefore, the scientific contribution of this chapter is,

Contribution 2. a novel feedforward design method to deal with system which have physically non-collocated measurement and performance location, which are time-varying due to the production process.

The second part of this thesis is related to research on over-actuated and over-sensed lightweight motion systems. In Chapter 4 the additional design freedom resulting from over-actuation is investigated to address **research challenge 2a**. The following scientific contributions are described in this chapter,

Contribution 3. the analysis of the design freedom resulting from over-actuation in a modal framework. First of all, this shows that input transformations exist, which do not affect the rigid-body behavior but render the desired flexible modes uncontrollable. Secondly, the formulation of conditions based on the system properties, which determine whether this design freedom is exploitable

Moreover, **research challenge 2b** is also addressed in this chapter, which leads to the following scientific contribution,

Contribution 4. the investigation of control structures, which can reflect the different control goals of the feedback and feedforward controller in over-actuated system. This investigation leads to the presentation of a novel control structure, which employs different input decoupling transformations for the feedback- and feedforward controller.

In Chapter 5 a data-based framework is investigated to address **research challenge 2c**. The scientific contribution described in this chapter is,

Contribution 5. the investigation of data-based method, which exploits the design freedom resulting from over-action, as investigated in Chapter 4. Secondly, the data-based feedforward method identifies the controller parameters which are optimal with respect to the actual plant. Additionally, it is investigated how to exploit the additional sensors in case of over-sensing.

1.6 Outline of this thesis

The research presented in this thesis is based on the following articles.

Chapter 2

- Ronde, M. J. C., van de Molengraft, M. J. G., and Steinbuch, M. (2012a). Model based feedforward for inferential motion systems, with application to a prototype lightweight motion system. In *American Control Conference*, pages 5324-5329, Montréal, Canada.
- Ronde, M. J. C., van de Molengraft, M. J. G., and Steinbuch, M. Model-based feedforward for inferential motion systems. *Submitted for journal publication*.

Chapter 3

- Ronde, M. J. C., van den Bulk, J. D. J. M., van de Molengraft, M. J. G., and Steinbuch, M. (2013a). Feedforward for flexible systems with time-varying performance locations. In *American Control Conference*, pages 6045-6050, Washington, DC, USA.

Chapter 4

- Ronde, M. J. C., Schneiders, M. G. E., van de Molengraft, M. J. G., de Haas, D., and Steinbuch, M. (2012b). Spatial feedforward for over-actuated flexible motion systems. In Scheidl, R. and Jakoby, B., (editors), *The 13th Mechatronics Forum International Conference*, volume 1/3, pages 254-260, Linz. Trauner-Verlag.
- Ronde, M. J. C., Schneiders, M. G. E., Kikken, E. J. G. J., van de Molengraft, M. J. G., and Steinbuch, M. (2013b). Model-based spatial feedforward for over-actuated motion systems. *Mechatronics, Article in press*, <http://dx.doi.org/10.1016/j.mechatronics.2013.09.010>

Chapter 5

- Ronde, M. J. C., Leenknecht, G. A. L., van de Molengraft, M. J. G., and Steinbuch, M. Data-based spatial feedforward for over-actuated motion systems. *Under review for journal publication*

This thesis consists of four research chapters. Three chapters are submitted for journal publication, the remaining chapter is based on a conference publication. Therefore, each chapter is self contained and can be read independently. The outline of the remaining part of this thesis is as follows.

In Chapter 2, a model-based feedforward method for inferential motion systems is presented, where a feedforward method is presented which provides performance at the performance location. Moreover, the feedforward controller can be designed independently from the feedback controller.

In Chapter 3, an exploratory study towards systems with time-varying inferential performance locations is presented. The problem of time-varying performance locations naturally occurs in many manufacturing systems, i.e. pick-and-place machines or wafer stages.

In Chapter 4, a model-based spatial feedforward method for over-actuated motion systems is introduced. This chapter presents design methods and conditions for the existence of spatial feedforward. Furthermore, this method has been experimentally validated on an industrial prototype lightweight motion system.

In Chapter 5, a data-based spatial feedforward method for over-actuated systems is introduced. In the data-based method the feedforward controller and feedforward decoupling are tuned based on experimental data from previous task trials. Therefore, the requirement of a complex MIMO plant model can be relaxed, i.e. only a MIMO rigid-body model is required.

Finally, in Chapter 6 the conclusions of this thesis and recommendations for future research will be presented.

Chapter 2

Model-based feedforward for inferential motion systems

IN high-performance motion systems, e.g. wafer-stages or pick-and-place machines, there is an increasing demand for higher production throughput and accuracy. In the current design paradigm of rigid-body design, higher demands for production throughput and accuracy will lead, in an evolutionary way, to larger motion drives. This paradigm does not scale with a higher production throughput, i.e. a new paradigm is required. The new paradigm is to design a lightweight machine and to deal with the resulting flexibilities by employing control. The location where the tool operates, e.g. the area to be exposed or the component to be placed, is typically non-collocated with the sensor locations. This gives additional problems to control the performance location if the system is flexible due to the lightweight design. This chapter presents a model-based feedforward method for lightweight motions systems, with non-collocated sensor and performance locations. Inferential control is considered, because the point of interest for performance is typically different from the location of the measured feedback signals.

2.1 Introduction

Driven by the fierce competition in the semiconductor industry, faster and more advanced integrated circuits (ICs) are desired, which can be produced at lower cost and consume less energy. This can be achieved by reducing the size of the features of ICs. Moreover, increased production speed leads to additional cost reduction. These ICs are manufactured in a process called *photo-lithography* (Mack, 2007) in a wafer-scanner. A key part of a wafer-scanner is the wafer stage, responsible for positioning the wafer with respect to the optical system. To increase the production speed more aggressive motion profiles (i.e. higher accelerations) and/or larger wafer sizes (i.e. higher mass) are required. Moreover, both miniaturization and higher accelerations lead to higher bandwidth requirements, which require a design with higher stiffness. This design paradigm, called rigid-body design, will lead to systems with an increase of the moving mass. Therefore, the required (acceleration) forces will become larger, resulting in stricter demands on actuators, amplifiers and cooling. For Lorentz type actuators, the dissipated power is quadratically proportional to the required force and thus to the required acceleration (Rovers, 2013). Lorentz type actuator have reached their physical limits with respect to the requirements on force on efficiency (Katalenic, 2013). Therefore, this paradigm has reached the boundary of its scalability, and becomes infeasible due to size requirements and thermal constraints (Oomen et al., 2013).

Lithographic and pick-and-place applications require accurate positioning at the location where the processing is done, i.e. the area to be exposed (lithography) or the location of the component to be placed (pick-and-place). However, measurements of the system are typically done at the edges of the moving mass, due to the production process and placement constraints. Therefore, the performance location is physically non-collocated with the sensor location and is immeasurable during normal operation.

A new design paradigm is required that reduces the moving mass of the machine and, consequently, allows for the presence of internal elastic deformations. This has several consequences for control design:

1. resonances in the frequency region of interest, i.e. near to the objective bandwidth of the control loop, and
2. the transfer between sensor output y and performance location z becomes dynamical due to internal elastic deformations and non-collocated sensor- and performance variables. This implies that the performance cannot be calculated or controlled using simple geometrical transformations. Such control problems are known as inferential control (Parrish and Brosilow, 1985).

Lower resonance frequencies limit the attainable bandwidth and thus the disturbance rejection is more limited. Increased performance specifications due to miniaturization and more severe excitation of the flexible dynamics due to aggressive

setpoint trajectories require higher levels of disturbance rejection. Due to these conflicting requirements, it is expected that feedforward becomes increasingly important. The consequences for planar actuator design implied by the reduction of the moving mass are investigated in Rovers (2013). As an alternative, other types of actuators can be considered, such as reluctance actuators (Katalenic, 2013). Furthermore, the excitation of the flexible dynamics by the setpoint trajectory leads to significant internal deformations and undesired vibrations. For example, it is shown in Butler (2011, Fig. 34) that the flexible modes in a wafer stage indeed are excited by the setpoint trajectory. Moreover, it is suggested that this can be solved by applying advanced feedforward control. Direct control at the sensors does not lead to satisfactory performance at the performance location due to these deformations. Therefore, it is required to explicitly deal with the performance outputs z . Furthermore, due to changes in the production process, such as different IC sizes, different photo-reactive properties or cycles with less accelerations, the setpoint trajectory may vary. The presence of disturbances also requires these machines to be operated in feedback control. The feedback controllers may be subject to (re-)tuning and/or gain scheduling (Butler, 2011). Therefore, the feedforward design method is required to be independent of the feedback control design and the setpoint trajectory. Traditional design methods for feedforward control, such as position, damping and inertia feedforward, do not take the flexible dynamics into account and will not lead to satisfactory results for systems with resonances in the bandwidth of interest, i.e. the setpoint trajectory will excite the flexible dynamics leading to undesired vibrations. In order to deal with the presence of significant elastic deformations, lightweight systems can be equipped with more actuators than rigid-body modes, i.e. these systems can be over-actuated (OA), see Schneiders et al. (2003, 2004a,b). Also the number of performance variables is not necessarily equal to the number of sensors. Both over-actuation and the number of performance variables itself can result in non-square system descriptions (unequal number of inputs and outputs). However, feedforward design for this class of systems has received little attention in literature yet.

Feedforward in nano-positioning (Butterworth et al., 2009; Clayton et al., 2009) deals with resonances in the bandwidth of interest. However, these methods typically deal with diagonal feedforward design, since the scanning directions are well decoupled. Furthermore, the performance variables are typically assumed to be directly measurable in contrast to our application.

In Brinkerhoff and Devasia (2000) a feedforward design method for non-square systems is presented using an optimal control approach. However, this approach is not suitable for inferential problems, i.e. designing a feedforward will not result in zero error on the performance variables due to the control structure.

The methods presented in Boerlage (2006) allow for a non-square system, but only square systems are considered. Furthermore, the assumption that the flexible dynamics occur far beyond the target bandwidth of the feedback controller

is generally not valid for lightweight motion systems considered in this chapter. Moreover, the jerk derivative feedforward from Boerlage (2006) only deals with the contribution of the compliant part of the flexible modes. However, the setpoint trajectory excites the resonant dynamics, which leads to performance deterioration.

Inferential control dealing with performance outputs z , that are different from the sensor output y , is well known in process industry (Parrish and Brosilow, 1985), but has only recently been introduced in the field of motion control (Oomen et al., 2009; Oomen, 2010; Oomen et al., 2011). However, existing work deals with the feedback part or simultaneous two degrees-of-freedom designs only.

In Zhang and Agustriyanto (2003), multivariable inferential feedforward is presented with an application in process industry, where the problem considered is a regulation problem. The dominant disturbance, i.e. the disturbance with the biggest effect on performance, is immeasurable in contrast to the servo-problem considered in this chapter, where the dominant disturbance, i.e. the setpoint trajectory, is known *a priori*.

Input shaping (Singer et al., 1999; Baumgart and Pao, 2007) is a suitable technique to reduce vibrations in flexible systems. However, this results in extra delays and thus an increased settling time, which is generally not acceptable in high-performance motion systems.

Spatial feedforward (see Chapter 4 and Ronde et al. (2013b)) can prevent the excitation of flexible modes for over-actuated systems. However, this method is only suitable if additional actuators are present. Furthermore, if a single inferential performance location is considered, this constraint might be too strict.

Learning-based approaches (Moore, 1998; Longman, 2000; Bristow et al., 2006), such as Iterative Learning Control (ILC), require a measurement of the performance variable during the learning process, which is not available in the considered class of inferential motion systems. Furthermore, ILC requires a new learning phase for every different setpoint trajectory.

In Heertjes and van de Molengraft (2009) the learned feedforward signal from ILC is approximated by a FIR filter, such that a setpoint-invariant feedforward controller is obtained. Such methods only guarantee performance at the sensor locations.

In van der Meulen et al. (2007, 2008) a fixed structure feedforward controller is presented, which combines the benefits of model-based feedforward and ILC, i.e. setpoint invariance and data-based tuning for performance, respectively. However, the approach still relies on jerk derivative feedforward, i.e. only the deformations due to the compliant dynamics of the flexible modes are compensated.

In Heertjes et al. (2010) the fixed-structure of van der Meulen et al. (2008) is replaced by a generic FIR filter. Finally, in Bruijnen and van Dijk (2012) a combination of two FIR filters is optimized, such that theoretically a zero error can be obtained. However, only the performance at the sensors is considered in

contrast to this chapter.

In van de Wijdeven and Bosgra (2007, 2008) an ILC approach for MIMO systems is presented. Although this approach does not explicitly deal with inferential feedforward problems, it is possible to do this in the presented framework. However, the presented approach is not setpoint-trajectory-invariant, i.e. a new learning sequence is required for every setpoint trajectory.

This chapter takes a different approach as (van de Wijdeven and Bosgra, 2007, 2008), resulting in a setpoint-invariant approach under the following condition:

Assumption 2.1. *The (performance) error is assumed to be dominated by the setpoint-trajectory disturbance. Other disturbances are assumed to be negligible or compensated otherwise.*

Under this assumption, model-based feedforward control can be used for inferential motion systems. Compared to previous work (Ronde et al., 2012a),

1. the feedforward control design can be done independently of the feedback control design, and
2. it is shown that different setpoint trajectories for the performance and sensor locations are required for the formulation of consistent control goals, and
3. the implementation has been improved, such that generating a constant feedforward signal does not pose a problem.

The contribution of this chapter is a feedforward control design method for inferential, lightweight flexible motion systems, which are possibly over-actuated. System resonances can be within the bandwidth of interest, the performance variable z is not necessarily measured, and systems can be non-square due to over-actuation. Moreover, the stability of the presented framework is investigated. Performance is only enforced at the location of the performance variable z , i.e. *local performance* is obtained. Moreover, the conditions formulated for inferential performance in the indirect control structure are not limited to the lifted framework, but generalize to other model-based methods for feedforward design.

The outline of the chapter is as follows, in Section 2.2 the problem formulation is given. Subsequently, in Section 2.3 the indirect control structure is shown, which provides a method to deal with $y \neq z$. The lifted framework which is used to compute the feedforward controller is briefly discussed in Section 2.4. The experimental validation is presented in Section 2.5. Furthermore, in the same section the proposed method is compared to two other methods as a benchmark. Finally in Section 2.6 the conclusions and recommendations for future research are given.

2.2 Problem formulation

Consider a flexible motion system described by the following discrete-time state representation,

$$\mathcal{G} : \begin{cases} x(k+1) &= Ax(k) + Bu(k) \\ y(k) &= C_y x(k) + D_y u(k) \\ z(k) &= C_z x(k) + D_z u(k) \\ x(0) &= 0 \end{cases}, \quad (2.1)$$

in the feedback interconnection structure of Fig. 2.1. Here $u(k) \in \mathbb{R}^{n_u \times 1}$, $y(k) \in \mathbb{R}^{n_y \times 1}$ and $z(k) \in \mathbb{R}^{n_z \times 1}$ are the inputs, sensor outputs and the performance outputs, respectively. It is assumed that the performance output $z(k)$ cannot be measured during operation. The sensor outputs $y(k)$ are used to generate the feedback signal.

Remark 2.2. Note that $x(0) = 0$ is not a strict requirement for the method presented. Any non-zero initial condition $x(0)$ can be absorbed into the setpoint trajectory.

Furthermore, the servo- and performance-errors are defined as,

$$\begin{aligned} e_y(k) &= r_y(k) - y(k), \\ e_z(k) &= r_z(k) - z(k), \end{aligned} \quad (2.2)$$

where $r_z(k)$ is the setpoint trajectory for the performance output $z(k)$. The setpoint trajectory $r_y(k)$ is related to $r_z(k)$ by $r_y(k) = Fr_z(k)$, where the prefilter F takes the difference in dimensions and/or dynamics into account. Now the control goal is defined as,

$$\arg \min_{K_{ff}} \|e_z\|_2,$$

where $e_z = [e_z(0) \ \dots \ e_z(N-1)]^T$, i.e. the designed feedforward controller should minimize the 2-norm of the performance error.

Definition 2.3 (Body modes Schneiders et al. (2004b)). The body modes are defined as the set of rigid-body modes ($\omega_r = 0$) and suspension modes. The suspension modes are defined as the modes where the moving parts can be regarded as rigid, but are attached to the fixed world by elastic elements. The suspension modes have, by design, a significantly lower resonance frequency than the internal modes, i.e. the structural stiffness of the suspension system to the fixed world is much smaller as the body stiffness. The number of body modes is denoted by n_b .

Definition 2.4 (Internal modes Schneiders et al. (2004b)). The internal modes are the modes where elastic deformation of the moving parts occurs. These internal modes are the undesired behavior of the system due to the limited stiffness.

Definition 2.5 (Indirect control). The indirect control of an immeasurable performance variable by controlling an auxiliary measurement variable.

The class of motion systems considered in this chapter, can be characterized by the following properties and assumptions:

1. linear time-invariant (LTI) system behavior,
2. lightweight system, i.e. resonances near the objective bandwidth,
3. sensor- and performance location are physically non-collocated ($G_y \neq G_z$),
4. number of sensor outputs $n_y \geq n_b$. During operation $n_y = n_b$ sensors are required, during system identification extra sensor(s) at z are required to obtain a model,
5. number of inputs $n_u \geq n_b$,
6. number of performance outputs $n_z \geq n_b$, and finally,
7. the setpoint trajectory r_z is known in advance.

Remark 2.6. For the method presented in this chapter it is not required that the system is over-actuated. However, it is beneficial due to the fact that zeros and thus non-minimum phase (NMP) zeros are less likely to appear (Maciejowski, 1989), (Skogestad and Postlethwaite, 2005, Section 4.5).

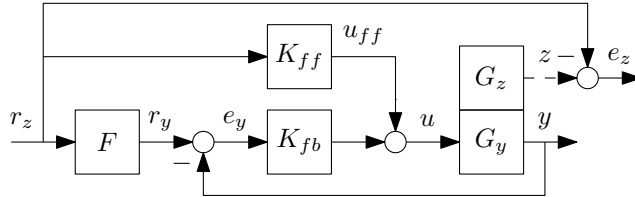


Figure 2.1: Indirect control structure (Skogestad and Postlethwaite, 2005, Section 10.4) with additional feedforward controller K_{ff} . The performance output z is represented by a dashed arrow, showing that this signal may not be measurable and is not used for feedback control.

2.3 Feedforward for indirect control structures

2.3.1 Motivating example

In this example it will be shown that different setpoint trajectories are required, when considering different output of the same dynamical system. In general, the dynamic response of the system to the sensors outputs and the performance outputs are different, leading to the requirement for different setpoint trajectories. The following simple example will show that even in the steady-state situation

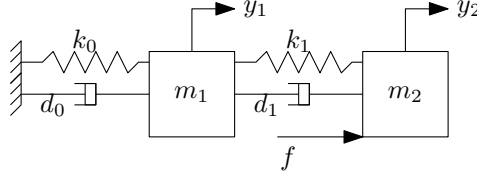


Figure 2.2: Example system with two masses (m_1, m_2) and stiffness to the fixed world (k_0).

problems can occur. Therefore, the following simple motion system in Fig. 2.2 is considered. For this system, the equations of motion are given by,

$$M\ddot{q}(t) + D\dot{q}(t) + Kq(t) = \begin{bmatrix} 0 & f(t) \end{bmatrix}^T, \quad q = \begin{bmatrix} y_1 & y_2 \end{bmatrix}^T,$$

where $M = \text{diag}(m_1, m_2)$ and,

$$D = \begin{bmatrix} d_0 + d_1 & -d_1 \\ -d_1 & d_1 \end{bmatrix}, \quad K = \begin{bmatrix} k_0 + k_1 & -k_1 \\ -k_1 & k_1 \end{bmatrix}.$$

Now consider the static situation, i.e. $\ddot{q} = 0$, $\dot{q} = 0$, then the equations of motion reduce to,

$$\begin{bmatrix} k_0 + k_1 & -k_1 \\ -k_1 & k_1 \end{bmatrix} \begin{bmatrix} y_1 \\ y_2 \end{bmatrix} = \begin{bmatrix} 0 \\ f \end{bmatrix}.$$

Solving this system of equations leads to,

$$y_1 = \frac{k_1}{k_0 + k_1} y_2, \tag{2.3}$$

and

$$f = -k_1 y_1 + k_1 y_2 = \frac{k_0 k_1}{k_0 + k_1} y_2.$$

From (2.3) it follows immediately that $y_1 \neq y_2$, except for the trivial solution ($y_1 = y_2 = 0$), provided that $k_0 \neq 0$. This is even the case in static situations, i.e. when there are no dynamics involved. This simple example shares the same relevant properties with all motion systems, i.e. any stiffness to the fixed world leads to a stiffness matrix $K \succ 0$, which physically means that there are no rigid-body modes present anymore. Thus, any other position than the equilibrium position will involve internal deformations in the system. This shows that even for steady-state ($\omega = 0$) different setpoint trajectories are required in case of stiffness to the fixed world. This motivates the requirements for different setpoint trajectories to avoid conflicting control goals.

2.3.2 Controller structures for inferential control

As motivated in the previous section, the standard feedforward control structure from Fig. 1.2 is not suitable, since this structure cannot handle different setpoint trajectories. Moreover, several other challenges exist for inferential control problems as motivated in Oomen (2010, Ch. 3&7) and Oomen et al. (2009, 2011):

1. in general $\dim y \neq \dim z$, i.e. the difference between the setpoint trajectory r_z and the measured output y cannot be computed, and
2. in case $\dim y = \dim z$, e.g. the outputs may be scaled arbitrarily, i.e. minimization of $r_z - y$ does not imply minimization of $r_z - z$. Moreover, if suspension modes are present then simultaneous minimization of $r_z - y$ and $r_z - z$ is impossible in general.

Relation with the general two degrees-of-freedom configuration

The general two degrees-of-freedom controller structure for inferential control as proposed in Oomen (2010, Ch. 3&7) and Oomen et al. (2009, 2011) is shown in Fig. 2.3. The controller K admits the following structure,

$$u = \underbrace{[K_1 \ K_2]}_{=:K} \begin{bmatrix} r_z \\ -y \end{bmatrix}. \quad (2.4)$$

Both extensions to the single degree-of-freedom control configuration to deal with immeasurable performance variables, i.e. inferential control (Parrish and Brosilow, 1985) and indirect control (Skogestad and Postlethwaite, 2005, Section 10.4), can be regarded as special cases of the general two degree-of-freedom control configuration.

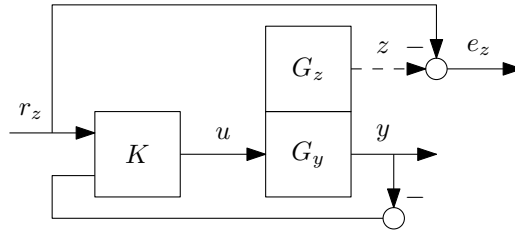


Figure 2.3: Two degrees-of-freedom controller structure for inferential control. The dashed line indicates that the performance output z is immeasurable during operation.

The proposed indirect control structure with additional feedforward controller of Fig. 2.1 fits in the general two degrees-of-freedom controller structure for inferential control. For the control structure of Fig. 2.1 the controller parametrization

from (2.4) reads,

$$u = [K_{fb}F + K_{ff} \quad K_{fb}] \begin{bmatrix} r_z \\ -y \end{bmatrix}. \quad (2.5)$$

The controller from (2.5) is indeed over-parameterized, i.e. there are three elements to be designed (K_{fb} , K_{ff} and F) for two degrees-of-freedom. However, this parametrization allows for independent design of the feedback controller and feedforward controller. This will be shown in the next section.

2.3.3 Independent feedforward design for indirect control structures

To prevent the feedback controller from deteriorating the feedforward signal, the servo-error e_y and the performance error e_z have to be zero simultaneously. From

$$e_y = S_i(F - G_y K_{ff})r_z,$$

it follows that e_y can be made small by choosing,

$$F = \overline{G_y} K_{ff}, \quad (2.6)$$

assuming $\overline{G_y}$ is close to G_y . Here $\overline{(\cdot)}$ indicates the use of a nominal model. The transfer function from the setpoint trajectory r_z to performance error e_z is given by,

$$e_z = (I - G_z S_i(K_{ff} + K_{fb}F)) r_z, \quad (2.7)$$

where $S_i = (I + K_{fb}G_y)^{-1}$ is the input sensitivity. Inserting (2.6) in (2.7) results in,

$$\begin{aligned} e_z &= (I - G_z S_i(K_{ff} + K_{fb}F)) r_z, \\ &= (I - G_z S_i(I + K_{fb}\overline{G_y})K_{ff}) r_z, \end{aligned}$$

which reduces to,

$$e_z = (I - G_z K_{ff}) r_z, \quad (2.8)$$

under the assumption that $\overline{G_y} = G_y$. From (2.6) and (2.8) it follows that the ideal feedforward controller is,

$$K_{ff} = \overline{G_z}^\dagger.$$

Here, $(\cdot)^\dagger$ indicates the use of a pseudo-inverse as G_z might be non-square as $n_u \geq n_z$, which coincides with the regular inverse if $n_u = n_z$.

Remark 2.7. In the case of rigid-body modes, $\overline{G_y}$ in (2.6) might be approximated by a constant at low frequencies, since at low frequencies the difference between y and z is just a compliant effect. Hence if the setpoint trajectory has its main frequency content at low frequencies, the pre-filter F can be approximated as the feedforward controller times a static gain, see (2.6).

Discussion

Stability is required to obtain the desired behavior. The stability of this control scheme is determined by:

1. the closed-loop stability, and
2. the stability of the feedforward controller K_{ff} , and
3. the stability of the prefilter F .

The closed-loop stability is ensured by proper design of the feedback controller. If the feedforward controller K_{ff} is unstable either an approximation (Tomizuka, 1987) or stable-inversion (Zou and Devasia, 1999) technique can be used. The stability of the pre-filter immediately follows from the stability of the feedforward controller, which is shown in Lemma 2.9.

Remark 2.8. In Lemma 2.9 below, the proof is given for SISO transfer function G_y and G_z for reasons of simplicity. The proof can be extended to MIMO by using matrix fraction descriptions.

Lemma 2.9. *The prefilter $F = G_y G_z^{-1}$ is stable if and only if G_z^{-1} is stable.*

Proof: Let G_y and G_z be the transfer function from a minimal realization of \mathcal{G} in (2.1), then

$$G_y = \frac{b(\xi)}{a(\xi)}, \quad G_z = \frac{c(\xi)}{a(\xi)}.$$

Here, ξ can be replaced by s (continuous-time) or z (discrete-time). If no pole-zero cancellation occur in either G_y or G_z the prefilter F is equal to,

$$F = G_y G_z^{-1} = \frac{b(\xi)}{a(\xi)} \frac{a(\xi)}{c(\xi)} = \frac{b(\xi)}{c(\xi)}$$

Now let G_y and G_z be factorized such that $\phi(\xi)$ and $\psi(\xi)$ contains all the pole-zero pairs which cancel in G_y and G_z respectively, then

$$G_y = \frac{b(\xi)}{a(\xi)} = \frac{\bar{b}(\xi)\phi(\xi)}{\bar{a}(\xi)\phi(\xi)}, \quad G_z = \frac{c(\xi)}{a(\xi)} = \frac{\hat{c}(\xi)\psi(\xi)}{\hat{a}(\xi)\psi(\xi)}.$$

Because G_y and G_z have the same poles, it holds that

$$\bar{a}(\xi)\phi(\xi) = \hat{a}(\xi)\psi(\xi).$$

Then, the prefilter results in,

$$F = G_y G_z^{-1} = \frac{\bar{b}(\xi)\phi(\xi)}{\bar{a}(\xi)\phi(\xi)} \frac{\hat{a}(\xi)\psi(\xi)}{\hat{c}(\xi)\psi(\xi)} = \frac{\bar{b}(\xi)\phi(\xi)}{\hat{c}(\xi)\psi(\xi)},$$

which shows that the poles of G_y exactly cancel, which is possible because both G_y and G_z are models with the same underlying state-space description. Therefore, the stability is determined by the zeros of the polynomial $\hat{c}(\xi)\psi(\xi)$, i.e. the poles of G_z^{-1} . ■

Furthermore, to enforce a unique solution for the pose of the system $n_z \geq n_b$, i.e. the number of constraints must be larger or equal to the number of (rigid-)body modes.

2.4 Lifted feedforward

Consider the system of (2.1) with output $z(k)$ only. For an LTI system, the lifted description (Bamieh et al., 1991; Dijkstra, 2004; van de Wijdeven, 2008) which is a static map representing convolution, results in,

$$\begin{bmatrix} z(0) \\ z(1) \\ \vdots \\ z(N-1) \end{bmatrix} = \begin{bmatrix} D_z & 0 & \cdots & 0 \\ C_z B & D_z & \cdots & 0 \\ \vdots & \vdots & \ddots & \vdots \\ C_z A^{N-2} B & C_z A^{N-3} B & \cdots & D_z \end{bmatrix} \begin{bmatrix} u(0) \\ u(1) \\ \vdots \\ u(N-1) \end{bmatrix}.$$

This can both represent an open- or closed-loop mapping, by taking the appropriate A , B , C , D . For MIMO systems, the convolution matrix becomes block-Toeplitz, with $n_z \times n_u$ blocks and remains valid for both square and non-square blocks. Also it is possible to include initial conditions, pre- and post-actuation and different actuation and observation windows (van de Wijdeven, 2008). It is also possible to model LTV systems in this framework (Dijkstra, 2004), which makes it possible to use a varying C matrix to take into account the varying location of the performance variable z . However, this is outside the scope of the chapter and subject to future research, see Chapter 3 and Dijkstra (2004); Sato (2003, 2008); Ronde et al. (2013a).

The class of systems considered here are typically strictly proper, i.e. with a relative degree $\rho > 0$. As a consequence the direct feedthrough matrix $D_z = 0$ and the convolution matrix will be rank deficient. This can be solved by using a shifted representation,

$$\begin{bmatrix} z(1) \\ z(2) \\ \vdots \\ z(N) \end{bmatrix} = \begin{bmatrix} C_z B & 0 & \cdots & 0 \\ C_z A B & C_z B & \cdots & 0 \\ \vdots & \vdots & \ddots & \vdots \\ C_z A^{N-1} B & C_z A^{N-2} B & \cdots & C_z B \end{bmatrix} \begin{bmatrix} u(0) \\ u(1) \\ \vdots \\ u(N-1) \end{bmatrix}.$$

The compact notation of this is

$$z = J_z u. \quad (2.9)$$

If additional delays are present, subsequent terms of the convolution, $C_z B, C_z AB, \dots$, are zero as well. This can be solved in a similar manner, i.e. by applying a larger shift.

For square systems, designing a feedforward mapping as $K_{ff} = J_z^{-1}$, results in $z = J_z J_z^{-1} r_z = r_z$. However for every non-minimum phase (NMP) zero of the represented system, there is a singular value of J_z which is approximately zero (Hashemi and Hammond, 1996; Dijkstra, 2004), resulting in an unbounded feedforward signal. For non-square systems J_z is non-square and direct inversion is not possible.

Proposition 2.10 (van de Wijdeven (2008)). *Consider the singular value decomposition of J_z from (2.9),*

$$\begin{aligned} J_z &= U \Sigma V^T, \\ &= [U_1 \mid U_2] \left[\begin{array}{c|c} \Sigma_1 & 0 \\ \hline 0 & \Sigma_2 \end{array} \right] \left[\begin{array}{c} V_1^T \\ V_2^T \end{array} \right], \end{aligned}$$

where the singular values $\Sigma_2 \approx 0$ due to non-minimum phase zeros. The matrices U and V are partitioned such that they match the dimensions of Σ_1 and Σ_2 . Now J_z can be approximated by,

$$J_z \approx U_1 \Sigma_1 V_1^T,$$

and a bounded u_{ff} can be computed as,

$$u_{ff} = J_z^\dagger r_z = (U_1 \Sigma_1 V_1^T)^\dagger r_z = V_1 \Sigma_1^{-1} U_1^T r_z,$$

which minimizes the 2-norm of the performance error $e_z = r_z - J_z u_{ff}$.

The resulting feedforward controller $K_{ff} = J_z^\dagger$ is not necessarily LTI and causal, i.e. (block)-Toeplitz and lower triangular respectively.

Remark 2.11. Note that causality of the feedforward controller is not considered to be an issue, since the setpoint trajectory is assumed to be known in advance. Constructing causal LTI feedforward controllers is outside the scope of this chapter.

2.5 Experimental validation

The prototype lightweight motion system, shown in Fig. 2.4, is made of a steel beam, with a length of 0.5 m. The beam is constrained by 5 wire springs such that

4 rigid-body modes are suppressed. The translation and rotation of the beam are the remaining degrees of freedom (DOFs). The experimental setup is driven by 3 Akribis AVM19-5 voice-coils using current controlled amplifiers with ± 2.5 V input range, which is approximately proportional to the output current. The output current is limited to 1.3 A. The position is measured contactless by three Philtec D64-NQ fiberoptic sensors used at the far side, with a resolution of $1 \mu\text{m}$ at a bandwidth of 20 kHz. The absolute accuracy of the specific sensor and target combination is unknown. Data-acquisition is done using a Beckhoff EtherCAT stack and real-time Linux at a sampling frequency $f_s = 2048$ Hz. Furthermore, the non-actuated equilibrium position is taken as the zero position of the sensor coordinate system. For the feedback control design, the system is decoupled, such that SISO controllers can be designed on the basis of the diagonal elements.

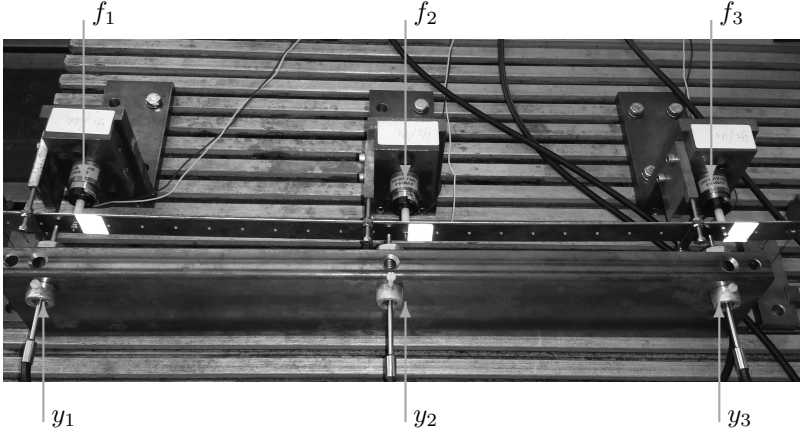


Figure 2.4: Prototype lightweight motion system, with actuators f_1, f_2 and f_3 and sensors y_1, y_2 and y_3 .

2.5.1 Performance variables and geometric decoupling

Consider the model shown in Fig. 2.5, where f_i , $i = 1, 2, 3$ are the force inputs and y_i , $i = 1, 3$ are the measurable sensor outputs during operation. In this case, the position of the center of gravity (COG) and the rotation around COG should be controlled. Therefore, the performance variable is chosen as,

$$z = \begin{bmatrix} y_{COG} \\ R_z \end{bmatrix} \approx \begin{bmatrix} y_2 \\ \frac{y_3 - y_1}{L} \end{bmatrix}, \quad (2.10)$$

such that the orientation of the system is uniquely constrained. However, the sensor y_2 is assumed to be immeasurable during operation and there is no sen-

sor present to directly measure R_z . Therefore, direct control of the performance variables is impossible.

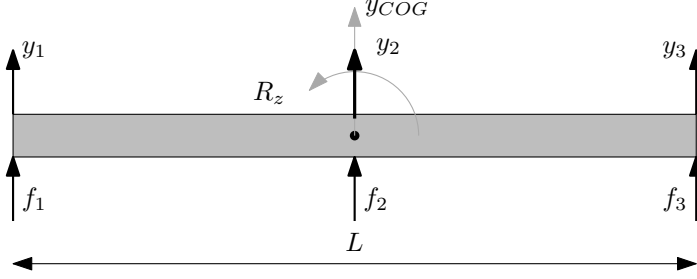


Figure 2.5: Geometric model of the experimental setup of Fig. 2.4. Here, the black dot indicates the center of gravity. Furthermore, the black arrows represent the decoupled coordinate system.

To decouple the system for feedback, it is assumed that the system approximately behaves like a rigid-body at low frequencies. This assumption is valid, since the suspension stiffness is by design much smaller than the internal stiffness of the beam. The actuator forces in terms of the decoupled forces around the center of gravity are defined by,

$$\begin{bmatrix} f_1 \\ f_2 \\ f_3 \end{bmatrix} = \underbrace{\begin{bmatrix} 1/3 & -2 \\ 1/3 & 0 \\ 1/3 & 2 \end{bmatrix}}_{T_{u,fb}} \begin{bmatrix} f_z \\ T_{R_z} \end{bmatrix}.$$

The motion coordinates $m(t)$, without the use of sensor y_2 , which is not measurable during operation, results in,

$$m(t) = T_y y(t), \quad (2.11)$$

with,

$$m(t) = \begin{bmatrix} y_{COG} \\ R_z \end{bmatrix}, \quad T_y = \begin{bmatrix} \frac{1}{2} & \frac{1}{L} \\ \frac{-1}{L} & \frac{1}{L} \end{bmatrix}, \quad y(t) = \begin{bmatrix} y_1 \\ y_3 \end{bmatrix}.$$

Therefore, the decoupled plant is equal to $G_{y,dec} = T_y G_y T_{u,fb}$.

2.5.2 Setpoint trajectory

The setpoint trajectory for y_{COG} is a 4-th order motion profile using the algorithm of Lambrechts et al. (2005) and the setpoint trajectory for R_z is zero. Both the setpoint trajectories are shown in Fig. 2.6. The maximum snap (not shown), i.e. jerk derivative equals $\bar{s} = 500 \text{ m/s}^4$.

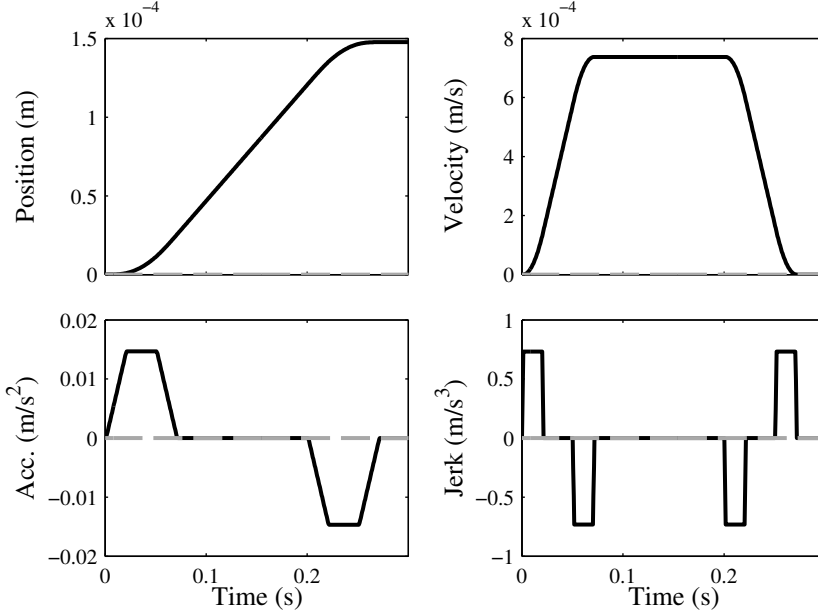


Figure 2.6: Setpoint trajectory r_z for y_{COG} (—) and R_z (--) and its derivatives for prototype lightweight system.

2.5.3 Identification and feedback design

As a first step, a frequency response function (FRF) is measured in open-loop (not shown). With this model, the amount of interaction after decoupling can be evaluated using the Relative Gain Array (RGA) (Skogestad and Postlethwaite, 2005). Since the RGA is close to identity, SISO controllers can be designed based on the diagonal terms of the plant.

The controller structure for the experiments is given by $K = \text{diag}(K_{11}(s), K_{22}(s))$, where

$$K_{ii}(s) = k_i \cdot \frac{s + 2\pi f_{int,i}}{s} \cdot \frac{\frac{1}{2\pi f_{z,i}}s + 1}{\frac{1}{2\pi f_{p,i}}s + 1} \cdot \frac{1}{\frac{1}{2\pi f_{lp,i}}s + 1} \cdot \frac{\frac{1}{(2\pi f_{nz,i})^2}s^2 + \frac{2\beta_{nz,i}}{2\pi f_{nz,i}}s + 1}{\frac{1}{(2\pi f_{np,i})^2}s^2 + \frac{2\beta_{np,i}}{2\pi f_{np,i}}s + 1},$$

with parameters and resulting bandwidths as shown in Table 2.1 and 2.2. This feedback controller consists of the following elements: gain, integrator, lead-filter, first-order lowpass and a notch-filter. The lead-filter is required to obtain the correct phase at the zero crossing of the open-loop. The integrator is included to improve the tracking at low frequencies. The notch-filter is included to prevent additional zero-crossings of the open loop, which allows to increase the bandwidth

without endangering stability. Finally, the lowpass filter is included to enforce the desired roll-off and to prevent the amplification of noise. The stability of the MIMO system is assessed by evaluating the characteristic loci (Skogestad and Postlethwaite, 2005) (not shown). For implementation the controller is discretized using a Tustin discretization scheme.

Axis i	k_i	$f_{int,i}$	$f_{z,i}$	$f_{p,i}$	$f_{lp,i}$	f_{BW}
1	0.21	2.1	8/3	24	60	8
2	0.025	5	15/3	45	100	15

Table 2.1: Controller parameters and resulting bandwidth f_{BW} (Hz). f_{BW} is defined as the zero dB crossing of the open-loop.

Axis i	$f_{nz,i}$	$\beta_{nz,i}$	$f_{np,i}$	$\beta_{np,i}$
1	33.5	0.15	50	0.5
2	-	-	-	-

Table 2.2: Controller parameters of the notch-filter.

A non-parametric model of the prototype lightweight system is shown in Figs. 2.7 and 2.8. This model has been identified in closed-loop by subsequently exciting each channel with zero mean white noise. As can be seen in Fig. 2.7, two suspension modes are present at 3 and 5 Hz, i.e. the stiffness to the fixed world, which is caused by the wire springs to constrain the other DOFs. The first internal flexible mode of the beam is located at 33 Hz.

2.5.4 Parametric model

Based on the non-parametric model as shown in Fig. 2.7, a parametric model has been obtained by a MIMO complex curve fitting method. The model from all inputs to all outputs has been obtained at the same time, such that the underlying structure is equal to (2.1). The resulting order is 14, i.e. the two suspension modes and the first five flexible modes. The estimated resonance frequencies and the corresponding damping values are presented in Table 2.3. The model approximates the non-parametric model with

$$\sum \|G_{\text{FRF}}(\omega_k) - G_{\text{model}}(\omega_k)\|_F^2 = 0.5940,$$

where $\omega_k \in [2\pi 0.5, 2\pi 500]$ is evaluated at the measurement frequency grid with a resolution of $2\pi 0.5$ rad/s.

By visual inspection, it can be seen that the diagonal and off-diagonal terms are modelled with a comparable deviation between model and FRF. The largest

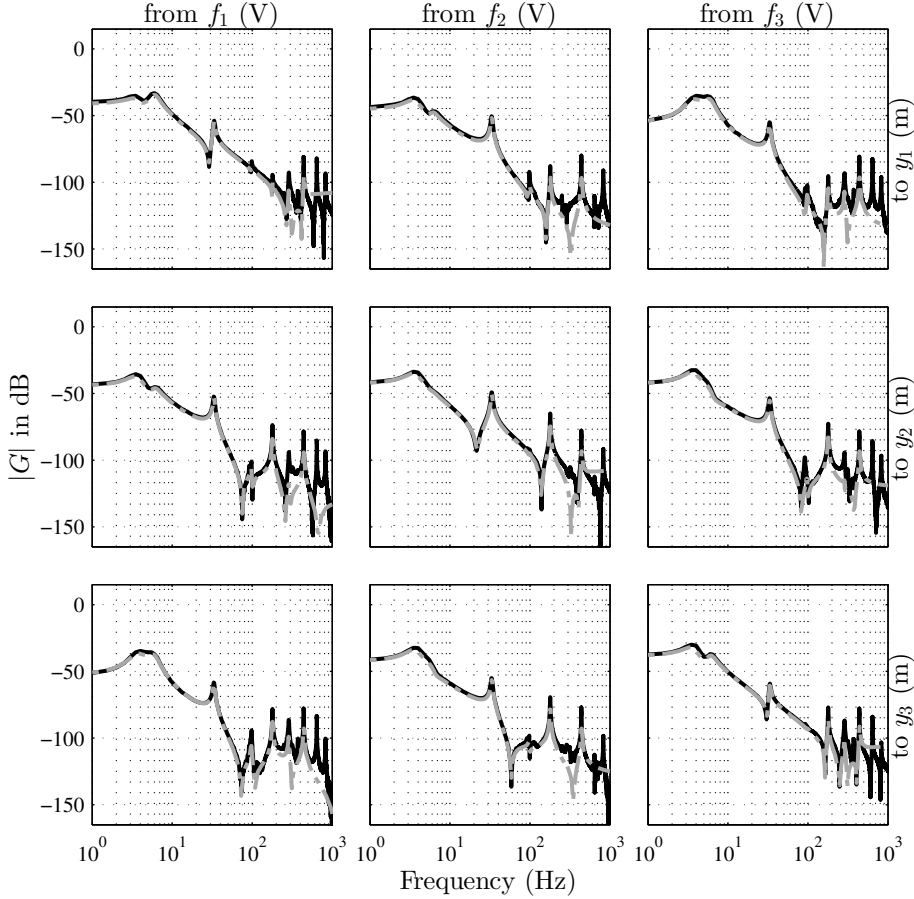


Figure 2.7: Bode magnitude diagram of the prototype lightweight motion system (without decoupling), measured FRF (—) and 14-th order parametric model (---).

deviations at low frequencies, where the most energy of the setpoint trajectory is concentrated, can be found around the resonance frequencies of the suspension modes. It is likely that improving the model quality also improves the final performance.

Subsequently, the parametric model of G is used to extract G_y (from u_1, u_2, u_3 to y_1, y_3) and G_z (from u_1, u_2, u_3 to y_2). The parametric model of G_z , with performance output definition of (2.10), will be used to construct the impulse response map J_z in (2.9). The parametric model of G_y and the feedforward controller from (2.14) will be used to construct the prefilter F .

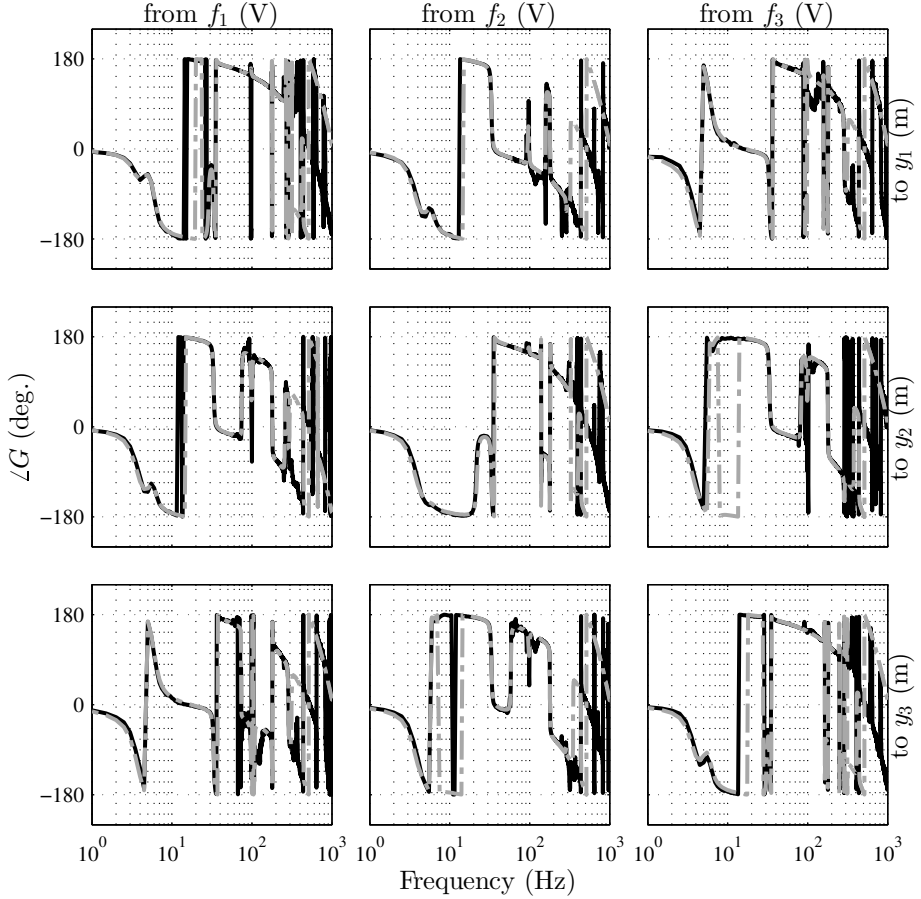


Figure 2.8: Bode phase diagram of the prototype lightweight motion system (without decoupling), measured FRF (—) and 14-th order parametric model (---).

2.5.5 Feedforward implementation aspects

Due to the suspension modes present in the system, a constant force is required to keep the system at rest except at the initial position (type 0 system, see Franklin et al. 2005). Although the suspension modes are included in the model, finite time implementation aspects lead to undesired oscillatory effects for systems with stiffness to the fixed world. A solution can be found by adding an integrator to the inputs of the system (van de Wijdeven and Bosgra, 2007), which is used to compute the feedforward controller. The integrator and the feedforward controller will be combined to obtain a solution in terms of the physical inputs. The new

i	f_i (Hz)	ζ_i (-)
1	3.6	0.2094
2	6.1	0.1404
3	33.4	0.0198
4	97.5	0.0157
5	179.4	0.0040
6	286.2	0.0101
7	439.5	0.0022

Table 2.3: Resonance frequencies and damping of the parametric model.

feedforward inputs $\overline{u_{ff}}$ are related to the old feedforward inputs u_{ff} by,

$$u_{ff} = J_{int} \overline{u_{ff}}, \quad (2.12)$$

where

$$J_{int} = \begin{bmatrix} I_{n_u} & & 0 \\ \vdots & \ddots & \\ I_{n_u} & \cdots & I_{n_u} \end{bmatrix}.$$

By combining (2.9) and (2.12) the new system description is obtained as,

$$z = J_z J_{int} \overline{u_{ff}} = \overline{J_z} \overline{u_{ff}}. \quad (2.13)$$

The feedforward controller for (2.13) can be computed as,

$$\overline{K_{ff}} = \overline{J_z}^\dagger.$$

Finally, the feedforward signal for the physical inputs is computed as,

$$u_{ff} = J_{int} \overline{K_{ff}} r_z. \quad (2.14)$$

2.5.6 Results

In this section the results from three different methods for tracking the setpoint trajectory of Fig. 2.6 are presented, which are:

1. no feedforward,
2. conventional feedforward, and
3. inferential feedforward.

All these methods will be used in conjunction with a feedback controller, which is required to operate the system and to take disturbances and modeling errors into account. Both the conventional and inferential feedforward controllers are

Case	K_{ff}	F	$\max e_z \text{ } (\mu\text{m})$	$\ e_z\ _2$
1	—	I	29.2	$5.43 \cdot 10^{-4}$
2	G_y^\dagger	I	13.7	$3.40 \cdot 10^{-4}$
3	G_z^\dagger	$G_y K_{ff}$	13.8	$2.39 \cdot 10^{-4}$

Table 2.4: Summary and numerical values for the experimental results.

constructed in the lifted domain with the parametric model from Fig. 2.7. This allows for a fair comparison between the different methods. The experiment without feedforward is included as a reference case. An overview of the feedforward controllers and prefilters is presented in Table 2.4.

To construct the convolution matrix J_z , the first $N = 1700$ Markov parameters of the model are used, which is equal to the number of samples in the setpoint trajectory. This results in a convolution matrix of size 3400×5100 . From this convolution matrix, the feedforward controller is constructed using all singular values, i.e. truncation is not required in absence of non-minimum phase zeros. In the ideal case without any modelling errors, increasing the number of singular values will increase the final performance in general.

The resulting feedforward signals for conventional and inferential feedforward are shown in Fig. 2.9. The resulting feedforward signal from both methods resemble the combination of inertia and position feedforward, which compensate for the mass and suspension stiffness, respectively. The dip at $t = 0.2$ can be attributed to the combination of position feedforward and the deceleration of the system. The differences between conventional - and inferential feedforward are due to differences between the models of G_y and G_z . Furthermore, for both methods it holds that there are less constraints than degrees-of-freedom (the convolution matrix is fat), thus the minimum energy solution is taken. Moreover, it can be seen that the feedforward controller is able to generate a constant force in contrast to previous work (Ronde et al., 2012a).

In Figs. 2.10, 2.11 and 2.12 the position outputs of the three different experiments are presented. For the experiment without feedforward and conventional feedforward it can be seen in Figs. 2.10 and 2.11 that the motion system arrives at the desired setpoint value. However, the difference between y_1 and y_3 on the one hand and y_2 on the other hand indicates that the beam is bent, which can be attributed to the same reasons as in the example of Section 2.3.1. Moreover, conventional feedforward significantly improves the settling time from approximately 0.6 s to 0.45 s. Nevertheless, for the translation of the performance location an offset remains for both conventional and no feedforward, i.e. this is not an artifact of the feedforward design method. In Fig. 2.12 the sensor outputs and their setpoint trajectories are shown for the proposed method. The setpoint trajectory r_y is calculated based on the model G_y and the feedforward controller K_{ff} . It can be observed that both the sensor- and performance output arrive at the desired

setpoint values without any offsets.

The servo-errors are defined by, $e_y = r_y - m(t)$, where $r_y = Fr_z$ and $m(t)$ is defined by (2.11). In Fig. 2.13 the translation servo-errors and its power spectral density (PSD) are shown. Here it can be seen that the translation servo-error is improved by applying feedforward. In the PSD only significant differences are found at low frequencies. In Fig. 2.14 the rotation servo-errors and its power spectral density are shown. For both feedforward methods and no feedforward these servo-errors are approximately equal.

The translation error and its power spectral density at the performance location are shown in Fig. 2.15. Both feedforward methods result in a peak error of approximately $13.7 \mu\text{m}$ compared to $29.2 \mu\text{m}$ without feedforward. Furthermore, in the proposed method the steady-state offset has been removed by explicitly taking the difference in dynamic behavior into account. This also leads to a lower energy contents of the translation error at the performance location, see Table 2.4. For both conventional and inferential feedforward control the remaining error during motion can be attributed to model inaccuracies and small non-linearities in the experimental setup.

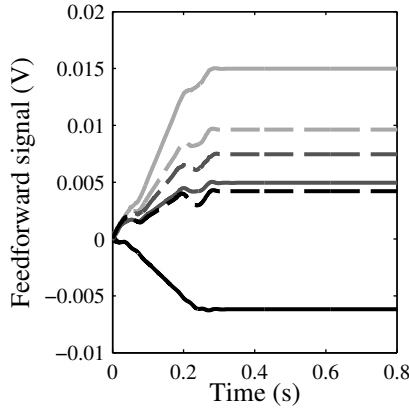


Figure 2.9: Feedforward signal u_{ff} , $u_{ff,1}$ (—), $u_{ff,2}$ (—) and $u_{ff,3}$ (—) for conventional feedforward (dashed) and inferential feedforward (solid).

2.6 Conclusions

In this chapter a novel method for feedforward design of a non-square inferential motion systems is presented. The method presented is independent of the setpoint trajectory and feedback control design. The sensor(s) at the performance location z is only required to obtain the non-parametric and parametric models, but is not required during operation.

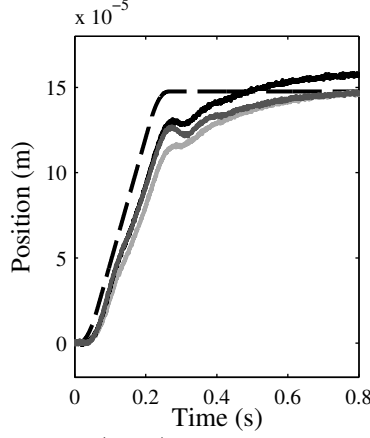


Figure 2.10: Position output (solid) and setpoint trajectory r_z (--) for $K_{ff} = 0$ and $F = I$. Position outputs y_1 (—), y_2 (—) and y_3 (—).

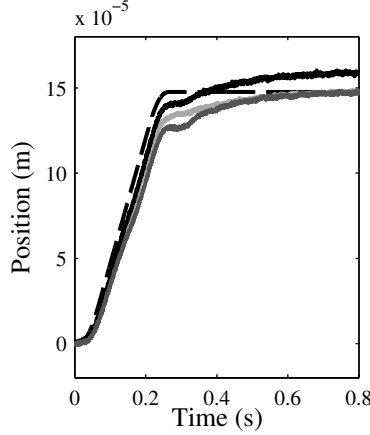


Figure 2.11: Position output (solid) and setpoint trajectory r_z (--) for $K_{ff} = G_y^T$ and $F = I$. Position outputs y_1 (—), y_2 (—) and y_3 (—).

The proposed inferential feedforward method has been validated on a prototype lightweight system showing an improvement of a factor 2 approximately, both in terms of peak error and 2-norm, compared to no feedforward. Compared to conventional feedforward the peak error of the proposed method is similar, but the 2-norm of the error is approximately 40% smaller. The performance is limited by disturbances, the repeatability of the system and the model quality, which is the same for any other feedforward method.

The control structure of Section 2.3 can be used to design feedforward controllers for this class of systems using other model based techniques as well, i.e.

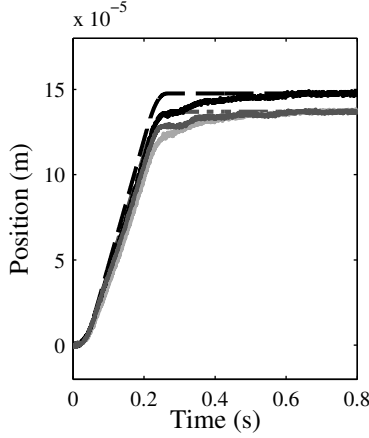


Figure 2.12: Position output (solid) and setpoint trajectory r_z (---) and r_y (-·- and -·-) for $K_{ff} = G_z^\dagger$ and $F = G_y K_{ff}$. Position outputs y_1 (—), y_2 (—) and y_3 (—).

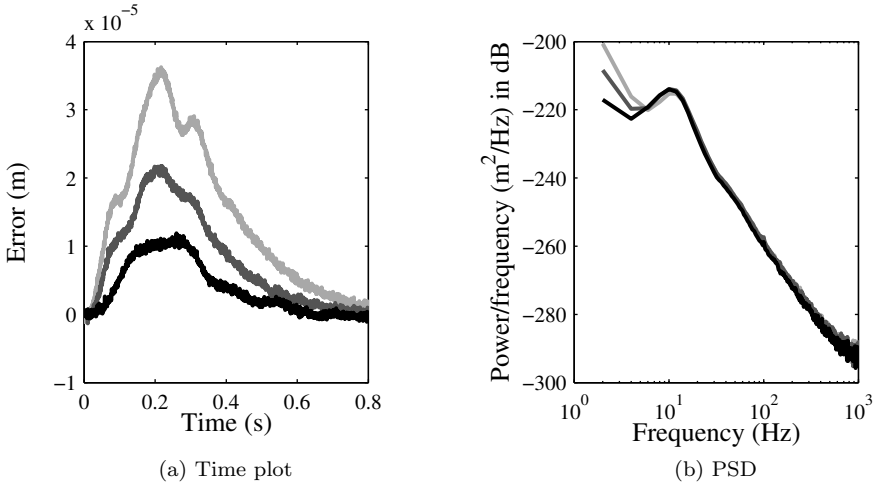


Figure 2.13: Servo-error (translation) of the three different methods, i.e. no feedforward (—), conventional feedforward (—) and inferential feedforward (—).

this method is not limited to the lifted system representation but generalizes to other model-based techniques.

In the next chapter, the framework from this chapter is extended to inferential motion systems with time-varying performance locations.

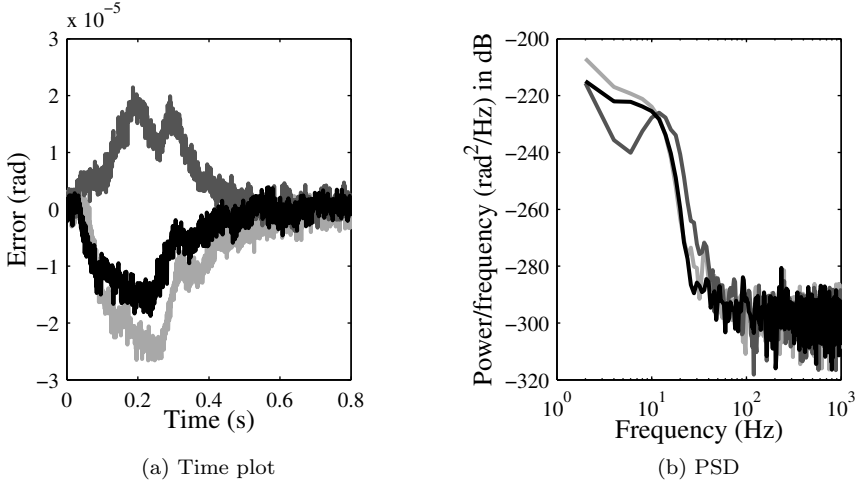


Figure 2.14: Servo-error (rotation) of the three different methods, i.e. no feedforward (—), conventional feedforward (—) and inferential feedforward (—).

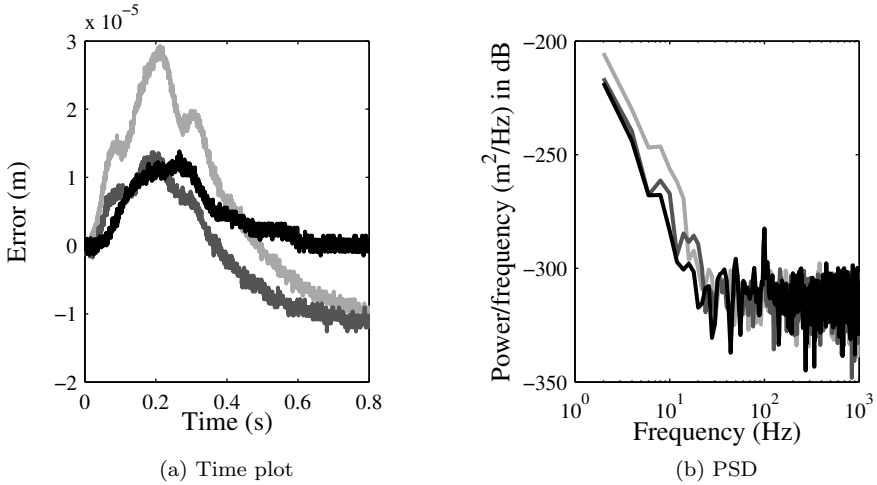


Figure 2.15: Performance-error (translation) of the three different methods, i.e. no feedforward (—), conventional feedforward (—) and inferential feedforward (—).

Chapter 3

Feedforward for flexible systems with time-varying performance locations

INCREASING demands for higher throughput in high-performance motion systems, e.g. waferstages or pick-and-place machines, lead to more aggressive motion profiles (higher accelerations), a stiffer design and/or larger wafer sizes (higher mass). Therefore, larger actuation forces are required, which puts stricter demands on actuators, amplifiers and cooling. However, this design paradigm has reached the boundary of its scalability. Therefore, the next generation of high-performance motion systems are designed to be lightweight. For this class of systems the location where the tool operates, e.g. the area to be exposed or component to be placed, is constantly varying. Due to the lightweight design and the changing position of the performance output location, the system dynamics to be considered for feedforward are changing as well, i.e. the flexible modes are observed differently. This chapter presents a model-based feedforward method for flexible systems with time-varying performance locations. This method is experimentally validated on a two-mass setup with flexible shaft.

This chapter is based on: "Michael Ronde, John van den Bulk, René van de Molengraft, Maarten Steinbuch. Feedforward for flexible systems with time-varying performance locations", *American Control Conference*, p. 6045-6050, Washington, DC, USA.

3.1 Introduction

Driven by Moore's law (Moore, 1965) and the fierce competition in the semiconductor industry, a higher throughput is desired. This requires more aggressive motion profiles (i.e. higher accelerations), a design with higher stiffness and/or larger wafer sizes (i.e. higher mass). Therefore, the required forces will become larger ($F = m \cdot a$). This results in stricter demands on actuators, amplifiers and cooling, e.g. the force density, required power and the generated heat respectively, which is infeasible due to its scalability. Therefore, a new design paradigm is required, which is to decrease the mass and to allow for internal flexibilities. However, this has several consequences for control design:

1. lightly damped resonances within the region of interest, i.e. the bandwidth, and
2. the transfer between sensor output y and performance location z , becomes dynamical due to flexibilities, i.e. there is no static transformation of the measurements possible anymore to calculate/control the performance variable. Furthermore, the location where the tool is operating, i.e. the area to be illuminated or the component to be placed is constantly varying. This is illustrated in Fig. 3.1. Therefore, the dynamics to be considered for feedforward control need to be varying accordingly.

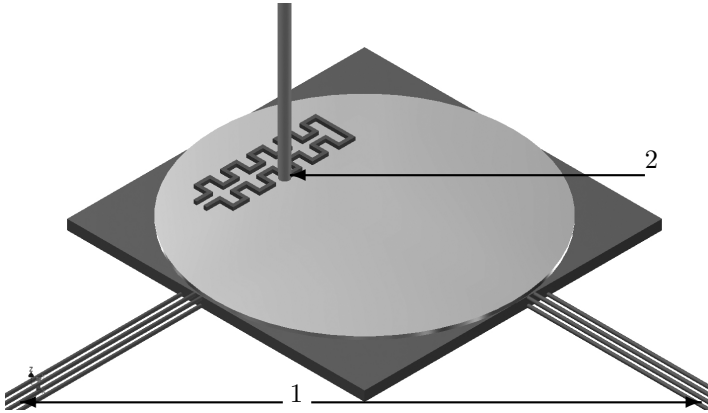


Figure 3.1: Example of a lithographic system with wafer-stage, with the sensors at the edges of the stage (1), while the area to be processed (performance location) is indicated by (2). Due to the production process, the performance location is changing in time.

Mass or inertia feedforward, which is commonly used in industry, does not take the flexible dynamics into account and will not lead to satisfactory results for

lightweight systems with flexibilities within the bandwidth of interest.

Snap feedforward (Boerlage et al., 2004; Boerlage, 2006; Steinbuch et al., 2010) additionally compensates for the quasi-static deformation during motion, which is not sufficient to address the resonant behavior if lightly damped flexible modes are present in the frequency band of interest.

Iterative learning control (ILC) (Van de Wijdeven, 2008; Dijkstra, 2004), which uses the measured error from previous experiments to learn a better feedforward signal, has the drawback that the solution is setpoint trajectory dependent, i.e. a new learning sequence is required for every new setpoint trajectory. Also, it is required that the errors are measured at the performance location, which may not be achievable in practice.

Input shaping (Singer et al., 1999; Baumgart and Pao, 2007; Singh, 2010) can be used to reduce residual vibrations for flexible systems that are subject to a setpoint trajectory. However, only the vibrations after the rest-to-rest motion are counteracted. Furthermore, these methods typically introduce delays, resulting in longer settling times, which is generally undesired.

For over-actuated systems, i.e. systems with more actuators than rigid body modes, spatial feedforward (see Chapter 4 and Ronde et al. (2013b)) can be used to prevent excitation of the flexible modes. This method can suppress as many flexible modes as there are additional actuators present. Therefore, the spatial feedforward method is only suitable for over-actuated systems, in contrast to the method presented in this chapter.

Both input shaping and spatial feedforward prevent the excitation of one or more flexible mode(s), leading to performance over the complete structure, i.e. global performance. However, these methods are not always suited for traditionally actuated systems, due to the undesired longer settling times or the lack of extra actuators.

In Sato (2003) a method is presented to design a gain-scheduled inverse of an LPV system. The drawback of this method is that an infinite number of LMI's has to be solved. This is solved in Sato (2008), but the solution is based on LMI's, which might not lead to numerically tractable solutions for practical systems. Furthermore, both methods require extensive modeling and obtain performance at the sensor location only.

In the previous chapter, the extension towards systems with time-varying performance (TVP) locations was suggested. However, direct application of the method from Ronde et al. (2012a) for these systems leads to infeasible feedforward signals, which can not be applied to any practical system. By including additional weightings (actuator and amplifier models), a feasible feedforward signal can be obtained.

Compared to Chapter 2 this chapter provides an extension towards systems with time-varying performance locations. Furthermore, the expressions for the feedforward design from Ronde et al. (2012a) are simplified, providing more in-

sight and easier implementation. Therefore, the contribution of this chapter is to provide:

1. a feedforward design for systems with time-varying (inferential) performance locations, and
2. a method to include weightings on the input signal, and
3. a computationally tractable feedforward synthesis method.

This chapter is organized as follows, in Section 3.2 the problem is formulated. Subsequently, in Section 3.3 lifted feedforward is briefly introduced. In Section 3.4 input weightings are introduced to include limits on actuators and amplifiers. Subsequently, in Section 3.5 the experimental results are presented. Finally, in Section 3.6 the conclusions and recommendations are presented.

3.2 Problem formulation

Consider a flexible system described by the following discrete-time state space representation,

$$\mathcal{G} : \begin{cases} x(k+1) &= Ax(k) + Bu(k) \\ y(k) &= C_y x(k) + D_y u(k) \\ z(k) &= C_z(k)x(k) + D_z(k)u(k) \\ x(0) &= 0 \end{cases} , \quad (3.1)$$

in the feedback interconnection depicted in Fig. 3.2. Here $k, u(k) \in \mathbb{R}^{n_u \times 1}$, $y(k) \in \mathbb{R}^{n_y \times 1}$ and $z(k) \in \mathbb{R}^{n_z \times 1}$ are the discrete-time index, inputs, sensor outputs and performance outputs of the system respectively. $C_z(k)$ and $D_z(k)$ denote a time-varying output- and throughput matrix at index k , respectively, so z can be a time-varying performance output.

Remark 3.1. Note that a zero initial condition $x(0) = 0$ is not a strict requirement for the method presented. Any non-zero initial condition $x(0) \neq 0$ can be absorbed into the setpoint trajectory.

Now the performance error can be defined as

$$e_z(k) = r_z(k) - z(k),$$

where $r_z(k)$ denotes the setpoint trajectory for the performance output. The control goal is defined as

$$\arg \min_{u_{ff}} \|e_z\|_2 ,$$

where $e_z = [e_z(0) \ \dots \ e_z(N-1)]^T$, thus minimizing the energy in the performance error signal by designing a feedforward signal.

Remark 3.2. In this chapter a single-input multi-output (SIMO) system is presented as example for the sake of simplicity. However, the proposed method is suitable for MIMO as well.

In this chapter it is assumed that y and z are represented in the same physical unit. Additionally, it is assumed that $G_y(0) = G_z(0)$, such that the solution is equivalent to the solution of Chapter 2, see Appendix A.2.

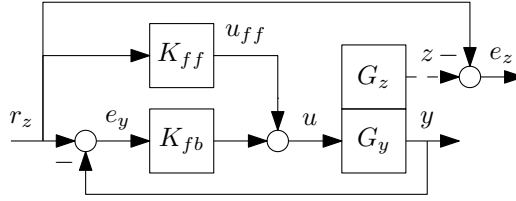


Figure 3.2: Indirect control structure (Skogestad and Postlethwaite, 2005). The performance output z is represented by a dashed line, indicating that it can not be measured (at all times).

3.3 Lifted Feedforward

Consider the system (3.1) in the interconnection of Fig. 3.2 with input u_{ff} and output $z(k)$ only. For an LTV system in full generality, the lifted system description (Dijkstra, 2004; Owens and Feng, 2003), which is a static convolution mapping, results in,

$$z = J_z u_{ff},$$

where

$$z = [z(0) \quad \cdots \quad z(N-1)]^T,$$

$$u_{ff} = [u_{ff}(0) \quad \cdots \quad u_{ff}(N-1)]^T,$$

and $J_z =$

$$\begin{bmatrix} D_z(0) & \cdots & 0 \\ \vdots & \ddots & \\ C_z(N-1) \prod_{k=1}^{N-2} A(N-1-k)B(0) & \cdots & D_z(N-1) \end{bmatrix}$$

The lifted system description can both represent an open- or closed-loop mapping, by taking the appropriate A , B , C , D matrices. For MIMO systems, the convolution matrix becomes block-diagonal with $n_z \times n_u$ blocks and remains valid

for both square and non-square blocks. Also it is possible to include initial conditions, pre- and post-actuation and different actuation and observation windows (Van de Wijdeven, 2008). This lifted system description makes it possible to take into account the time-varying performance output z .

Typically, motion systems are strictly proper systems ($D_z = 0$) and/or delays are present, resulting in J_z being rank deficient. This can be solved by shifting the output vector by an appropriate number of samples, as presented in Section 2.4.

From Hashemi and Hammond (1996), it is well known that unstable poles and non-minimum phase (system or sampling (Aström et al., 1984)) zeros are reflected in the magnitude of the singular values of the lifted system matrix J_z . This causes problems when inversion is used, i.e. a calculated feedforward signal may be unbounded due to singular values close to zero. In order to solve this problem, the Moore-Penrose pseudo-inverse (Ben-Israel and Greville, 2003) is used.

Consider the singular value decomposition of J_z ,

$$\begin{aligned} J_z &= U\Sigma V^T, \\ &= \begin{bmatrix} U_1 & U_2 \end{bmatrix} \begin{bmatrix} \Sigma_1 & 0 \\ 0 & \Sigma_2 \end{bmatrix} \begin{bmatrix} V_1^T \\ V_2^T \end{bmatrix}. \end{aligned}$$

where Σ_2 contains the singular values close to zero. The dimensions of U_2 and V_2 are such that they match the dimension of Σ_2 . Then J_z can be approximated by only taking into account the largest singular values contained in Σ_1 , giving,

$$J_z \approx U_1 \Sigma_1 V_1^T.$$

Now, a bounded feedforward u_{ff} can be computed as,

$$u_{ff} = J_z^\dagger r_z = V_1 \Sigma_1^{-1} U_1^T r_z, \quad (3.2)$$

which minimizes the 2-norm of the performance error $e_z = r_z - J_z u_{ff}$. The resulting feedforward controller $K_{ff} = J_z^\dagger$ is not necessarily LTI or causal, i.e. (block-)Toeplitz or lower triangular respectively.

3.4 Lifted feedforward with input weightings

Directly using the pseudo-inverse in (3.2) to compute a feedforward signal for a system with time-varying performance locations may result in undesired solutions, i.e. the feedforward signal may have a large magnitude and frequency contents at high-frequencies. In order to restrict high frequency contents, an extra weighting can be added to the cost-criterion to obtain a feasible feedforward signal.

Typically, the input to a system is limited by the actuators and amplifiers in both magnitude and frequency contents, therefore the resulting solution from Section 3.3 is undesired in general. Also, the high-frequency and not modeled modes

may be excited by the high-frequency contents of the input signal. Therefore, an additional weighting W is added to the cost-criterion to reflect the limitations of the actuators and amplifiers. This results in,

$$\begin{bmatrix} z \\ 0 \end{bmatrix} = \begin{bmatrix} J_z \\ J_w \end{bmatrix} u_{ff} = J_{zw} u_{ff},$$

where J_w is input-output mapping of $W(z)$ and its dimension is compatible with u_{ff} . Then the feedforward input can be computed as,

$$u_{ff} = J_{zw}^\dagger \begin{bmatrix} z \\ 0 \end{bmatrix}. \quad (3.3)$$

The filter $W(z)$ is typically chosen as a high-pass filter, penalizing the high-frequency contents in the feedforward signal. An example of $W(z)$ is given by,

$$W(z) = \alpha \frac{z-1}{z}, \quad (3.4)$$

with convolution representation,

$$J_w = \alpha \begin{bmatrix} 1 & & & & \\ -1 & \ddots & & & \\ & \ddots & \ddots & & \\ & & \ddots & \ddots & \\ & & & -1 & 1 \end{bmatrix},$$

with scaling parameter α . The Bode diagram of (3.4) is shown in Fig. 3.3, where it can be seen that $W(z)$ indeed acts as a high-pass filter.

3.5 Experiments

The experimental setup shown in Fig. 3.4 consists of 2 masses connected by a flexible shaft. The mass at one side is driven by a 10 Watt Maxxon DC-motor, which is torque controlled. The positions of the two masses are measured by incremental encoders with a resolution of $\frac{2\pi}{2000} = 0.0031$ rad. Note that the encoder y_2 is only used to obtain a model, which is used to compute the feedforward controller. During operation this encoder is not required and is only used to evaluate the performance. The data-acquisition is done using a custom built EtherCAT device using a real-time Linux distribution at a sample frequency of $f_s = 2048$ Hz. The input to the system is limited by ± 2.5 V.

In this section the following methods will be presented:

1. the direct formulation in (3.2), and
2. the proposed method with additional weightings in (3.3).

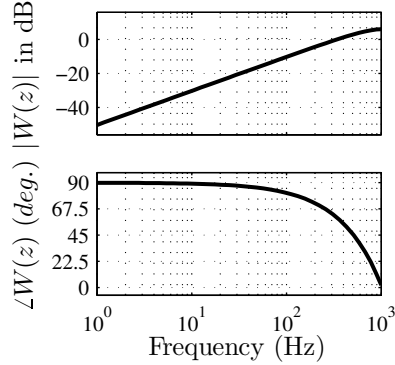


Figure 3.3: Bode magnitude diagram of an example of $W(z)$ for $\alpha = 1$ and $f_s = 2048$ Hz, which is included in the cost-criterion to penalize high-frequency contents in the feedforward signal.

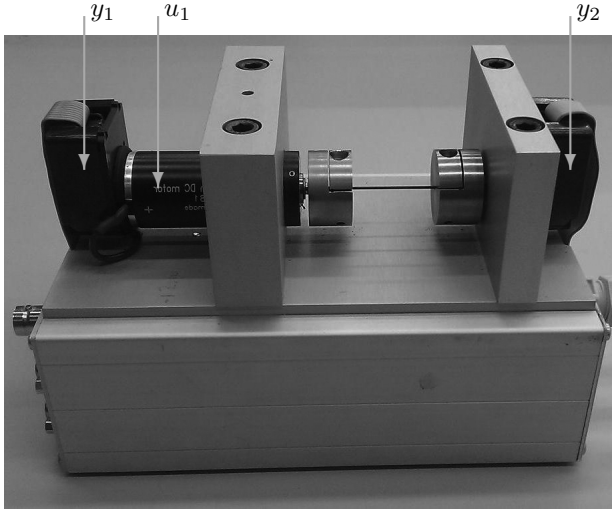


Figure 3.4: Experimental 2-mass system with flexible shaft. The position of the left and right masses are measured by encoder y_1 and y_2 respectively.

3.5.1 Identification and modeling

The experimental setup from Fig. 3.4 has been identified in closed-loop by exciting the system with noise and recording the responses of both outputs. The resulting frequency response function (FRF) is shown in Fig. 3.5.

Subsequently, a model of the system is obtained by fitting the FRF-measurement data in Fig. 3.5. The result is shown in the same figure in light-grey. The motor-

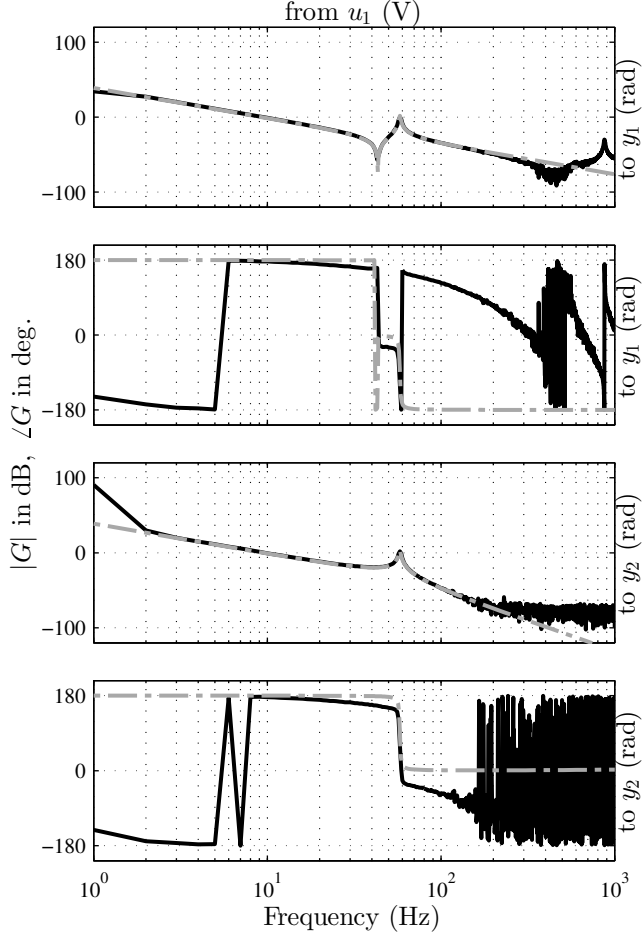


Figure 3.5: Bode diagram of the measured FRF (—) and model (---) of the experimental setup, where y_1 and y_2 are the encoders at the motor and load side respectively.

and load-side models are denoted by $G_1(s)$ and $G_2(s)$ respectively.

$$G_1(s) = \frac{Y_1(s)}{U(s)} = \frac{6172s^2 + 3193s + 4.567e8}{s^4 + 6.145s^3 + 1.327e5s^2},$$

$$G_2(s) = \frac{Y_2(s)}{U(s)} = \frac{3193s + 4.567e8}{s^4 + 6.145s^3 + 1.327e5s^2}.$$

3.5.2 Feedback control design

The feedback controller for motor feedback, i.e. $G_y = G_1(s)$, is manually tuned using loopshaping techniques using the FRF measurement data of Fig. 3.5. The feedback controller structure is given by,

$$K_{fb}(s) = k \cdot \frac{s + 2\pi f_i}{s} \cdot \frac{\frac{1}{2\pi f_z}s + 1}{\frac{1}{2\pi f_p}s + 1} \cdot \frac{\frac{1}{(2\pi f_1)^2}s^2 + \frac{2\beta_1}{2\pi f_1}s + 1}{\frac{1}{(2\pi f_2)^2}s^2 + \frac{2\beta_2}{2\pi f_2}s + 1} \cdot \frac{1}{\frac{1}{(2\pi f_{lp})^2}s^2 + \frac{2\beta_{lp}}{2\pi f_{lp}}s + 1}. \quad (3.5)$$

k	f_i	f_z	f_p	f_1	β_1	f_2	β_2	f_{lp}	β_{lp}
0.9	2	5	45	57.95	0.008	200	0.5	400	0.7

Table 3.1: Controller parameters for the experiments.

The controller (3.5) with parameters given in Tab. 3.1 results in a bandwidth of approximately 15 Hz, with sufficient stability margins ($\|S\|_\infty = 6$ dB, $PM = 31.9^\circ$, $GM = 25.1$ dB). The stability of the closed-loop is assessed by evaluating the Nyquist plot (not shown).

3.5.3 Setpoint trajectory

The fourth order setpoint trajectory is designed using the algorithm of (Lambrechts et al., 2005). The resulting trajectory is show in Fig. 3.6. At the left of the vertical dash-dotted line, performance is required at the mass at the motor side. At the right of the vertical dash-dotted line, performance is required at the load-side. This will be formalized in the next section.

3.5.4 Feedforward control design

As shown in Chapter 2 and Ronde et al. (2012a), to obtain an error equal to zero boils down to pre-filtering the setpoint trajectory or taking the closed-loop dynamics into account. In the intended application, changing the setpoint trajectory is not desired. Therefore, the closed-loop dynamics are taken into account.

The performance error e_z for the control structure of Fig. 3.2 is given by,

$$e_z = (I - G_z S_i (K_{ff} + K_{fb})) r_z, \quad (3.6)$$

where $S_i = (I + K_{fb} G_y)^{-1}$ is the input sensitivity. Hence, the choice of

$$K_{ff} = (\overline{G_z S_i})^\dagger - K_{fb}, \quad (3.7)$$

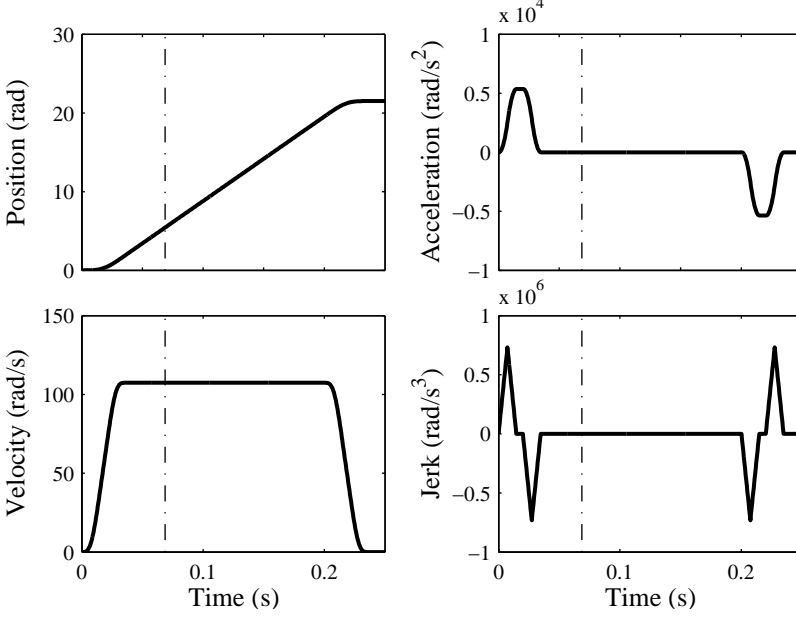


Figure 3.6: Fourth-order setpoint trajectory, where after approximately 0.25 (s) the position setpoint is kept at a constant level (not shown). The dash-dotted line indicates the time where a different performance location is considered.

ideally results in an error of zero. The bar indicates the part of the feedforward controller, which is based on a nominal model, which is subject to model uncertainty. Inserting (3.7) in (3.6) leads to,

$$e_z = (I - G_z S_i (\overline{G_z S_i})^\dagger) r_z.$$

From this, it is clear that all errors in the nominal model and due to truncation of the singular values, directly lead to an increase of the performance error.

The proposed method from Section 3.4 is applied to generate a feedforward controller for the experimental setup with time varying performance. In order to demonstrate this, the performance variable $z(k)$ is chosen as follows,

$$z(k) = \begin{cases} y_1(k) & k \in (1, \gamma) \\ y_2(k) & k \in (\gamma + 1, N) \end{cases}, \quad (3.8)$$

i.e. performance is required at the first mass at the first $\gamma = 141$ samples, from sample $\gamma + 1 = 142$ performance is required at the second mass. Similar changes in performance dynamics are also expected in application where the performance locations gradually change.

Now the lifted system description for $G_z S_i$ can be used which results in,

$$\begin{bmatrix} y_1 \\ y_2 \\ 0 \end{bmatrix} = \begin{bmatrix} J_1 \\ J_2 \\ W \end{bmatrix} u_{ff} = J_{zw} u_{ff}, \quad (3.9)$$

where the proper parts of y_1 and y_2 are chosen corresponding to the time-varying performance variable in (3.8). The matrices J_1 and J_2 are the corresponding parts of the lifted system descriptions of $G_1 S_i$ and $G_2 S_i$, respectively. Furthermore, a filter W is included as shown in Section 3.4. Subsequently, a bounded feedforward u_{ff} can be computed as,

$$u_{ff} = J_{zw}^\dagger \begin{bmatrix} r_z \\ 0 \end{bmatrix} - K_{fb} r_z. \quad (3.10)$$

3.5.5 Design of $W(z)$

The filter $W(z)$ has to be stable for the 2-norm of the weighted input signal to exist. However, the choice of $W(z)$ is not limited to FIR filters. The choice of the shape and gain of $W(z)$ influences the effect on the feedforward signal. The choice of higher order filters allows to penalize the high-frequencies more severely, while the low frequencies are almost not penalized. This allows to take the actuator and amplifier dynamics into account and/or to take the unmodeled dynamics of the plant into account. However, this does not result in an explicit constraint on the input signal, but in a trade-off between tracking performance and the input signal. Therefore, the design of $W(z)$ is an iterative procedure. First, an initial design is computed. Subsequently, the input constraints are evaluated for the worst case setpoint trajectory. In case that the input constraints are not satisfied, the filter $W(z)$ is iteratively redesigned until the input constraints are satisfied.

For the experiments, $W(z)$ is chosen as a 6th-order high-pass Butterworth filter with a cut-off frequency (−3 dB point) of 560 Hz and $\alpha = 1$, i.e. frequencies above the cut-off frequency should be penalized, indicating that the actuators and amplifiers can follow signals up to approximately the cut-off frequency. Here, a 6-th order filter is chosen to prevent too much penalization at low frequencies.

3.5.6 Results

Directly applying the method from Section 3.3 for the LTV system of (3.9), i.e. by not applying any weighting, leads to the feedforward signal in Fig. 3.7. Note that for the computation of the feedforward signal, the one singular value which is close to zero already has been removed according to (3.2). Implementing the feedforward signal from Fig. 3.7, if possible, also leads to undesired behavior due to the parasitic dynamics being excited which are not present in the model.

The infeasible feedforward signal can be understood from a physical point of view. The two masses vibrating in the first flexible mode move exactly in anti-phase, i.e. their position and speed are opposite when the rigid-body movement is subtracted. If the performance definition is then switched, a very large amount of energy is required to correct for the difference in position and speed. Although, this is a relatively simple system, it is expected that similar problems occur in more complex systems, like for example wafer stages.

For practical implementation, a compensation for the Coulomb friction (Olsson et al., 1998) has been added to the feedforward controller as, $F_c = k_c \cdot \text{sign}(\dot{r}_z)$, i.e. the value of the friction is only dependent on the direction of the velocity. The parameter $k_c = 0.0007$ has been obtained by manual tuning. Furthermore, the present delay in the system, as can be seen in Fig. 3.5, has been compensated.

The feedforward computation method in (3.10) results in the feedforward signal as shown in Fig. 3.8a. The two singular values, which are close to zero, have been removed according to (3.2). The power spectral density of the feedforward signal is shown in Fig. 3.8b, where it can be seen that the obtained feedforward signal u_{ff} is indeed band-limited and satisfies the input constraint of ± 2.5 V. The oscillations of the feedforward signal around the switch time can be explained by the change in dynamics. Increasing the weighting on the input signal can reduce these oscillations at the cost of decreased performance.

The performance error e_z obtained by using the feedforward signal from Fig. 3.8a is shown in Fig. 3.9. Here, it can be seen that performance can be obtained for systems with TVP. The obtained performance is represented by the black line, which switches from y_1 (light-grey line) to y_2 (dark-grey line). On the left of the dash-dotted line performance is obtained at y_1 , which is significantly smaller than

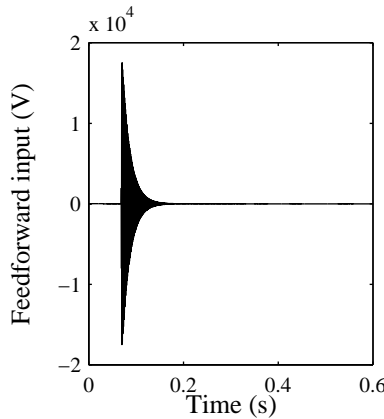


Figure 3.7: Infeasible feedforward signal u_{ff} for the system without actuator and amplifier weightings, i.e. $\alpha = 0$.

the obtained error e_2 in this interval. On the right of the dash-dotted line performance is required on y_2 , where it can be seen that the performance for y_2 is indeed better than for y_1 .

These results are also numerically presented in Table 3.2 for the different intervals. Here, it can be seen that the 2-norm of the performance error is smaller than the 2-norm of the individual errors, i.e. there is a trade-off in the achievable performance.

This results shows that the proposed method indeed can deal with systems where the performance location is time-varying. For traditionally actuated systems, i.e. systems with as many actuators as (rigid-)body modes, it is not possible to prevent excitation of the flexible modes without changing the setpoint trajectory, i.e. without the use of input shaping. However, the proposed method can deal with different system dynamics without changing the setpoint trajectory. If the switch between the different performance output occurs at steady state, the feedforward control design problem can be separated in two problems by taking the proper initial conditions into account. However, this is a much simpler problem than the problem statement considered in this chapter.

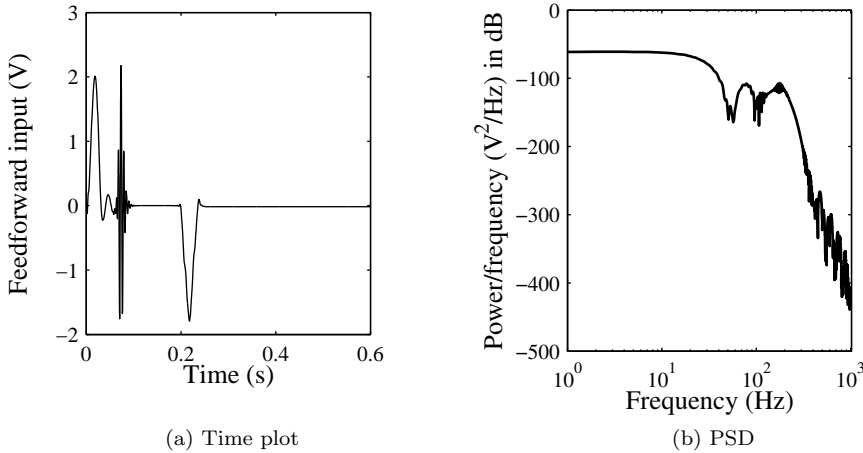


Figure 3.8: Feedforward signal u_{ff} with actuator and amplifier weightings included, such that a signal with limited magnitude and frequency content is obtained. At the time of the switch in performance there is a clear distinction visible from the (scaled) acceleration, which takes the time-varying performance location into account.

Samples	$\ e_1\ _2$	$\ e_2\ _2$	$\ e_z\ _2$
$(1, \gamma)$	$3.8 \cdot 10^{-1}$	$5.59 \cdot 10^{-1}$	$3.8 \cdot 10^{-1}$
$(\gamma + 1, N)$	$8.2 \cdot 10^{-1}$	$5.92 \cdot 10^{-1}$	$5.92 \cdot 10^{-1}$
$(1, N)$	0.9052	0.8153	0.7051

Table 3.2: Errors and performance evaluated in different intervals.

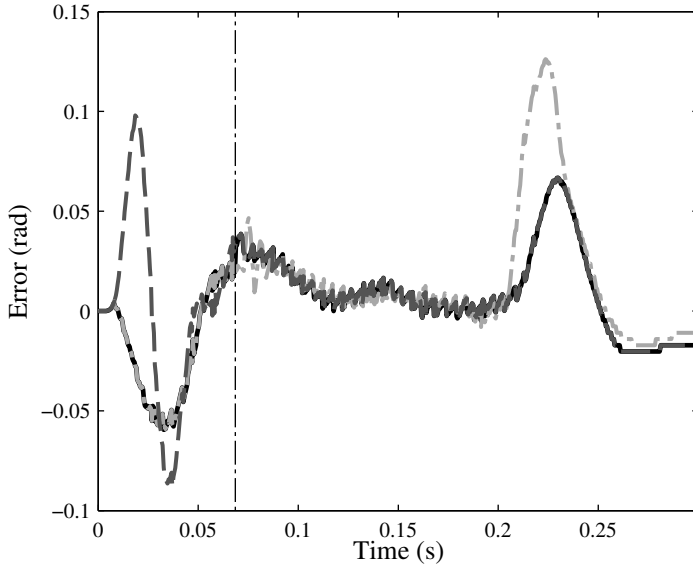


Figure 3.9: Performance $e_z = r_z - z$ (—) and $e_1 = r_z - y_1$ (— ·) and $e_2 = r_z - y_2$ (— —). The vertical dash-dotted line indicates the time instance where the switch in performance definition occurs.

3.6 Conclusions

This chapter presents a design method for feedforward controllers for systems with time-varying performance locations. The proposed method employs a formulation in the lifted framework. Direct formulation in this framework leads to infeasible input signals. By incorporating the filter W high-frequency inputs are penalized, depending on the magnitude and shape of W , which leads to feasible input signals. The shape of the input signal resembles mass feedforward, with an additional oscillation around the switch in performance definition.

The feedforward controller, designed using the proposed method, is independent on the chosen setpoint trajectory. However, the performance definition is predetermined, i.e. the switching time between different performance outputs, is fixed after design of the feedforward controller. Changing the performance definition would required a redesign of the feedforward controller. The solution is also dependent on the feedback controller, i.e. changing the feedback controller requires redesign of the feedforward controller as well, similar to ILC. This can be solved by using by including different setpoint trajectories as presented in Chapter 2.

Further research includes the application to intrinsically multivariable systems with time-varying performance locations, e.g. a plate or wafer stage.

The next two chapters of this thesis deal with feedforward design for over-actuated motion systems. In the next chapter a model-based method to exploit the design freedom from over-actuation in feedforward control is presented.

Chapter 4

Model-based spatial feedforward control for over-actuated motion systems

IN high-performance motion systems, e.g. wafer-stages and pick-and-place machines, there is an increasing demand for higher throughput and accuracy. The rigid-body design paradigm aims at very stiff designs, which lead in an evolutionary way to increasingly heavier systems. Such systems require more and more power, such that this paradigm rapidly approaches the boundary of its scalability. An alternative paradigm is to design a lightweight machine with over-actuation and over-sensing, to deal with the resulting flexibilities. This chapter presents a spatial feedforward method for over-actuated flexible motions systems, which aims at reducing the vibrations over the complete flexible structure during motion. The proposed method is experimentally validated on an industrial prototype and compared to mass feedforward and a standard zero-vibration input shaper.

4.1 Introduction

In the semiconductor industry higher throughput and higher accuracy are desired to keep up with Moore's law (Moore, 1965) and to stay ahead of competition. More aggressive motion profiles (i.e. higher accelerations) and a design with higher stiffness (i.e. higher mass) are required to obtain the desired higher throughput, while maintaining desired accuracy. This will require larger forces, which put stricter demands on actuators, amplifiers and cooling, which is expected to become infeasible in the near future. For a general overview of the control of high-performance motion systems see (Clayton et al., 2009; Butler, 2011).

The next generation of advanced motion systems is expected to be lightweight, which results in significant internal flexibilities. An example of the mode shapes of such systems is shown in Fig. 4.1. This has several consequences for control design:

1. resonances in the region of interest, i.e. close to or even below the objective bandwidth, and
2. transfer between sensor output y and performance location z becomes dynamical due to the limited stiffness, i.e. there is no geometrical transformation possible anymore to analyse/control the performance.

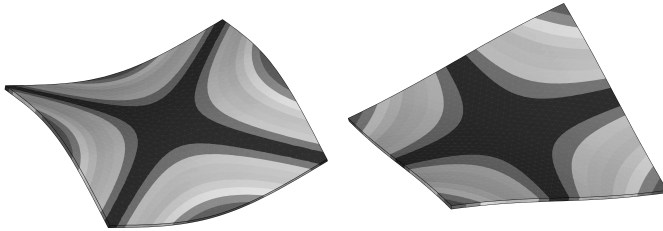


Figure 4.1: Mode shapes of a plate as an example for the problems faced in advanced motion systems. The stage is typically measured at the edges, while processing takes place at a different location, i.e. a good performance at the sensors does not guarantee good performance at the location where processing takes place due to the different dynamics.

Common feedforward methods, which do not take the flexible dynamics into account, will not lead to satisfactory results for lightweight systems. Lightweight systems are typically over-actuated (Schneiders et al., 2003, 2004a,b), i.e. the system contains more actuators than rigid-body degrees of freedom. The additional actuators provide extra design freedom, which is not exploited by the current feedforward design methods. Therefore, the goal is to exploit this design freedom to obtain a better performance than traditionally designed systems with rigid-body

feedforward.

Snap-feedforward (Lambrechts et al., 2005; Steinbuch et al., 2010) is a common method to compensate for the compliance of the low frequency contribution of flexible modes in feedforward control, i.e. the deformation during motion. However, this method only guarantees local performance, i.e. at the sensor location only.

Data-based tuning of the feedforward parameters (Van der Meulen et al., 2008) can improve performance, but still suffers from the same drawbacks as snap-feedforward. Also similar work with a more generic structure, such as (Heertjes et al., 2010; Bruijnen and van Dijk, 2012), only guarantees performance at the sensor location.

For the class of lightweight systems, local performance at the sensors is generally not sufficient, since this does not provide any guarantees at the performance location, i.e. the location where the tool operates (Oomen, 2010; Oomen et al., 2011).

A common method to reduce vibrations in motion systems is input shaping, where the objective is to remove the frequency content at the eigenfrequencies of the flexible structure from the input signal. This is typically done by convolving the input signal with an input shaper (Singhose, 1997; Pao, 1999; Singh and Singhose, 2002; Lau and Pao, 2003; Cutforth and Pao, 2004; Singh, 2008, 2010). Such methods aim at increasing the performance after setup-time, i.e. the residual vibrations after the point-to-point motion are attenuated. However, these methods obtain global performance, i.e. performance at any point of the structure.

If positive shapers are considered (Baumgart and Pao, 2007), the shaped input signal satisfies the same bounds as the original input signal at the cost of extra delay, which may be undesired in the intended application. Negative shapers can reduce this delay (Singhose et al., 1995; Singh and Singhose, 2002), however there are no guarantees provided on the bound of the shaped input signal. For MIMO systems this delay can be reduced (Baumgart and Pao, 2007), if the input signal is known in advance. However, in this chapter the setpoint trajectory is assumed not to be known a priori. Also, application of input shaping changes the setpoint trajectory which is typically not desired in many high-performance motion applications.

Learning based approaches (Moore, 1998; Longman, 2000; Bristow et al., 2006), such as Iterative Learning Control (ILC), require a measurement of the performance variable during the learning process, which is not available in the considered class of motion systems. Furthermore, ILC requires a new learning sequence for every new setpoint trajectory. In van de Wijdeven and Bosgra (2007, 2008) ILC compensation for residual vibration prevents excitation of modes by using an actuation and observation window. In this method only local performance is guaranteed.

The proposed method in this chapter can be considered as a special case of static input-output decoupling (Maciejowski, 1989; Vaes et al., 2003). Typically,

static decoupling aims at diagonalization of the plant, by pre- and post-multiplying the plant with a static matrix, to allow for decentralized control. However, the method proposed here aims at independent control of the rigid-body modes and preventing the excitation of flexible modes. This is achieved by pre-multiplying the plant with a static matrix in the feedforward path. Therefore, there is less freedom compared to standard decoupling techniques, since only an input transformation is applied. Hence, the standard decoupling techniques cannot be applied for the problem considered in this chapter.

The proposed method, called **spatial feedforward**, exploits the freedom induced by over-actuation explicitly. This design freedom is used to prevent excitation of the performance-relevant flexible modes. Compared to existing methods, the proposed method does not introduce extra delay in the input signal.

The techniques in this chapter aim at obtaining *global performance*, i.e. performance at any point of the flexible structure, in contrast to the previous chapters and (Ronde et al., 2012a, 2013a) where *local (inferential) performance* is obtained. Compared to earlier work on spatial feedforward (Ronde et al., 2012b), this chapter provides the extension to multiple modes, including conditions for the existence of the solution. The contributions of this chapter are to provide a feedforward method which has the following properties:

1. explicit use of over-actuation, and
2. no additional delays introduced, and
3. prevent the excitation of multiple flexible modes, and
4. performance guarantee over the whole structure, i.e. global performance, and
5. independent of the setpoint trajectory.

The outline of this chapter is as follows. In Section 4.2 the problem is formulated. Subsequently, spatial feedforward is introduced in Section 4.3. The conditions for the existence of solutions are formulated in Section 4.4. In Section 4.5 a method to compute partial solutions is provided. In Section 4.6 input shaping, which is used as a benchmark, is briefly discussed. In Section 4.7 and 4.8 the experimental validation and conclusions are presented, respectively.

4.2 Problem formulation

Consider a system with proportionally damped modes. Such systems can be written in the following modal description (Gawronski, 2004):

$$\begin{aligned}
 G(s) &= C_m [Is^2 + 2Z\Omega s + \Omega^2]^{-1} B_m, \\
 &= [C_b \mid C_{int}] \left[\frac{\Theta^{(b)}(s)}{\Theta^{(int)}(s)} \right] \left[\frac{B_b}{B_{int}} \right], \quad (4.1)
 \end{aligned}$$

with Z and Ω diagonal, due to proportional damping. Therefore, the matrices $\Theta^{(b)}(s)$ and $\Theta^{(int)}(s)$ are diagonal and contain the second order transfer functions of the body modes and internal modes respectively. Furthermore B_{mi} , i.e. the i -th row of B_m , is associated with the i -th mode only.

The plant $G(s)$ has n_u inputs and n_y outputs and is controlled using the control structure shown in Fig. 4.2.

The goal is to find a static input transformation $T_{u,ff}$, such that the body-modes are independently controllable and the flexible modes are not excited by feedforward control, i.e. the flexible modes become uncontrollable.

The static transformation matrices $T_{u,fb}$ and T_y are used to decouple the system as $G_d = T_y G T_{u,fb}$, to allow for decentralized feedback control. The motion $m(t)$ represents the pose of a motion system. The mapping between the sensors $y(t)$ and the measured rigid-body motion $m(t)$ is given by:

$$m(t) = T_y y(t), \quad (4.2)$$

where $m(t)$ typically has dimension n_b .

Remark 4.1. The choice of T_y is not unique, i.e. scaling or a linear combination of translations/rotations occur. In Section 4.7.4 a choice for T_y will be made based on physical interpretation.

Definition 4.2 (Body mode). The body modes are defined as the set of rigid-body and suspension modes. The number of body modes is denoted by n_b .

Definition 4.3 (Suspension mode). A suspension modes has, by design, a significantly lower resonance frequency than the internal modes, i.e. the structural stiffness of the suspension system to the fixed world is much smaller than the body stiffness.

Definition 4.4 (Internal mode). The undesired flexible modes are called the internal modes, i.e. the flexible modes excluding the suspension modes. The number of internal modes is denoted by n_r .

Definition 4.5. The number of internal modes to be suppressed by spatial feedforward is denoted by n_m .

Lemma 4.6. A single mode of a system in the modal form 3 (Gawronski, 2004, p.37) is controllable if and only if $b_{mi} \neq 0$

Proof: Consider a single mode in modal form 3 (Gawronski, 2004, p.37). The controllability of this system with state matrix A and input matrix B can be tested by (Antsaklis and Michel, 2006; Kailath, 1980),

$$\text{rank} \begin{bmatrix} B & AB \end{bmatrix} = \text{rank} \begin{bmatrix} 0 & b_{mi} \\ b_{mi} & -2\zeta_i \omega_i b_{mi} \end{bmatrix},$$

which has clearly full row rank if and only if $b_{mi} \neq 0$. ■

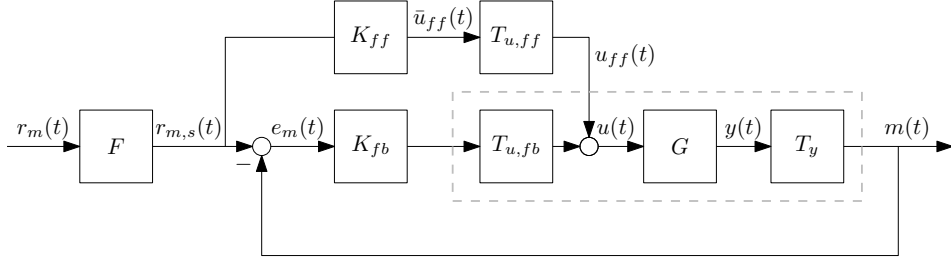


Figure 4.2: Control structure for spatial feedforward. The plant G has inputs $u(t)$ and sensor outputs $y(t)$. The feedback- and feedforward controller are denoted by K_{fb} and K_{ff} respectively. Furthermore, $T_{u,fb}$, $T_{u,ff}$ and T_y denote the (static) coordinate transformation matrices. The desired motion, the measured motion and the motion error are represented by $r_m(t)$, $m(t)$ and $e_m(t)$ respectively. The filter F is used in case of input shaping, which is used as a reference case. For all other methods $F = I$.

4.2.1 Assumptions

In this chapter we assume:

1. a linear time-invariant (LTI) system with force/torque inputs and position/rotation outputs, and
2. proportional or modal damping, and
3. no model uncertainty, and
4. functional motion system, i.e. $\text{rank}(B_b) = n_b$.

The first three assumptions lead to a model in the form of (4.1). The fourth assumption guarantees the independent controllability of all rigid-body modes.

For spatial feedforward, additional assumptions are:

1. over-actuated (OA) $n_u > n_b$, where the degree of over-actuation is given by $n_s = n_u - n_b$, and
2. modes to be suppressed is given.

The first assumption ensures that there is sufficient design freedom, which can be employed by spatial feedforward. However, this condition is not sufficient to guarantee the existence of solutions. This will be formulated in Section 4.4.

4.3 Spatial feedforward

The body modes of the system (4.1) are used to position the system at the desired position, while the internal modes result in undesired vibrations of the system.

Therefore, the goal is to find a new set of feedforward inputs $\bar{U}_{ff}(s)$ by a static input transformation $T_{u,ff}$, such that

1. each body-mode is independently controllable,
2. a selection of the flexible modes is not excited by the feedforward.

The new feedforward inputs \bar{U}_{ff} are related to the old feedforward inputs U_{ff} by,

$$U_{ff}(s) = T_{u,ff} \bar{U}_{ff}(s), \quad (4.3)$$

where $T_{u,ff} \in \mathcal{R}^{n_u \times n_b}$. This results in a reduced input dimension, i.e. from n_u to n_b .

4.3.1 Body-mode feedforward

For each body mode to be independently controllable, it is required that,

$$B_b T_{u,ff} = \Lambda, \quad B_b \in \mathcal{R}^{n_b \times n_u}, \quad \Lambda \in \mathcal{R}^{n_u \times n_u}$$

with $T_{u,ff}$ from (4.3) and where Λ is a diagonal matrix. Here, $\Lambda = I$ is chosen, which can be done without loss of generality, i.e. this just introduces a scaling. Due to over-actuation B_b is fat, i.e. non-square, a pseudo-inverse is required. A pseudo-inverse of the matrix A is defined as the solution X to $AXA = A$. This solution is denoted as A^\dagger , i.e. the Moore-Penrose pseudo-inverse (Ben-Israel and Greville, 2003). For a fat real matrix A with full row rank, the property $AA^\dagger = I$ holds. In this case $A^\dagger = A^T (AA^T)^{-1}$. The minimum energy solution is given by,

$$T_{u,ff} = B_b^\dagger,$$

which allows individual control of each body mode. Therefore, this specific choice for $T_{u,ff}$ for body-mode feedforward control is denoted as,

$$T_b := B_b^\dagger, \quad (4.4)$$

In the case of rigid-body modes only, the input directions can be aligned with the desired motion direction by using an appropriate coordinate transformation under similarity.

For systems with suspension modes, the body-modes cannot be aligned with the desired motion $m(t)$, hence a combination of the body modes should be found, such that this results in the desired movement. For details see (Ronde et al., 2012b).

4.3.2 Design freedom

Since the system is functionally over-actuated, the input matrix B_b is fat, i.e. there are multiple solutions which have the same effect on the body modes. Therefore, an extra design freedom is present in the selection of $T_{u,ff}$,

$$\dim \ker(B_b) = n_s,$$

i.e. there are n_s free directions that can be selected without affecting the body-mode behaviour. This design freedom can be exploited, such that a certain chosen flexible mode is not excited.

4.3.3 Spatial feedforward control, desired solution

Ideally, the spatial feedforward design would be such that

$$\begin{bmatrix} B_b \\ B_{int} \end{bmatrix} T_{u,ff} = \begin{bmatrix} I_{n_b} \\ 0_{n_r} \end{bmatrix},$$

i.e. all body modes are independently controllable and none of the flexible modes are excited. However, in practice this cannot be achieved due to the limited number of actuators. Therefore, a limited number of n_m internal modes is chosen in \widetilde{B}_{int} , where \widetilde{B}_{int} is a selection of the rows of B_{int} , i.e. a selection which determines which flexible modes are desired to be suppressed. This leads to,

$$\begin{bmatrix} B_b \\ \widetilde{B}_{int} \end{bmatrix} T_{u,ff} = \begin{bmatrix} I_{n_b} \\ 0_{n_m} \end{bmatrix}. \quad (4.5)$$

The conditions for the existence of solutions will be formulated in the next section.

4.4 Existence of solutions

The input matrix with a selected number of modes is given by,

$$\widetilde{B} = \begin{bmatrix} B_b \\ \widetilde{B}_{int} \end{bmatrix}. \quad (4.6)$$

In Table 4.1 the conditions for the existence of solution are summarized.

In general, problem (4.5) can be solved if and only if,

$$\begin{bmatrix} I_{n_b} \\ 0_{n_m} \end{bmatrix} \in \text{Im}(\widetilde{B}), \quad (4.7)$$

where $\text{Im}(\cdot)$ denotes the image of the matrix.

A sufficient condition to satisfy (4.7), which guarantees the existence of a solution, is given in Lemma 4.7.

There are several special cases regarding the input directions, namely,

Constraint	Existence of solutions
$\text{rank}(B_b) = n_b$ and $n_u > n_b$	Functional over-actuated motion system
$n_m = n_u$ and $\text{rank } \tilde{B} = n_u$	Guaranteed solution (Lemma. 4.7)
$n_m = n_u$ and $\text{rank } \tilde{B} < n_u$	Solution if and only if (4.7) holds
$n_m < n_s$	Design freedom left
$n_m > n_s$	Overconstrained problem (Theorem 4.11)

Table 4.1: Summary of the existence conditions for spatial feedforward.

1. *intrinsically uncontrollable internal modes*, i.e. all actuators are exactly placed in the nodes of a mode. Therefore, this mode will never be excited,
2. *internal modes aligned with body modes*, i.e. the direction of the body modes and internal modes are equal. Therefore, it is not possible to make this mode uncontrollable, without changing the actuator configuration, and
3. *iso-directional internal modes*, modes with the same input direction, which can be made uncontrollable at the same time.

Lemma 4.7. *The controllability of n_m internal modes of a system can be arbitrarily selected by a static transformation matrix if the matrix (4.6) is square, i.e. $n_u = n_b + n_m$ and has*

$$\text{rank}(\tilde{B}) = n_u \quad (4.8)$$

Proof: Let $\widetilde{B_{int}}$ be a selection of rows, i.e. modes, from B_{int} , such that the matrix (4.6) is square and has full rank. Then, the solution of (4.5) is given by,

$$T_{u,ff} = \begin{bmatrix} B_b \\ \widetilde{B_{int}} \end{bmatrix}^{-1} \begin{bmatrix} I_{n_b} \\ 0_{n_m} \end{bmatrix}.$$

■

Typically, a system has more relevant modes than the degree of over-actuation, which means that the matrix in (4.6) is not square. Lemma 4.7 guarantees the existence of a solution for a number of modes equal to the degree of over-actuation. The rank condition in (4.8) essentially means that the extra actuators need to add extra degrees of freedom to the input space. If this (sufficient) condition is not satisfied, there can still be solutions, namely if (4.7) holds. If (4.7) does not hold, then not all internal modes can be suppressed from all channels. However, it may still be possible to make certain modes uncontrollable in certain input channels.

4.5 Partial solutions

The solution presented in Lemma 4.7 is only suitable to solve the complete case, i.e. for all input channels at once. However, in some cases it is more desirable to

obtain a partial solution of spatial feedforward, i.e. different internal modes might be relevant in the different input channels.

For spatial feedforward $T_{u,ff}$ is selected as,

$$T_{u,ff} = T_b + T_s,$$

where $T_b = B_b^\dagger$ and

$$T_s \mid \text{Im}(T_s) = \ker(B_b), \quad (4.9)$$

i.e. T_s is such that the image of T_s lies in the kernel of B_b .

In Section 4.3.1 it was shown that the selection of T_b allows independent control of the body modes. In Lemma 4.8 it will be shown that the selection of T_s as in (4.9) does not affect the controllability of the body modes. Subsequently, the conditions for a mode to become uncontrollable will be shown in Lemma 4.9.

Lemma 4.8. *The controllability of a body mode r is not affected by the selection of T_s if and only if*

$$T_s \mid \text{Im}(T_s) = \ker(B_b),$$

Proof: Let $b_{b,r}$ be the r -th row of B_b and let $t_{f,i}$, $t_{b,i}$ and $t_{s,i}$ be the i -th column of $T_{u,ff}$, T_b and T_s respectively. Furthermore, let T_b be selected as (4.4) and let $\text{rank}(B_b) = n_u$. Then,

$$b_{b,r}t_{f,i} = 1 \Leftrightarrow b_{b,r}t_{b,i} + b_{b,r}t_{s,i} = 1 \Leftrightarrow b_{b,r}t_{b,i} = 1,$$

i.e. the columns of $T_{u,ff}$ can be decomposed into T_b and T_s . Furthermore $b_{b,r}t_{s,i} = 0$, due to the selection of T_s in (4.9). ■

Lemma 4.9. *An internal mode r is uncontrollable from input i if and only if*

$$b_{int,r}t_{b,i} = -b_{int,r}t_{s,i}. \quad (4.10)$$

Proof: Let $b_{int,r}$ be the r -th row of B_{int} and let $t_{f,i}$, $t_{b,i}$ and $t_{s,i}$ be the i -th column of $T_{u,ff}$, T_b and T_s respectively.

$$b_{int,r}t_{f,i} = 0 \Leftrightarrow b_{int,r}(t_{b,i} + t_{s,i}) = 0 \Leftrightarrow b_{int,r}t_{b,i} = -b_{int,r}t_{s,i}.$$

■

For a single mode, computing the spatial feedforward using Lemma 4.9 boils down to solving the scalar equation (4.10) per input channel.

Let $\mathcal{U} = \mathbb{R}^{n_u}$ be the space of all input vectors. Furthermore, let \mathcal{V}, \mathcal{W} be subspaces of \mathcal{U} , such that $\mathcal{U} = \mathcal{V} \oplus \mathcal{W}$ and $\mathcal{V} \cap \mathcal{W} = 0$.

$$\begin{aligned} V &= [v_1 \quad \dots \quad v_{n_s}] \mid \text{span}(V) = \ker(B_b), \quad V \in \mathbb{R}^{n_u \times n_s}, \\ W &= [w_1 \quad \dots \quad w_{n_b}] \mid \text{span}(W) = \text{Im}(B_b^T), \quad W \in \mathbb{R}^{n_u \times n_b} \end{aligned}$$

i.e. V and W are a basis for $\ker(B_b)$ and $\text{Im}(B_b^T)$ respectively. Due to assumptions for functional OA and the Rank-Nullity theorem (Meyer, 2000),

$$\dim(V) = n_s, \quad \dim(W) = n_b.$$

Let the spatial design freedom of $t_{s,i}$ be parameterized as,

$$t_{s,i} = V\alpha_i, \quad \alpha_i \in \mathbb{R}^{n_s \times 1}. \quad (4.11)$$

This parametrization is used in Theorem 4.10, such that a selected number of internal modes can be made uncontrollable.

Theorem 4.10. *Let \widetilde{B}_{int} be a selection of n_s internal modes, i.e. rows, from B_{int} , then the internal modes selected in \widetilde{B}_{int} are uncontrollable from input i if and only if*

$$T_{u,ff} = T_b + V\alpha_i,$$

with

$$\alpha_i = -\left(\widetilde{B}_{int}V\right)^{-1}\widetilde{B}_{int}t_{b,i}.$$

and $\text{rank}(\widetilde{B}) = n_b + n_s$.

Proof: Proof follows from the application of Lemma 4.9 with (4.11).

$$\begin{aligned} \widetilde{B}_{int}t_{f,i} = 0 &\Leftrightarrow \widetilde{B}_{int}(t_{b,i} + t_{s,i}) = 0 \Leftrightarrow \widetilde{B}_{int}(t_{b,i} + V\alpha_i) = 0 \Leftrightarrow \\ \widetilde{B}_{int}t_{b,i} &= -\widetilde{B}_{int}V\alpha_i \Leftrightarrow \alpha_i = -\left(\widetilde{B}_{int}V\right)^{-1}\widetilde{B}_{int}t_{b,i}. \end{aligned}$$

Due to the selection of n_s modes, $\widetilde{B}_{int} \in \mathbb{R}^{n_s \times n_u}$, therefore the product $\widetilde{B}_{int}V$ is square. To prove that $\widetilde{B}_{int}V$ has full rank, consider the product $\widetilde{B}V$,

$$\begin{bmatrix} B_b \\ \widetilde{B}_{int} \end{bmatrix} V,$$

which has full rank due to Sylvester's rank inequality (Bernstein, 2009) and the condition $\text{rank}(\widetilde{B}) = n_b + n_s$. Since $B_bV = 0$, by construction of V (V is a basis for $\ker(B_b)$), this does not contribute to the rank. Therefore, it can be concluded that $\text{rank}(\widetilde{B}_{int}V) = n_s$. \blacksquare

If $n_m > n_s$, there are more constraints than there is design freedom. Of course, one can choose to apply a standard least-squares solution to (4.5), i.e. replace the inverse by a pseudo-inverse. However, this would lead to an approximate solution, thereby compromising the independent controllability of the body modes. Therefore, a constrained solution is presented in Theorem 4.11.

If $n_m < n_s$, a limited amount of the design freedom is used, which can be solved by applying a least-squares solution to (4.5) or by application of Theorem 4.11.

Theorem 4.11. Let \widetilde{B}_{int} be a selection of $n_m > n_s$ internal modes from B_{int} , then the internal modes selected in \widetilde{B}_{int} are the 2-norm optimal solution of (4.12) with constraint (4.13) from input i

$$\min \left\| 0 - \widetilde{B}_{int} t_{f,i} \right\|_2, \quad (4.12)$$

$$B_b T_{u,ff} = I. \quad (4.13)$$

if and only if

$$T_{u,ff} = T_b + V \alpha_i,$$

with

$$\alpha_i = - \left(\widetilde{B}_{int} V \right)^\dagger \widetilde{B}_{int} t_{b,i}$$

and $\text{rank}(\widetilde{B}) = n_u$.

Proof: Due to the selection of n_m modes $\left(\widetilde{B}_{int} V \right) \in \mathbb{R}^{n_m \times n_s}$. To prove that $\widetilde{B}_{int} V$ has full column rank, consider the product $\widetilde{B} V$. By applying Sylvester's rank inequality (Bernstein, 2009),

$$\begin{aligned} \text{rank}(\widetilde{B}) + \text{rank}(V) - n_u &\leq \text{rank}(\widetilde{B} V), \\ n_u + n_s - n_u &\leq \text{rank}(\widetilde{B} V), \end{aligned}$$

therefore $\text{rank}(\widetilde{B} V) = n_s$. Since $B_b V = 0$, by construction of V , this does not contribute to the rank. Therefore, it can be concluded that $\text{rank}(\widetilde{B}_{int} V) = n_s$. This means that computing α boils down to a “conventional least-squares problem”. To show that this indeed minimizes (4.12), consider

$$\begin{aligned} \min \left\| 0 - \widetilde{B}_{int} t_{f,i} \right\|_2 &= \min \left\| -\widetilde{B}_{int} (t_{b,i} + V \alpha_i) \right\|_2, \\ &= \min \left\| \underbrace{-\widetilde{B}_{int} t_{b,i}}_y - \underbrace{\widetilde{B}_{int} V}_A \underbrace{\alpha_i}_x \right\|_2, \end{aligned}$$

then the least-squares solution is given by $x = A^\dagger y$. ■

4.6 Input shaping

Both input shaping and the method proposed in this chapter have the property that these method prevent the excitation of flexible modes over the complete flexible structure. However, to achieve this input shaping modifies the setpoint in

Mode	Frequency (Hz)	ζ (-)
1	142.75	0.0013
2	501.05	0.0019

Table 4.2: Parameters used to design the zero-vibration input shaper.

contrast to the proposed method. Therefore, input shaping provides an excellent benchmark case for the proposed method. The remainder of this section will presents a short recap of zero-vibration input shaping (Singh, 2010). Since the method should be independent on the setpoint trajectory, it is not possible to derive shorter shapers for the MIMO system (Baumgart and Pao, 2007). Therefore, the problem reduces to designing a set of SISO shapers.

A general N^{th} -order input shaper is given by,

$$h(t) = \sum_{l=0}^N a_l \delta(t - t_l). \quad (4.14)$$

A closed-form solution of a Zero-Vibration (ZV) input shaper in the form of (4.14) is given by Singh and Singhose (2002) and in Appendix B,

$$\begin{aligned} a_0 &= \frac{1}{1+Q}, & t_0 &= 0, \\ a_1 &= \frac{Q}{1+Q}, & t_1 &= \frac{T_d}{2}, \end{aligned}$$

where Q is,

$$Q = \exp\left(\frac{\zeta\pi}{\sqrt{1-\zeta^2}}\right).$$

For the prototype lightweight motion system of Section 4.7 these parameters are given in Table 4.3. To allow a fair comparison, the frequencies and damping parameters have been updated for input shaping, since this method is sensitive to errors in the modal parameters. For input shaping the two most relevant frequencies are selected to be suppressed, for spatial feedforward this is limited by the number of additional actuators. Therefore, an input shaper will be designed to suppress the modes from Table 4.2. The intermediate design steps are only shown once, as they are similar for both input shapers.

For digital implementation the *nearest sampling time approximation* is chosen (Baumgart and Pao, 2007),

$$t_{1,\text{NST}} = \text{ceil}\left(\frac{t_1}{t_s}\right) = 35.$$

This results in the following discrete transfer functions of the input shapers,

$$H_1(z) = \frac{0.5015z^{35} + 0.4985}{z^{35}}, \quad H_2(z) = \frac{0.5015z^{10} + 0.4985}{z^{10}}.$$

This results in the total shaper,

$$\begin{aligned} H(z) &= H_1(z)H_2(z) \\ &= \frac{0.2515z^{45} + 0.25z^{35} + 0.25z^{10} + 0.2485}{z^{45}} \end{aligned} \quad (4.15)$$

with $t_s = 1/10000$ s. For input shaping, the setpoint trajectory $r_m(t)$ is filtered by (4.15) prior to applying to the system.

4.7 Experimental validation

4.7.1 Prototype lightweight motion system

The industrial prototype lightweight motion stage, shown in Fig. 4.3, can move in all 6 degrees of freedom over a range of approximately 0.5 mm in x, y and z -direction and approximately 1 mrad in R_x, R_y and R_z -direction. The sensor- and actuator layout of the stage is schematically shown in Fig. 4.4. The stage is driven by 4 Lorenz-actuators for the x, y, R_z -directions. For the z -direction 9 actuators are available on a 3 by 3 grid. The position is measured at the corners of the stage using linear incremental encoders with a resolution of 1 nm. The stage is lifted by gravity compensators, such that ideally the stage is freely floating and the actuators do not need to generate any force in the working point.

The goal is to perform a point-to-point motion in z -direction, while preventing the excitation of flexible modes by using spatial feedforward. Therefore, the experiments in this section will be focussed on the z, R_x, R_y -direction, this allows for a more compact presentation of the results. The modes to be suppressed in the feedforward path are selected on the basis of results of standard mass feedforward. Additionally, both standard- and spatial feedforward will be compared to input shaping.

To verify the fact that the selected internal modes are not excited by the spatial feedforward, an additional sensor will be employed at the performance location in Fig. 4.3. In the intended application this typically would be the area to be exposed or the location of the component to be placed. Therefore, a capacitive sensor is placed such that the position of the center of the stage can be measured in z -direction with a resolution of approximately 10 nm. This sensor will only be used for validation purposes.

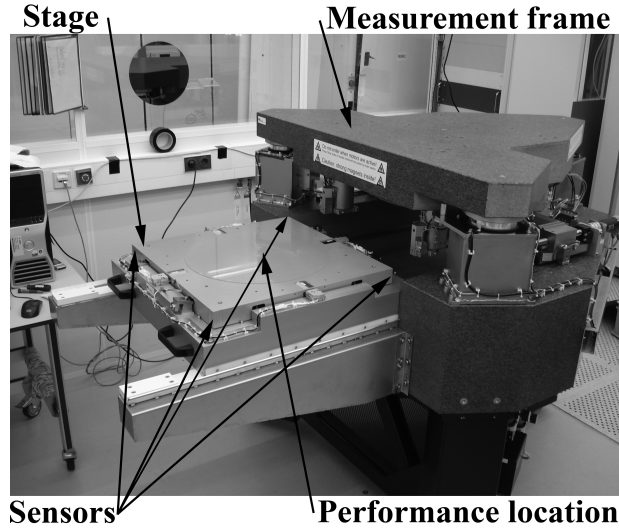


Figure 4.3: Industrial prototype lightweight motion system with over-actuation. The position of the stage is measured with respect to the measurement frame using sensors. The performance location indicates the area where processing takes place.

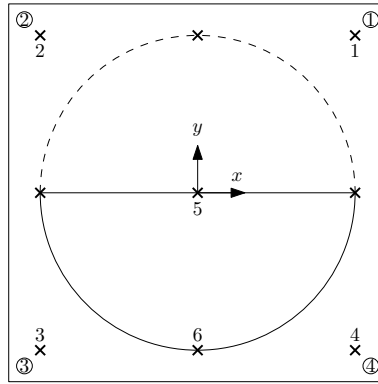


Figure 4.4: Schematic actuator- and sensor layout of stage in Fig. 4.3 of the prototype lightweight motion system. The crosses mark the location of the actuators in z -direction. Only the numbered actuators are actually used. The circles represent the sensors in z -direction. Furthermore, an extra sensor in z -direction can be placed within the solid semicircle, which can be used for verification.

4.7.2 Identification

In this section, the identification of the prototype lightweight motion system will be presented. A non-parametric model will be used for the design of the feedback

Description	i	Frequency f_i (Hz)	Damping ζ_i (-)
Internal modes	1	143.0	0.005
	2	382.8	0.005
	3	517.3	0.005
	4	517.3	0.005
	5	523.5	0.005
	6	760.0	0.005

Table 4.3: Eigenfrequencies and damping of the parametric model. The third and fourth modes are bending modes with a geometric multiplicity of two, i.e. these modes have the same eigenvalues, but their corresponding modeshapes are orthogonal.

controller and for the stability evaluation of the system under decentralized control. Furthermore, the non-parametric model is used to validate the parametric model. The parametric model in the form of (4.1) is obtained from the FEM. Subsequently, Theorem 4.10 is applied with the model from (4.1).

Non-Parametric model

In Fig. 4.5 and Fig. 4.6 a non-parametric model of the prototype lightweight motion stage is shown. This model has been identified by subsequently exciting each input with a multisine in closed-loop, while the x, y and R_z -direction are controlled at a fixed position.

Parametric model

A parametric model of order 200 has been obtained from a Finite Element Method (FEM) model. The result is shown in Fig. 4.5 and Fig. 4.6. By visual inspection it can be seen that the main characteristics of the measured plant are correctly represented by the model. Furthermore, it can be seen that the initial estimate of the value of the damping in the model can be improved. However, the presented method is invariant for modelling errors in frequency and damping, i.e. the method only depends on the input directions, i.e. the mode shapes. Therefore, this does not pose a problem. The eigenfrequencies and corresponding damping of the model are given in Table. 4.3.

4.7.3 Actuator- and sensor selection

For the z, R_x, R_y -directions the actuators at the four corners will be employed both for feedback and for the standard rigid-body feedforward in order to obtain a symmetric, equal distribution of the forces during acceleration.

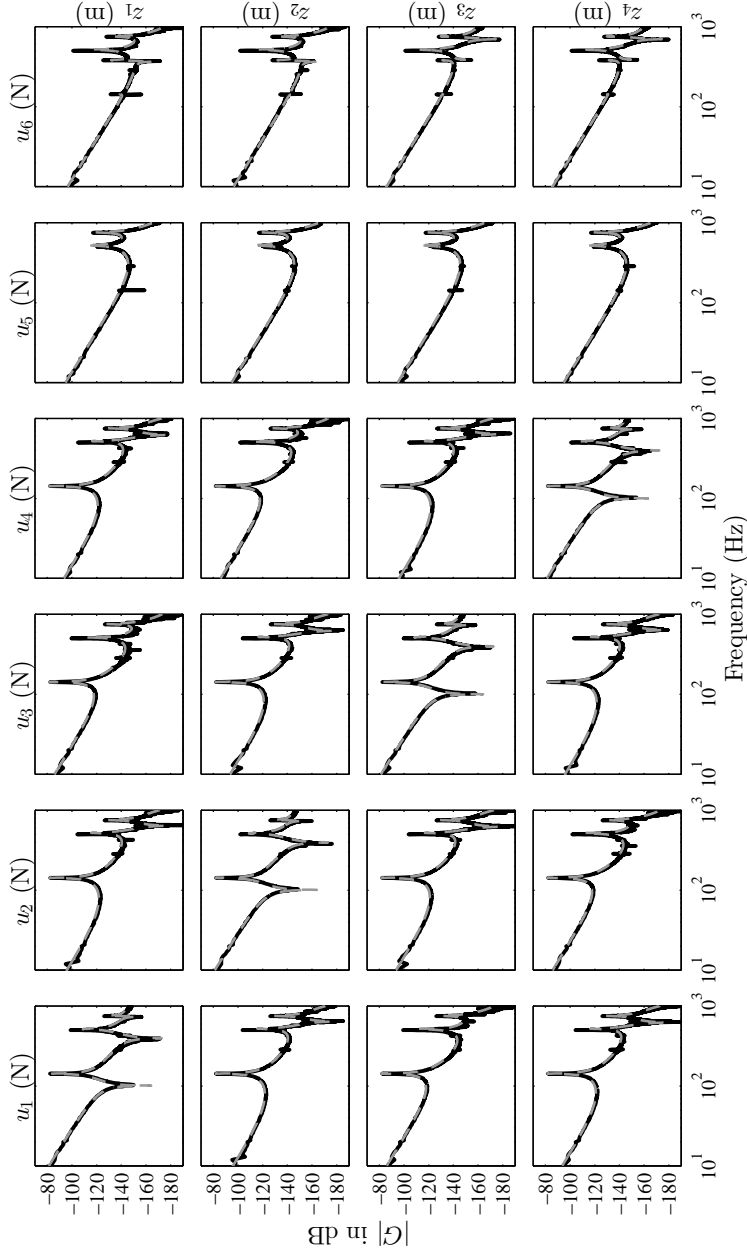


Figure 4.5: Bode magnitude diagram of the prototype lightweight motion system, measured FRF (—) and parametric model (--).

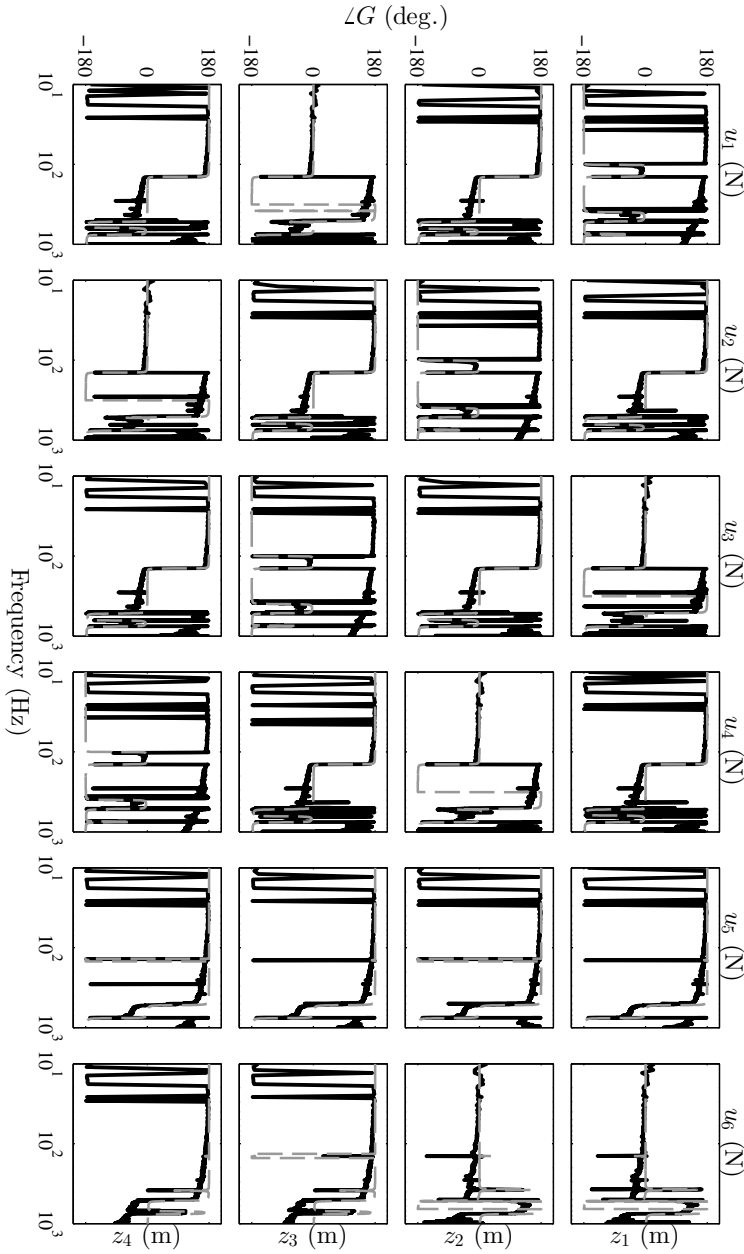


Figure 4.6: Bode phase diagram of the prototype lightweight motion system, measured FRF (—) and parametric model (---).

For the feedforward six actuators will be employed as shown in Fig. 4.4. This configuration has been selected, such that the matrix \widetilde{B}_{int} is well invertible (condition number close to 1) on the basis of the FEM-model of the waferstage.

For both the feedback and feedforward control the 4 sensors at the corners will be used.

4.7.4 Decoupling and feedback control design

The physical coordinates are used for geometric decoupling of the system. The four actuators and sensors will be used for feedback control of the translation and rotation in the z, R_x, R_y -direction of the prototype motion system as in (4.2). For the experimental setup (4.2), is equal to,

$$\begin{bmatrix} z \\ R_x \\ R_y \\ \text{torsion} \end{bmatrix} = \begin{bmatrix} 0.25 & 0.25 & 0.25 & 0.25 \\ 0.90 & 0.90 & -0.90 & -0.90 \\ -0.84 & 0.84 & 0.83 & -0.83 \\ 0.35 & -0.35 & 0.35 & -0.35 \end{bmatrix} \begin{bmatrix} z_1 \\ z_2 \\ z_3 \\ z_4 \end{bmatrix}, \quad (4.16)$$

where the last motion direction represents the deformation of the stage in terms of torsion. This direction is used for an additional feedback control loop to control the first internal mode (torsion).

The decoupled plant is then given by,

$$G_{dec} = T_y G T_{u,fb}. \quad (4.17)$$

The feedback controller is given by

$$K_{fb} = \text{diag}(K_x, K_y, K_{R_z}, K_z, K_{R_x}, K_{R_y}, K_{\text{torsion}}), \quad (4.18)$$

where

$$K_j(s) = k_j \frac{s + 2\pi f_{int,j}}{s} \frac{\frac{1}{2\pi f_{z,j}} s + 1}{\frac{1}{2\pi f_{p,j}} s + 1} \frac{1}{\frac{1}{(2\pi f_{lp,j})^2} s^2 + \frac{2\beta_{lp}}{2\pi f_{lp,j}} s + 1} \cdot \frac{\frac{1}{(2\pi f_{nz,j})^2} s^2 + \frac{2\beta_{nz,j}}{2\pi f_{nz,j}} s + 1}{\frac{1}{(2\pi f_{np,j})^2} s^2 + \frac{2\beta_{np,j}}{2\pi f_{np,j}} s + 1},$$

with $\beta_{lp} = 0.5$ and other parameters as shown in Table 4.4 and 4.5. The controller consists of the following elements: gain, integrator, lead-filter, second-order lowpass and a notch-filter. The lead-filter is required to obtain the correct phase at the zero crossing of the open-loop. The integrator is included to improve the tracking at low frequencies and to prevent steady-state errors. The notch-filter is included to prevent additional zero-crossings of the open loop, which allows to increase the bandwidth without endangering stability. Finally the lowpass filter is

Axis j	k_j	$f_{int,j}$	$f_{z,j}$	$f_{p,j}$	$f_{lp,j}$	f_{BW}
x	3.1318e5	10	50/4	200	250	48.2
y	3.0651e5	10	50/4	200	250	46.3
R_z	2.3773e4	10	50/4	200	250	53.4
z	3.3165e5	10	50/4	200	250	49.7
R_x	1.1252e4	10	50/4	200	250	58.9
R_y	1.1328e4	10	50/4	200	250	58.9

Table 4.4: Controller parameters and resulting bandwidth f_{BW} (Hz). f_{BW} is defined as the zero dB crossing of the open-loop.

Axis j	$f_{nz,j}$	$\beta_{nz,j}$	$f_{np,j}$	$\beta_{np,j}$
z	530	0.001	530	0.1
R_x	504	0.001	504	0.1
R_y	504	0.001	504	0.1

Table 4.5: Controller parameters for the notch filters.

included to enforce the desired roll-off and to prevent the amplification of noise. The controller K_{torsion} is given by (4.19).

$$K_{\text{torsion}} = \frac{60800}{\frac{1}{2\pi}s + 1} \frac{s + 2\pi}{s}. \quad (4.19)$$

4.7.5 MIMO stability

In order to be able to easily obtain stable closed-loop behavior, interaction between the individual feedback loops is ideally prevented by the diagonality of (4.17). However, in practice there will always be some interaction left. Therefore, the off-diagonal terms of the decoupled plant, G_{dec} , can be considered as an additive perturbation as shown in Fig. 4.7a, where $G_d = \text{diag}(G_{dec})$ and $G_{nd} = G - G_d$. The structured singular value can be used to evaluate the stability of the MIMO system with a decentralized (i.e. diagonal) feedback controller, K_d , (Skogestad and Postlethwaite, 2005; Grosdidier and Morari, 1986). The transfer function considering the diagonal terms only are given by,

$$\begin{aligned} S_d &= (I + G_d K_d)^{-1}, \\ T_d &= I - S_d. \end{aligned} \quad (4.20)$$

The output multiplicative error is then given by,

$$E = G_{nd} G_d^{-1}.$$

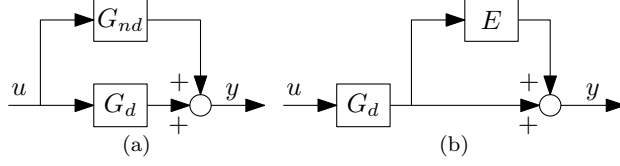


Figure 4.7: Plant representation with an (a) additive and (b) multiplicative output perturbation.

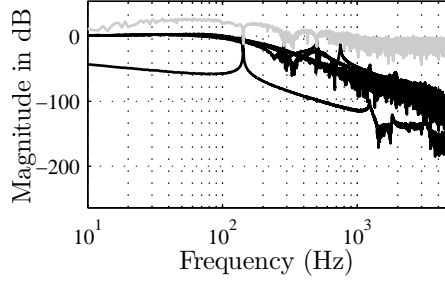


Figure 4.8: Sufficient condition for the stability of the system with decentralized controller K_{fb} . $\sigma(T_d)$ (—) and $\mu_{T_d}^{-1}$ (---). At the first internal mode, the sufficient criterion is not satisfied. Therefore, no conclusion can be drawn about stability from this condition.

If $(I + G_d K_d)^{-1}$ is stable, a sufficient condition for stability of $(I + G K_d)^{-1}$ is given by,

$$\bar{\sigma}(T_d(j\omega)) < \mu_{T_d}^{-1}(E(j\omega)), \quad \forall \omega, \quad (4.21)$$

where $\bar{\sigma}(\cdot)$ is the maximum singular value and μ_{T_d} is the structured singular value w.r.t. the diagonal structure of T_d from (4.20).

Remark 4.12. Typically it is assumed that G itself is stable to allow for independent design. In this case, the aim is only to evaluate the stability afterwards. Therefore, the stability of G is not required.

The condition (4.21) is shown in Fig. 4.8 for the decentralized controller K_{fb} in (4.18). It can be seen that condition (4.21) is not satisfied for all frequencies, therefore the stability of the system cannot be concluded using (4.21).

Therefore, the stability of the system is assessed using the characteristic loci (Skogestad and Postlethwaite, 2005) shown in Fig. 4.9. This figure shows that

the controlled MIMO system has a good MIMO phase margin. Furthermore, the circle of radius 0.5 around the -1 point is not entered. Therefore, the peak in the sensitivity function $\|S(j\omega)\|_\infty < 6$ dB, indicating sufficient robustness margins.

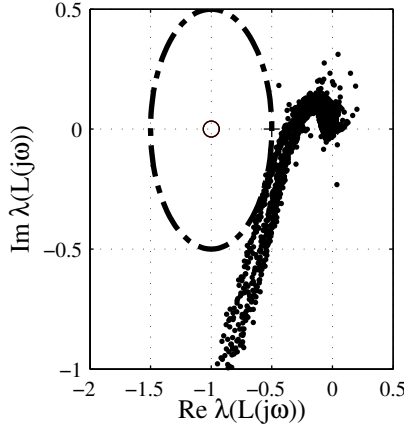


Figure 4.9: Characteristic loci.

4.7.6 Setpoint trajectory

The setpoint trajectory $r_m(t)$ for the z -direction is a third order point-to-point motion of $10 \mu\text{m}$, as shown in Fig. 4.10. The backward motion is exactly mirrored. After one sequence of forward and backward motion, a wait time of 0.25 s is introduced. This complete sequence is repeated six times. The setpoint trajectory for all other directions is zero.

For the input shaping case, the setpoint trajectory $r_m(t)$ is filtered by (4.15), such that the input shaped setpoint trajectory $r_{m,s}(t)$ is obtained.

4.7.7 Rigid-body and spatial feedforward design

To determine which modes are relevant, a standard rigid-body feedforward is applied to the system. The rigid-body decoupling matrix is defined by (4.4), with B_b from (4.1). For rigid-body feedforward design with four actuators, $T_{u,ff}$ is given in (C.1). The two last rows being zero indicates that only the first four actuators are employed to position the system.

The feedforward controller is given by,

$$K_{ff} = k_{fa} \cdot a, \quad (4.22)$$

where a is the acceleration of the (shaped) setpoint trajectory and k_{fa} is the mass parameter of the system. This parameter is determined by manual tuning.

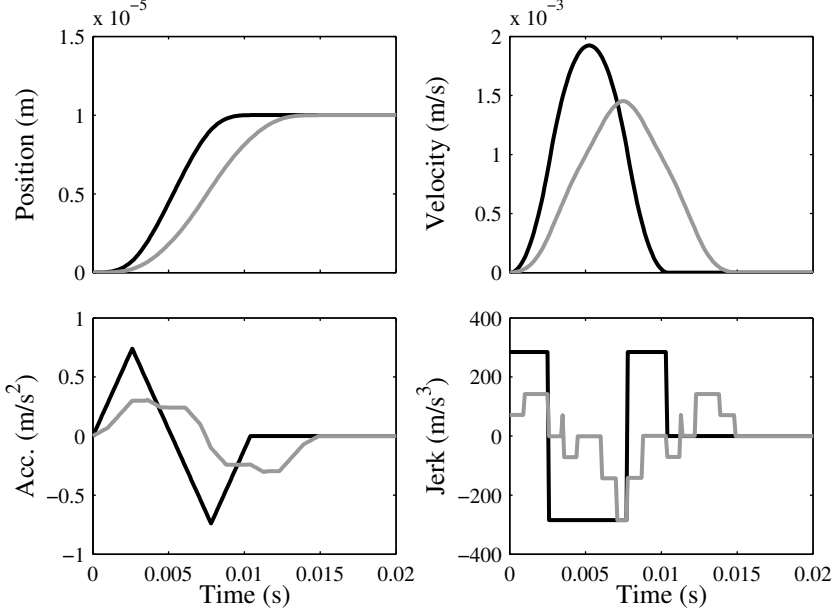


Figure 4.10: Setpoint trajectory for the position, velocity and acceleration and jerk for the translation in z -direction $r_m(t)$ (—) and shaped version $r_{m,s}(t)$ (—)

From the power spectral density of the servo-errors in Fig. 4.12 and Fig. 4.14 and the frequencies from Table 4.3, it is clear that the 5th internal mode is relevant for the z -direction. For the R_x and R_y direction, the internal modes 3 and 4 are relevant. Therefore, the spatial feedforward in the next section will be designed such that the internal modes 3, 4 and 5 are uncontrollable in the feedforward path.

The spatial feedforward decoupling $T_{u,ff}$ is designed such that the internal modes 3, 4 and 5 are uncontrollable according to Theorem 4.10. The numerical values of the spatial feedforward design are provided in Appendix C.

The result of both input transformations are shown in (C.2) and (C.3). In both cases it can be seen that the first three rigid-body modes are independently controllable, i.e. input one influences body-mode one, etc. In the case of rigid-body feedforward the third, fourth and fifth flexible modes are still excited from all input channels as can be seen in (C.2). However, in the case of spatial feedforward the third, fourth and fifth flexible mode are not excited, see (C.3). The first two flexible modes are still excited in both cases, however in the case of spatial feedforward this mode is excited more severely for all inputs, i.e. the same input signal will lead to a more severe excitation of the first two mode in case of spatial feedforward. Especially, the last column contains large numbers, which is not relevant for the presented case as the setpoint trajectory for the R_y direction is zero at all times.

In case of a non-zero setpoint trajectory for the R_y direction, a different selection of relevant modes has to be considered. Subsequently, the feedforward decoupling matrix can be solved according to Theorem 4.10 per input channel.

4.7.8 Results

In this section, the experimental results of the following three methods are presented,

Rigid body feedforward	$T_{u,ff} = T_b$	$F = I$
Spatial feedforward	$T_{u,ff} = T_b + T_s$	$F = I$
Input shaping	$T_{u,ff} = T_b$	$F = H(z)$

All methods use the same rigid-body feedforward controller (4.22). However, for spatial feedforward the static input transformation matrix $T_{u,ff}$ is different. For input shaping, the setpoint trajectory $r_m(t)$ is filtered by an ZV-input shaper as shown in Section 4.6. However, all tracking errors are determined with respect to the unshaped setpoint trajectory $r_m(t)$, i.e. $e_z(t) = r_m(t) - m(t)$. Here, $m(t)$ are the motion coordinates derived from the measurements by (4.16).

To illustrate the difference between these methods, the tracking errors for the z - and R_x -directions are shown in Fig. 4.11 and Fig. 4.13.

The three feedforward methods will be compared in terms of peak-error, RMS-error and added delay. These results are shown in Table. 4.6. The input shaping elongates the setpoint trajectory by 45 samples, i.e. approximately 4.5 ms.

If the z -direction is considered, input shaping performs the worst in terms of RMS- and peak error. Spatial feedforward perform the best in terms of RMS- and peak error. Furthermore, both spatial feedforward and input shaping don not excite the modes around 500 Hz, which are excited by rigid-body feedforward.

For the R_x -direction the difference is much more clear. Spatial feedforward outperforms both rigid-body feedforward and input shaping. Both the peak- and RMS-errors are approximately a factor 1.5 smaller for spatial feedforward compared to rigid-body feedforward. The results of spatial feedforward and input shaping are similar (within 20 %). However, it must be noted that the result for spatial feedforward has been obtained without introducing any delays in contrast to input shaping. The setpoint trajectory for input shaping is approximately 20% longer, see Fig. 4.10. The servo-error and its cumulative power spectral density in z -direction are shown in Fig. 4.11 and Fig. 4.12 respectively. In Fig. 4.11 it is clear that the error peaks during the non-zero phases of the setpoint as shown in Fig. 4.10, which can be expected due to the absence of snap feedforward. In the cumulative power spectral density of e_z , shown in Fig. 4.12, an increase of approximately 4 dB can be observed around 520 Hz for rigid-body feedforward. This can be explained by the internal modes 3, 4 and 5, which are excited by the setpoint trajectory. For spatial feedforward and input shaping this increase in

Method	$\max e_z $	$\text{RMS}(e_z)$	$\max e_{R_x} $	$\text{RMS}(e_{R_x})$
Rigid-body	0.4522	0.0976	0.1484	0.0323
Spatial	0.3057	0.0723	0.0969	0.0256
Input shaping	4.0257	0.8227	0.1261	0.0272

Table 4.6: Experimental results of the different methods. All values should be multiplied by 10^{-6} .

frequency content is much smaller compared to rigid-body feedforward. However, the slight increases in spectral content for spatial feedforward and input shaping indicate that compensation is still not perfect. Moreover, spatial feedforward performs worse than rigid-body feedforward in the frequency region below 520 Hz, which can be explained by the increased excitation of the modes which are not considered in the spatial feedforward design. However, the 2-norm of the error is significantly lower for spatial feedforward indicating a better overall performance.

The servo-error and its cumulative power spectral density in R_x -direction are shown in Fig. 4.13 and Fig. 4.14 respectively. The servo-error e_{R_x} , shown in Fig. 4.13, shows similar peaks during the nonzero jerk phases. In Fig. 4.14 the cumulative power spectral density of e_{R_x} is shown. For all three methods, a clear step in the spectral content around 500 Hz can be observed. Here, the difference between the methods is quite clear. For rigid-body feedforward the step is approximately 5 dB, while this is 0.3 dB and 0.9 dB respectively for input shaping and spatial feedforward.

In the cumulative power spectral density of e_{R_x} it is clearly visible that the proposed spatial feedforward improves the behavior of the system. This means that input directions are estimated with sufficient accuracy to design the spatial feedforward. However, the modes are still excited due to mismatches in the feedforward compensation and the model used to calculate the spatial feedforward. Any mismatch in the feedforward compensation leads to a servo-error. Since a different decoupling is used for the feedback controller, the relevant modes are possibly still excited by the feedback inputs. If additional sensors are present, additional feedback loops can be created to resolve this problem.

In Figs. 4.15 and 4.16 the measured tracking error in z -direction at the additional sensor (above the center of the stage) and its cumulative power spectral density are shown respectively. The tracking error in Fig. 4.15 is comparable to Fig. 4.11 despite the lower resolution of the additional sensor. In the CPSD in Fig. 4.16 it can be seen that rigid-body feedforward clearly excites the internal modes around 500 Hz. Moreover, some higher order internal modes can be observed as well. For spatial feedforward it is clear that the modes around 500 Hz are not excited anymore, which leads to an overall performance increase. Moreover, similar phenomena as in Fig. 4.12 can be observed, i.e. at frequencies below 520 Hz rigid-body feedforward performs better, but the overall performance of spatial feedforward is better.

4.8 Conclusion

In this chapter a novel feedforward control design method, called spatial feedforward, for over-actuated flexible motion systems is presented. This method employs the extra design freedom for the input, such that n_s (degree of over-actuation) of the internal modes will not be excited. Also, conditions for the existence of a spatial feedforward controller are explicitly derived. Furthermore, this method has been experimentally validated on an industrial prototype lightweight motion system. The method is compared to standard mass feedforward and input shaping. Input shaping is a common method to design input signals for flexible systems, such that this results in global performance. The proposed method has similar properties to input shaping, without altering the setpoint trajectory. Both methods result in global performance, i.e. at any point of the flexible structure.

The method presented in this chapter heavily relies on the availability of a complex MIMO plant model to compute a (non-square) feedforward decoupling, such that excitation of the flexible modes by the feedforward can be prevented. Since the mode shapes from the model are never exact, data-based methods to optimize the spatial feedforward may be applied to improve the final performance. In the next chapter a data-based feedforward control design method to exploit the design freedom from over-actuation and over-sensing is presented.

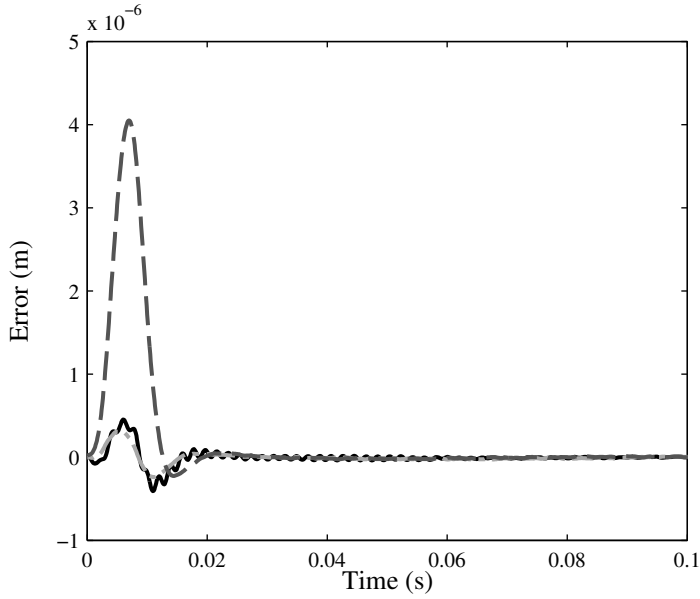


Figure 4.11: Measured servo-error e_z for rigid-body feedforward (—), spatial feedforward (—·) and input shaping (--).

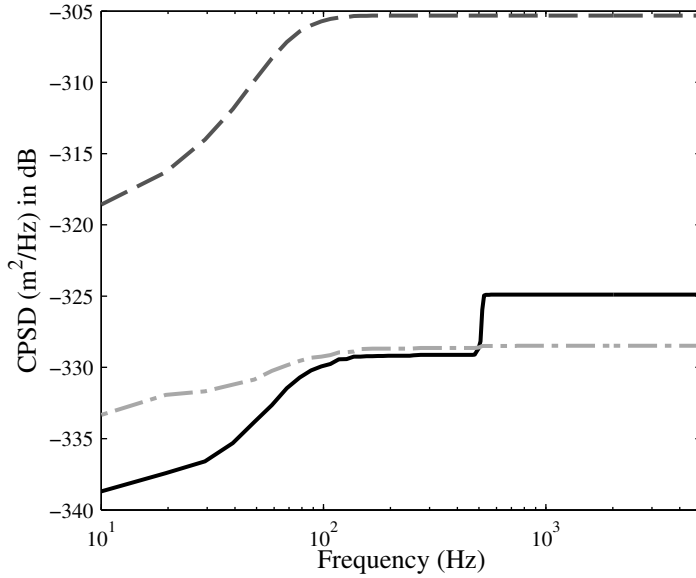


Figure 4.12: Cumulative power spectral density of measured e_z for rigid-body feedforward (—), spatial feedforward (—·) and input shaping (--).

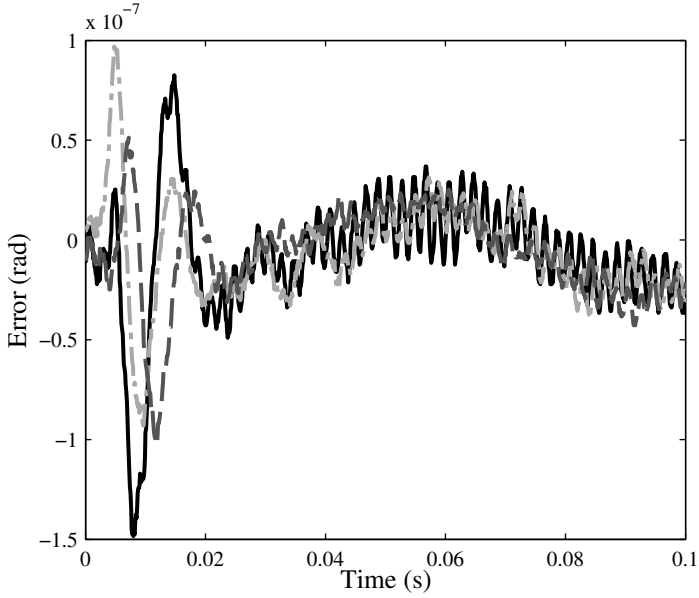


Figure 4.13: Measured servo-error e_{R_x} for rigid-body feedforward (—), spatial feedforward (---) and input shaping (-·-).

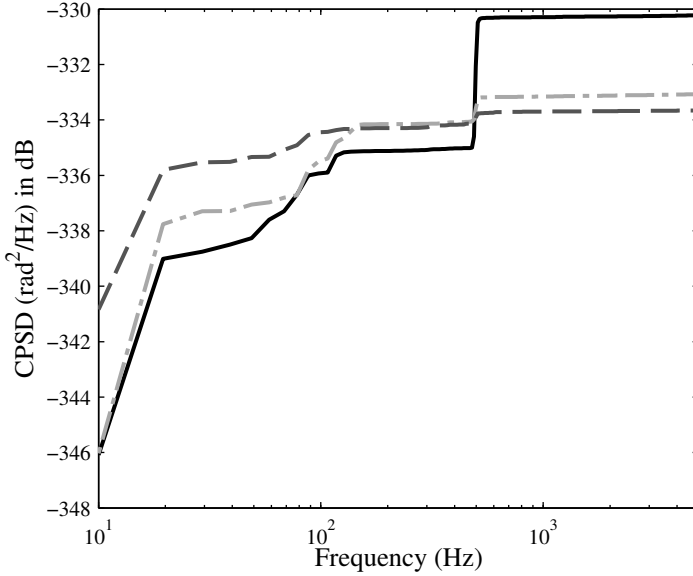


Figure 4.14: Cumulative power spectral density of measured e_{R_x} for rigid-body feedforward (—), spatial feedforward (---) and input shaping (-·-).

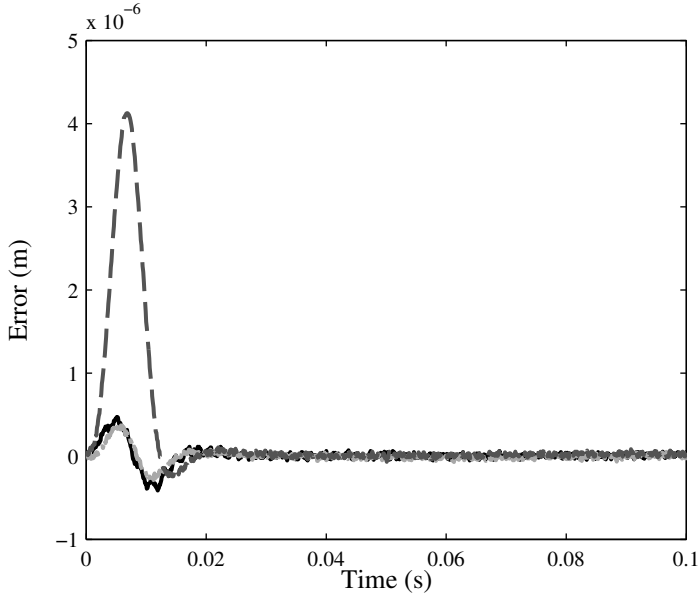


Figure 4.15: Measured servo-error e_z at the performance location for rigid-body feedforward (—), spatial feedforward (— ·) and input shaping (— —).

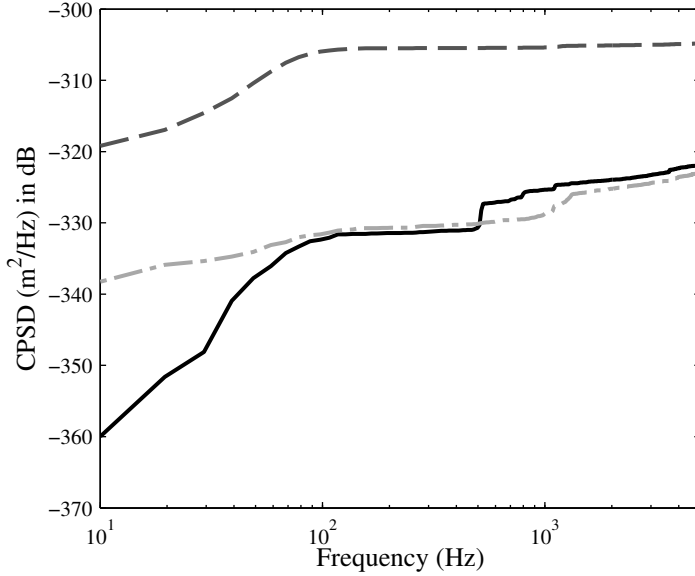


Figure 4.16: Cumulative power spectral density of measured e_z at the performance location for rigid-body feedforward (—), spatial feedforward (— ·) and input shaping (— —).

Chapter 5

Data-based spatial feedforward control for over-actuated motion systems

FOR advanced motion systems there is an increasing demand for higher production throughput and accuracy. Traditionally, such systems are designed using a rigid-body design paradigm, which aims at designs with high stiffness. The alternative is to design a lightweight system and deal with the resulting flexibilities by over-actuation and over-sensing. This chapter presents a data-based spatial feedforward method based on previous task trials, which aims at reducing the vibrations over the complete structure during motion. The proposed method is experimentally validated on an industrial prototype and compared to standard mass feedforward using rigid-body decoupling.

5.1 Introduction

In the semiconductor industry there is an ever increasing demand for higher throughput and accuracy (Moore, 1965). These demands lead to more aggressive motions and larger wafer sizes, which both lead to larger required forces to actuate the system. Moreover, miniaturization leads to higher demands on accuracy, which results in a higher required bandwidth of the system. Therefore, a system with increased stiffness is required, which possibly leads to more mass. The increased forces, due to increased mass and acceleration, lead to higher specifications on the actuators, amplifiers and cooling. In the rigid-body design paradigm this leads in an evolutionary way to systems with an increasing mass, which is expected to become infeasible in the near future due to thermal constraints. For a general introduction to the control of advanced motion systems see (Steinbuch and Norg, 1998; Clayton et al., 2009; Butler, 2011).

Therefore, the next generation of advanced motion systems, e.g. wafer-stages, pick-and-place machines and planar motors, will be lightweight. Compared to a rigid-body design, the differences in control design are:

1. mechanical resonances near the desired bandwidth of the feedback controlled system, and
2. due to the elastic deformations in the moving stage, the relation between the measured variables y and the performance variables z cannot be considered to be static anymore. Therefore, it does not suffice anymore to use geometric relations to calculate/control the performance variables. The difference between measurement and performance variables is illustrated in Fig. 3.1.

To deal with the challenges of advanced lightweight systems, such systems are typically equipped with extra sensors and actuators compared to traditional design, i.e. over-sensing and over-actuation is applied (Schneiders et al., 2003, 2004a,b). Furthermore, to obtain the desired performance it is typically required to apply feedforward control. However, traditional feedforward methods do not take advantage of over-sensing and over-actuation.

Snap feedforward (Lambrechts et al., 2005; Steinbuch et al., 2010) compensates the low-frequency contributions of the flexible modes, i.e. the deformation due to compliance during motion. However, such approaches only guarantee the performance at the sensors locations and not for the whole structure.

In van der Meulen et al. (2007, 2008) the parameters of a fixed-structure feedforward controller are optimized based on the measured tracking error of a previous experiment. Since this fixed-structure is based on snap feedforward, it suffers from the same drawbacks. In Baggen et al. (2008); Heertjes et al. (2010) a multivariable gradient-approximation-based algorithm is used to optimize a set of FIR feedforward filters. Since these feedforward filters can be of high order, it is possible to compensate more than the deformation due to compliance during motion. Never-

theless, no guarantees can be provided about the performance over the complete flexible structure. Additionally, in Bruijnen and van Dijk (2012) it is shown that a second FIR filter is required to exactly obtain a zero error at the sensor locations in the ideal case. All fixed-structure feedforward methods can be regarded as ILC with basis functions, as shown in van de Wijdeven and Bosgra (2010).

Learning control methods (Moore, 1998; Longman, 2000; Bristow et al., 2006; Ahn et al., 2007), such as iterative learning control (ILC) and repetitive control, use data from previous task trials to improve the performance. However, such methods do not provide any guarantees on global performance. Furthermore, the learned feedforward signal is specific for a chosen setpoint trajectory.

A different approach is presented in Heertjes and van de Molengraft (2009), where the feedforward signal from a converged ILC sequence is mapped into a FIR filter. In this way a setpoint trajectory invariant filter is created, which removes one of the common drawbacks of ILC.

In Butler (2013), an adaptive feedforward method with application to a long-stroke stage is presented. The advantage of this method is that differences due to position dependency can be compensated for, in contrast to ILC and fixed-structure feedforward. The presented framework aims at correcting the rigid-body behavior due to position dependency and does not exploit over-actuation. Therefore, only performance at the sensor locations can be guaranteed and it is expected that this will not result in the desired global performance for lightweight systems. Furthermore, actuators at fixed locations are considered in this chapter, which typically have less or no position dependency.

A common approach to prevent the excitation of flexible modes is input shaping (Pao, 1999; Singh, 2010). Typically, the setpoint trajectory is convolved with an input shaping filter, such that the resonance frequencies of the system are removed from the setpoint trajectory. Input shapers with positive coefficients are designed, such that the filtered signal satisfies the same bound as the original signal. However, by using such methods, a delay is introduced, which is not desired in the intended applications. It is possible to overcome this drawback by allowing negative coefficients for the input shaper. However, by doing so there are no guarantees for the filtered signals.

Model-based spatial feedforward as presented in Chapter 4 and in Ronde et al. (2012b, 2013b) is a novel feedforward method for over-actuated systems, which provides guarantees for performance over the whole structure, i.e. *global performance*. However, this method relies heavily on the availability of a complex MIMO plant model to compute a (non-square) feedforward decoupling, such that excitation of the flexible modes by the feedforward can be prevented. Spatial feedforward can in fact be viewed as a special case of static input-output decoupling, see Vaes (2005). However, the typical aim and design freedom are quite different from standard input-output decoupling. In standard input-output decoupling the aim is to diagonalize the decoupled plant, in order to facilitate decentralized feedback control

design. Furthermore, static pre- and post-transformation matrices are available in contrast to spatial feedforward, where only a pre-transformation matrix is available. Therefore, standard input-output decoupling methods cannot be applied in a straightforward manner.

The approach presented in this chapter shows an analogy with iterative feed-back tuning (IFT). For an overview of IFT see Hjalmarsson et al. (1998); Hjalmarsson (2002); Gevers (2002). The method presented in this chapter has the advantage over IFT that closed-loop stability is not endangered, since only the feedforward controller is optimized. An IFT approach to decoupling is presented in Gunnarsson et al. (2003); Mišković et al. (2007), which both suffer from the same drawbacks as standard input-output decoupling methods.

In contrast to Chapter 4 and Ronde et al. (2013b), it is assumed that only a model of the rigid-body behavior is available, i.e. without the flexible behavior. The intermediate step of obtaining a parametric MIMO plant model, such as is illustrated in Oomen et al. (2013), is replaced by a dedicated parameter identification experiment. Furthermore, a data-based approach results in optimal controller parameters with respect to the actual plant, which is typically not the case for manual tuning or model-based approaches.

In contrast to the approaches in van der Meulen et al. (2007, 2008) and Baggen et al. (2008); Heertjes et al. (2010), this chapter deals with over-actuated feedforward control, which results in feedforward controllers with an unequal number of input and outputs. Thereby exploiting the additional design freedom. Moreover, the class of systems considered in this chapter, i.e. lightweight motion systems, can be considered as proportionally damped systems due to their low damping. This allows for the representation of these systems in modal form, which is exploited in this chapter. The use of an initial feedforward controller with inaccurate estimates of the mass and principle moments of inertia of the system can cause errors which are orders of magnitude larger than the vibrations of the system. Therefore, the feedforward controller and feedforward decoupling are combined in one simultaneous optimization.

The contribution of the chapter is fourfold, namely to provide a method which:

1. optimizes the over-actuated feedforward design, based on measurement data, as an extension of Chapter 4 and Ronde et al. (2012b, 2013b),
2. estimates mass and principle moments of inertia,
3. does not require the selection of modes, and finally
4. exploits the use of over-sensing.

Moreover, similar to model-based spatial feedforward from Chapter 4 and Ronde et al. (2013b) the presented method results in a parametric feedforward controller, i.e. suitable for different setpoint trajectories. Furthermore, this method does not introduce any delay or modification of the setpoint trajectory in contrast to input shaping.

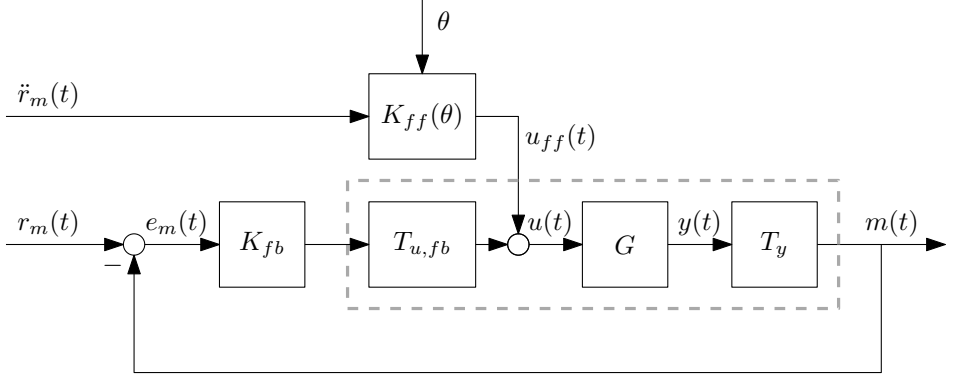


Figure 5.1: Control structure for spatial feedforward. Here G is the plant to be controlled, with input $u(t)$ and sensor outputs $y(t)$. The static pre- and post-transformation matrices $T_{u,fb}$ and T_y are used to decouple the system, such that a decentralized feedback controller K_{fb} can be used to control the individual feed-back loops. Furthermore, the post-transformation matrix T_y transforms the sensor output $y(t)$ to motion coordinates $m(t)$. The (non-square) feedforward controller $K_{ff}(\theta)$ is designed such that the motion errors are minimized. The setpoint trajectory and tracking error in motion coordinates are denoted by $r_m(t)$ and $e_m(t)$ respectively.

The outline of this chapter is as follows. In Section 5.2 the problem is formulated. Subsequently, in Section 5.3 spatial feedforward is briefly discussed. The proposed data-based optimization algorithm is presented in Section 5.4. Also different methods for gradient estimation are presented. The data-based optimization is applied to an industrial prototype motion system in Section 5.5, where the method is also compared to mass feedforward with standard body-mode decoupling. Finally, in Section 5.6 the conclusions and recommendations are presented.

5.2 Problem formulation

Consider a motion system with modal or proportionally damped modes. Such systems can be written in the following modal description (Gawronski, 2004):

$$\begin{aligned} G(s) &= C_m [Is^2 + 2Z\Omega s + \Omega^2]^{-1} B_m, \\ &= \begin{bmatrix} C_b & | & C_{int} \end{bmatrix} \left[\frac{\Theta^{(b)}(s)}{\Theta^{(int)}(s)} \right] \begin{bmatrix} B_b \\ B_{int} \end{bmatrix}, \end{aligned} \quad (5.1)$$

where B_m and C_m represent the model input- and output matrices respectively. The matrices Z and Ω contain the damping and resonance frequencies, respectively,

which are diagonal under the assumption of proportional damping. Therefore, the matrices $\Theta^{(b)}(s)$ and $\Theta^{(int)}(s)$ are diagonal and contain the second-order transfer functions of the (rigid) body modes and internal modes respectively. Furthermore B_{mi} , i.e. the i -th row of B_m , is associated with the i -th mode only. Moreover, the input- and output matrices B_m and C_m are divided corresponding to the (rigid)body and internal modes into the pair B_b and B_{int} and into the pair C_b and C_{int} , respectively.

Remark 5.1. The dependency on time or Laplace operator is dropped from the notation when this is clear from the context.

The system $G(s)$, having n_u inputs and n_y outputs, is controlled using the control structure shown in Fig. 5.1. The static transformation matrices $T_{u,fb}$ and T_y are used to decouple the system as $G_d = T_y G T_{u,fb}$, to allow for decentralized feedback control. The motion $m(t)$ represents the pose of a motion system. The mapping between the sensors $y(t)$ and the measured rigid-body motion $m(t)$ is given by:

$$m(t) = T_y y(t), \quad (5.2)$$

where $m(t)$ typically has dimension n_b .

The goal is to compute a non-square feedforward controller $K_{ff}(\theta)$, based on experimental data from previous task trials, such that:

1. the body-modes are independently controllable, and
2. the tracking errors $e_m(t)$ from Fig. 5.1 are minimized using the additional design freedom from over-actuation.

Remark 5.2. The choice of a static transformation matrix T_y is not unique, i.e. any scaling or linear combination of translations/rotations can be taken. In Section 5.5.3, a choice will be made based on physical interpretation.

Definition 5.3 (Body mode). The body modes are defined as the set of rigid-body and suspension modes. The number of body modes is denoted by n_b .

Definition 5.4 (Suspension mode). A suspension mode has, by design, a significantly lower resonance frequency than the internal modes, i.e. the structural stiffness of the suspension system to the fixed world is much smaller than the body stiffness.

Definition 5.5 (Internal mode). Internal modes are the non-intentional flexible modes due to the finite stiffness of the moving structure, which is in general undesired. Theoretically an infinite number of modes exist. However, the number of relevant internal modes (Hughes, 1987) is finite and is denoted by n_r .

Definition 5.6. The number of internal modes to be suppressed by spatial feedforward is denoted by n_m , with $n_m \ll n_r$.

In this chapter the following assumptions are made:

1. linear time-invariant (LTI) system behavior, and
2. proportional damping of the modes, and
3. over-actuated system, i.e. $n_u > n_b$, and finally
4. the relevant modes must be observable from the sensor outputs.

The first two assumptions are required for a model in the form of (5.1) to exist. The third assumption is required for spatial feedforward to exist. The last assumption is required to include the relevant phenomena in the cost-function.

The feedforward controller is assumed to have the following standard form,

$$K_{ff}(\theta) = T_{u,ff}(\theta) \overline{K_{ff}},$$

where

$$\overline{K_{ff}} = \begin{bmatrix} \hat{m} & & & & \\ & \hat{m} & & & \\ & & \hat{J}_z & & \\ & & & \hat{m} & \\ & & & & \hat{J}_x \\ & & & & & \hat{J}_x \end{bmatrix},$$

where \hat{m} is the estimated mass and \hat{J}_x, \hat{J}_y and \hat{J}_z are the estimated principle moments of inertia of the moving mass. Furthermore, the rigid-body dynamics of the plant are assumed to be decoupled by T_y and $T_{u,ff}(\theta)$ (typically into cartesian coordinates), i.e. the decoupled plant becomes diagonal.

Remark 5.7. In this chapter, the basis functions are limited to the setpoint trajectory acceleration. This is due to the fact that in the ideal case the system behaves as an inertia without flexibilities.

5.3 Spatial feedforward

This section will present a brief introduction of spatial feedforward as presented in Chapter 4 and Ronde et al. (2013b). For extensive details, the reader is referred to Chapter 4. Subsequently, the design space including mass and principle moments of inertia will be parameterized. This parametrization will be employed in the data-based optimization presented in this chapter.

For spatial feedforward, $T_{u,ff}$ is selected such that,

1. the body-modes can be controlled individually, and
2. the selected internal modes are not excited,

from the feedforward inputs. Hereto, the following equation must be satisfied,

$$B_b T_{u,ff} = \Lambda, \quad (5.3)$$

where Λ is any diagonal matrix, such that the body-modes can be feedforward controlled individually. Without loss of generality $\Lambda = I$ can be selected, see Lemma D.2. Hereto,

$$T_{u,ff} = B_b^\dagger,$$

where $(\cdot)^\dagger$ denotes the pseudo-inverse (Ben-Israel and Greville, 2003), which is selected to obtain the minimum energy solution. This solution is denoted as,

$$T_b := B_b^\dagger.$$

Remark 5.8. An alternative choice can be made such that the mass and principle moments of inertia of the feedforward decoupled system remain the same, i.e. they retain their physical relevance.

Since the system (5.1) is assumed to be over-actuated, the matrix B_b is fat, i.e. it has more actuators (inputs) than rigid-body modes. Therefore, there are multiple solutions having the same effect on the body modes of the system, as shown in Chapter 4 and Ronde et al. (2013b). Hence, the static transformation matrix for feedforward control can be represented as follows,

$$T_{u,ff} = T_b + T_s,$$

where

$$T_s \in \mathbb{R}^{n_u \times n_b} \mid \text{Im}(T_s) = \ker(B_b).$$

All the directions contained in T_s have the physical property that the sum of forces and the sum of moments around the centre of gravity are equal to zero. To achieve that the selected internal modes are not excited $T_{u,ff}$ should be selected such that,

$$\begin{bmatrix} B_b \\ \widetilde{B_{int}} \end{bmatrix} T_{u,ff} = \begin{bmatrix} I_{n_b} \\ O_{n_m} \end{bmatrix}.$$

This formulation takes into account that only the excitation of n_m modes from B_{int} can be prevented. The selection of n_m modes from B_{int} are contained in $\widetilde{B_{int}}$. To employ this design freedom, a basis W ,

$$W = [w_1 \quad \cdots \quad w_{n_s}] \mid \text{span}(W) = \ker(B_b), \quad (5.4)$$

which is a basis for $\ker(B_b)$ is constructed.

Subsequently, a parametrization of the spatial design freedom is constructed. Until now, it was implicitly assumed that the mass and inertia of the system are

exactly known, which is typically not the case in practice. The errors due to inaccurate mass and inertia estimates are typically large compared to the oscillations of the flexible modes. To obtain the desired solution it is required to estimate the mass and inertia as well. Therefore, this section provides an extended parametrization, such that the mass and inertia can be estimated. Furthermore, the parametrization is chosen such that the mass and inertia parameters retain their physical relevance.

The design freedom of the feedforward controller is parameterized as follows,

$$K_{ff}(\theta) = T_b \overline{K_{ff}} + \sum_{j=1}^{n_s} \Psi_j \Theta_j, \quad K_{ff}(\theta) \in \mathbb{R}^{n_u \times n_b}, \quad (5.5)$$

where Ψ_j is the matrix with the design freedom w_j and is defined as,

$$\Psi_j = \begin{bmatrix} w_j & w_j & w_j & w_j & w_j & w_j \end{bmatrix}, \quad \Psi_j \in \mathbb{R}^{n_u \times n_b}.$$

The diagonal matrices Θ_j contain the parameters θ_{jn_b+i} for the i -th body mode and the j -th design freedom. Considering all body-modes of interest, e.g. $n_b = 6$, this results in,

$$\Theta_j = \begin{bmatrix} \theta_{jn_b+1} & & & & & \\ & \theta_{jn_b+2} & & & & \\ & & \theta_{jn_b+3} & & & \\ & & & \theta_{jn_b+4} & & \\ & & & & \theta_{jn_b+5} & \\ & & & & & \theta_{jn_b+6} \end{bmatrix}, \quad \Theta_j \in \mathbb{R}^{n_b \times n_b}. \quad (5.6)$$

Furthermore, let $\Psi_0 := T_b$ and Θ_0 as defined in (5.6). Including these definitions in (5.5) results in,

$$K_{ff}(\theta) = \sum_{j=0}^{n_s} \Psi_j \Theta_j. \quad (5.7)$$

Without loss of generality, an initial estimate of the mass and principle moments of inertia can be included as,

$$K_{ff}(\theta) = \Psi_0 \overline{K_{ff}} + \sum_{j=0}^{n_s} \Psi_j \Theta_j. \quad (5.8)$$

This parametrization of the feedforward controller will be employed in the formulation of the optimization problem, which is presented in the next section.

5.4 Optimization

In contrast to Chapter 4 and Ronde et al. (2012b, 2013b) it is assumed that only a model of the body-modes is available. Therefore, without the model of the flexible

modes the model-based solutions cannot be computed. Using the model of the body-modes, the space which can be used to optimize the spatial feedforward can be computed using (5.4). This space is subsequently used in the optimization method as presented in the remainder of this section.

5.4.1 Objective function

To optimize the parameters of the spatial feedforward, an objective function has to be chosen, such that it represents the behavior that is subject to improvement. In this section, only the tracking errors $e_m(t)$ are minimized for simplicity of presentation. Additional signals, such as measurements of the elastic deformation, can be used in the objective function as well, which is shown in Section 5.5.

Definition 5.9 (Task trial). A task trial is the execution of one experiment with a length of N samples and starting from the same initial conditions.

$$\min_{\bar{\theta}_l} V(\bar{\theta}_l). \quad (5.9)$$

Here, a signal based objective function $V(\bar{\theta}_l) : \mathbb{R}^{Nn_b} \rightarrow \mathbb{R}$ is chosen,

$$V(\bar{\theta}_l) = e_{m,l}^T(\bar{\theta}_l) \Gamma e_{m,l}(\bar{\theta}_l), \quad \bar{\theta}_l = [\theta_1 \quad \cdots \quad \theta_n]^T, \quad (5.10)$$

where $e_{m,l}(\bar{\theta}_l)$ is the error in motion coordinates at the l -th task trial and $\bar{\theta}_l$ is the vector with the stacked parameters from (5.7). The matrix Γ is used to weight the relative importance of different directions in the optimization criterion.

$$e_{m,l} = \begin{bmatrix} e_{x,l} \\ e_{y,l} \\ e_{R_z,l} \\ e_{z,l} \\ e_{R_x,l} \\ e_{R_y,l} \end{bmatrix}, \quad \Gamma = \begin{bmatrix} \gamma_x & & & & & \\ & \gamma_y & & & & \\ & & \gamma_{R_z} & & & \\ & & & \gamma_z & & \\ & & & & \gamma_{R_x} & \\ & & & & & \gamma_{R_y} \end{bmatrix}, \quad \Gamma \in \mathbb{R}^{Nn_b \times Nn_b},$$

where $e_{m,l} \in \mathbb{R}^{Nn_b \times 1}$, $\gamma_i = \bar{\gamma}_i I \in \mathbb{R}^{N \times N}$, $i \in \{x, y, R_z, z, R_x, R_y\}$, with $\bar{\gamma}_i > 0$ being a scalar constant.

Remark 5.10. In this section, the objective function (5.10) is tailored towards non over-sensed systems to limit the length of the presentation. However, the objective function can be extended to an arbitrary number of motion directions, i.e. $\dim(m) > n_b$. An example will be shown in Section 5.5.

The second-order Taylor-approximation of (5.10) around $\bar{\theta}_l = 0$ is given by,

$$V(\bar{\theta}_l) = V(0) + \nabla V(0)^T \bar{\theta}_l + \frac{1}{2} \bar{\theta}_l^T \nabla^2 V(0) \bar{\theta}_l + \mathcal{O}(\bar{\theta}_l^3).$$

Therefore,

$$\begin{bmatrix} \frac{\partial V(\bar{\theta}_l)}{\partial \theta_1} \\ \vdots \\ \frac{\partial V(\bar{\theta}_l)}{\partial \theta_n} \end{bmatrix} = \nabla V(0) + \nabla^2 V(0) \bar{\theta}_l,$$

where n denotes the number of parameters and the gradient is given by,

$$\nabla V(0) = \begin{bmatrix} \frac{\partial V(0)}{\partial \theta_1} \\ \vdots \\ \frac{\partial V(0)}{\partial \theta_n} \end{bmatrix} = 2\nabla e_{m,l}^T(0) \Gamma e_{m,l}(0), \quad (5.11)$$

and the Hessian is given by,

$$\nabla^2 V(0) = 2\nabla e_{m,l}^T(0) \Gamma \nabla e_{m,l}(0) + 2\nabla^2 e_{m,l}^T(0) \Gamma e_{m,l}(0). \quad (5.12)$$

5.4.2 Gauss-Newton optimization

The parameters can be updated using Newton's method (Heath, 2002; Boyd and Vandenberghe, 2004) as,

$$\bar{\theta}_{l+1} = \bar{\theta}_l - \alpha_s (\nabla^2 V(\bar{\theta}_l))^{-1} \nabla V(\bar{\theta}_l), \quad (5.13)$$

where α_s is a fixed step size. To improve the convergence speed, α_s can be optimized using a line-search algorithm. However, in this case a fixed step size α_s is considered.

The Hessian in (5.12) can be approximated as,

$$\nabla^2 V(0) \approx 2\nabla e_{m,l}^T(0) \Gamma \nabla e_{m,l}(0), \quad (5.14)$$

since the motion errors $e_{m,l}$ are close to zero near the solution. Furthermore, the Hessian $\nabla^2 e_{m,l}(0)$ is assumed to be small.

Using (5.14) as approximation of the Hessian equals the Gauss-Newton method (Ruszczyński, 2006). The same method has been employed in both van der Meulen et al. (2007, 2008) and Baggen et al. (2008); Heertjes et al. (2010). The conditions for convexity of $V(\bar{\theta}_l)$ are shown in Theorem D.1.

Procedure 5.11. The optimization procedure can be applied as follows:

1. Do an experiment with $\bar{\theta}_0 = 0$.
2. Estimate the gradient (5.11) and the Hessian (5.14) of $V(\bar{\theta}_l)$ (offline).
3. Do a Gauss-Newton update of the parameters (5.13) (offline).
4. Increase the number of trials, i.e. $l = l + 1$.

5. Repeat steps 2-4 until convergence is achieved.

Corollary 5.12. *From (5.17) it is clear that $\frac{\partial e_m}{\partial \theta_k}$ is independent of $\bar{\theta}_l$. Therefore, the gradient (5.16) is independent of the parameters $\bar{\theta}_l$. By virtue of this property, an approximation $\nabla e_{m,l}^T(\bar{\theta}_l)$ around zero can be used for all task trials.*

5.4.3 Gradient-estimation methods

To estimate the gradient and the Hessian, two approaches can be followed:

1. model-based estimation, i.e. the Hessian is estimated using model-based knowledge, while the gradient is estimated using model-based and measurement information, and
2. perturbation of the parameters method. To estimate the gradient by perturbation of the parameters, using a finite difference approximation.

The model-based estimation is cheap, since the required number of experiments is limited, i.e. a model of the process sensitivity is required. The perturbation of parameters method is more accurate and more expensive in terms of required number of experiments. There are several techniques available to reduce the number of experiments (Spall, 1992, 1997). However, this is beyond the scope of this chapter.

Model-based gradient estimation

Even if a MIMO plant model, including the flexible modes, is available it is not obvious to select the modes which are not excited by the feedforward. Therefore, the model can be used to construct the gradient. Subsequently, the data-based optimization method can be employed to find the optimal solution given the cost-function in (5.9).

The tracking error $e_m(t)$ for the l -th task trial is given by,

$$\begin{aligned} e_{m,l}(\bar{\theta}_l) &= S_{o,d} (I - T_y G K_{ff}(\theta_l) s^2) r_m, \\ &= S_{o,d} \left(I - T_y G (\Psi_0 \overline{K_{ff}} + \sum_{j=0}^{n_s} \Psi_j \Theta_j s^2) \right) r_m, \end{aligned} \quad (5.15)$$

where the decoupled output sensitivity is given by,

$$S_{o,d} = (I + T_y G T_{u,fb} K_{fb})^{-1}.$$

In (5.15) it can be observed that the error is affine in the parameters $\bar{\theta}_l$. The

gradient of the motion error w.r.t. the parameters is given by,

$$\nabla e_{m,l}^T(\bar{\theta}_l) = \begin{bmatrix} \frac{\partial e_{m,l}^T(\bar{\theta}_l)}{\partial \theta_1} \\ \vdots \\ \frac{\partial e_{m,l}^T(\bar{\theta}_l)}{\partial \theta_n} \end{bmatrix}, \quad (5.16)$$

where the derivatives w.r.t. a single parameter are given by,

$$\frac{\partial e_{m,l}(\bar{\theta}_l)}{\partial \theta_k} = -S_{o,d} T_y G \bar{\Psi}_{ji} \ddot{r}_m. \quad (5.17)$$

Here, $\bar{\Psi}_{ji}$ denotes the j -th design freedom in the i -th input channel and is defined as,

$$\bar{\Psi}_{ji} = [0_{n_u \times i-1} \quad w_j \quad 0_{n_u \times n_b-i}],$$

i.e. the column of Ψ_j associated with the parameter $\theta_{j n_b + i}$.

Gradient estimation by parameter perturbation

The gradient and the Hessian can be approximated by doing perturbed-parameters experiments. The first-order Taylor series approximation of the motion error for a perturbation of the parameters is given by,

$$e_{m,l}(\delta\theta_k) = e_{m,l}(0) + \frac{\partial e_{m,l}(0)}{\partial \theta_k} \delta\theta_k + \mathcal{O}(\delta\theta_k^2). \quad (5.18)$$

Using (5.18) the gradient of the error w.r.t. the parameters can be constructed as,

$$\frac{\partial e_{m,l}(0)}{\partial \theta_k} \approx \frac{e_{m,l}(\delta\theta_k) - e_{m,l}(0)}{\delta\theta_k}, \quad (5.19)$$

where $e_m(0)$ and $e_m(\delta\theta_k)$ denote the motion error with non-perturbed parameters and the motion error with perturbed parameters. respectively. The size of the parameter perturbation is denoted by $\delta\theta_k$.

Remark 5.13. The feedforward controller and the 'spatial' decoupling are combined in this chapter, to provide one optimization framework. However, for implementation the feedforward controller and the decoupling can be separated again. The details are provided in Appendix D.1.

5.5 Experimental validation

In this section the data-based solution will be compared to mass feedforward using a standard body-mode decoupling.

5.5.1 Prototype lightweight motion system

In Fig. 4.3, an industrial prototype lightweight motion system is shown. This stage can move in all 6 degrees of freedom, with a limited stroke of approximately 0.5 mm in x, y and z -direction and 1 mrad in R_x, R_y and R_z -direction. To limit the complexity and length of the presentation only the out-of-plane directions, i.e. z , R_x , and R_y , will be considered. For these directions, 9 Lorenz type actuators are available on a 3 by 3 grid as shown in Fig. 5.2. The position of the stage in z -direction is measured at the corners by linear incremental encoders with a resolution of 1 nm. Additionally, an extra output has been added to the optimization, which measures the internal deformation (torsion) of the stage, i.e. over-sensing is applied. This is elaborated in Section 5.5.3. Moreover, a piezo strain sensor is present to measure internal deformation of the stage. This sensor will only be used for validation purposes. Furthermore, gravity compensators are present, such that ideally the stage is freely floating in its operating point.

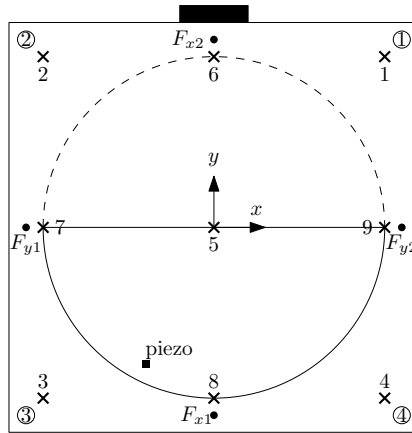


Figure 5.2: Sensor- and actuator layout of the industrial prototype motion system (top view). The crosses mark the actuators and the circles mark the sensors for the z -direction. The square indicates the location of the piezo strain sensor. The black rectangle on top represents the cable support to the fixed world.

5.5.2 Identification

A non-parametric frequency response function (FRF) is obtained by subsequently exciting each input with a multisine (Pintelon and Schoukens, 2001) in closed-loop. While doing these experiments, the stage is controlled to a fixed position in x, y and R_z -direction. As an example, the z -direction of the measured decoupled plant is shown in Fig. 5.3, where resonance phenomena can be observed at 143, 286, 502,

521, 751 and 1925 Hz. The resonance frequencies observed in the measurements differ from the resonance frequencies of the model as shown in Table 4.3, which can be attributed to model uncertainty. Moreover, not all resonance frequencies are observed from every input-output combination.

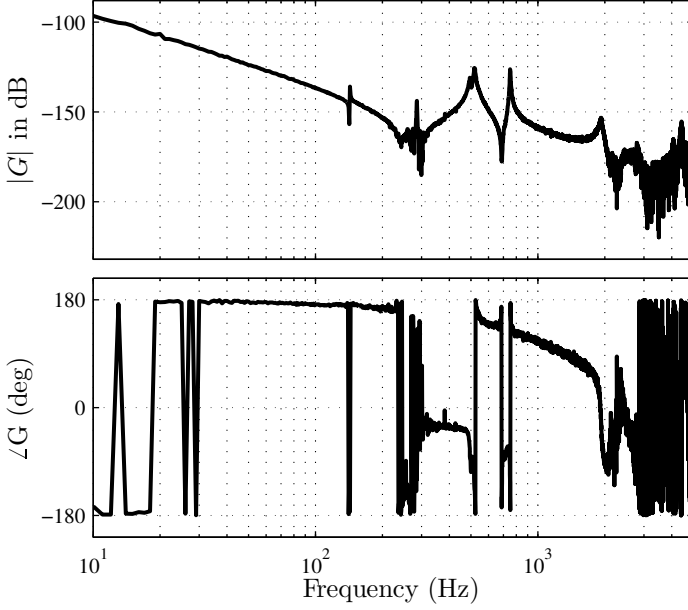


Figure 5.3: Bode diagram of the frequency response measurement of $T_y GT_{u,fb}$ in z -direction of the industrial prototype motion system.

A Finite Element Method (FEM) has been used to obtain a model in the form of (5.1) for the rigid-body modes of the system. The input matrix of the body-modes from the FEM model is given in Appendix D.4 in (D.1). The matrix $B_b \in \mathbb{R}^{3 \times 9}$, i.e. there are 9 actuators to control 3 body-modes. Therefore, the dimension of the additional design freedom is $n_s = 6$.

5.5.3 Decoupling and feedback control design

The plant has been decoupled using geometric decoupling. Therefore, T_y is chosen such that the motion $m(t)$ (Fig. 5.1) contains the rigid-body displacements in meters and radians. Since the system is over-sensed, an additional torsion output has been added, which measures the amount of internal deformation in the stage (no unit). To show the performance improvements by feedforward control, this extra output will not be used for feedback control, but is used for the optimization of the feedforward controller. The output decoupling matrix from (5.2) is given

by,

$$\begin{bmatrix} z \\ R_x \\ R_y \\ \text{torsion} \end{bmatrix} = \begin{bmatrix} 0.25 & 0.25 & 0.25 & 0.25 \\ 0.90 & 0.90 & -0.90 & -0.90 \\ -0.84 & 0.84 & 0.83 & -0.83 \\ 0.35 & -0.35 & 0.35 & -0.35 \end{bmatrix} \begin{bmatrix} z_1 \\ z_2 \\ z_3 \\ z_4 \end{bmatrix}. \quad (5.20)$$

Furthermore, $T_{u,fb}$ is chosen such that the mass and principle moments of inertia do not change. Afterwards, the remaining interaction has been analysed using the relative gain array (RGA), see Skogestad and Postlethwaite (2005). The RGA shows that the plant is sufficiently well decoupled for decentralized control design, since the RGA is close to identity around the target bandwidth.

The decentralized feedback controller is designed using manual loopshaping and is given by,

$$K_d(s) = \text{diag} (K_x, K_y, K_{R_z}, K_z, K_{R_x}, K_{R_y}), \quad (5.21)$$

where,

$$K_i(s) = k_i \frac{s + 2\pi f_{int,i}}{s} \frac{\frac{1}{2\pi f_{z,i}}s + 1}{\frac{1}{2\pi f_{p,i}}s + 1} \frac{1}{\frac{1}{(2\pi f_{lp,i})^2}s^2 + \frac{2\beta_{lp}}{2\pi f_{lp,i}}s + 1} \cdot \frac{\frac{1}{(2\pi f_{nz,i})^2}s^2 + \frac{2\beta_{nz,i}}{2\pi f_{nz,i}}s + 1}{\frac{1}{(2\pi f_{np,i})^2}s^2 + \frac{2\beta_{np,i}}{2\pi f_{np,i}}s + 1},$$

with $\beta_{lp} = 0.5$ and other parameters as shown in Table 5.1 and 5.2. The feedback controller (5.21) has been discretized using a Tustin transformation (no prewarping) with a sampling frequency of $f_s = 10000$ Hz.

Axis i	k_i	$f_{int,i}$	$f_{z,i}$	$f_{p,i}$	$f_{lp,i}$	f_{BW}
x	3.1318e5	10	50/4	200	250	48.2
y	3.0651e5	10	50/4	200	250	46.3
R_z	2.3773e4	10	50/4	200	250	53.4
z	3.3165e5	10	50/4	200	250	49.7
R_x	1.1252e4	10	50/4	200	250	58.9
R_y	1.1328e4	10	50/4	200	250	58.9

Table 5.1: Controller parameters and resulting bandwidth f_{BW} (Hz). f_{BW} is defined as the zero dB crossing of the open-loop.

5.5.4 MIMO stability

The overall stability of the MIMO system with decentralized controller (5.21) has been evaluated using the characteristic loci of the measured FRF (Skogestad and Postlethwaite, 2005), which shows that the system is closed-loop stable as can be seen in Fig. 4.9.

Axis i	$f_{nz,i}$	$\beta_{nz,i}$	$f_{np,i}$	$\beta_{np,i}$
z	530	0.001	530	0.1
R_x	504	0.001	504	0.1
R_y	504	0.001	504	0.1

Table 5.2: Controller parameters for the notch filters. Note that in the first three control loops (x, y, R_z) the notch filter is absent.

5.5.5 Setpoint trajectory

The setpoint trajectory for the z -direction is a third order point-to-point motion profile (Lambrechts et al., 2005). This setpoint trajectory is shown in Fig. 5.4 and has been designed such that it is challenging for the system, i.e. such that the actuators generating the largest forces are close to saturation. After 0.25 s a backward motion, which is exactly mirrored, is performed. Every 0.75 s this forward-backward sequence is repeated, resulting in 5 repetitions in 4 s. The setpoint trajectory for all other directions is zero.

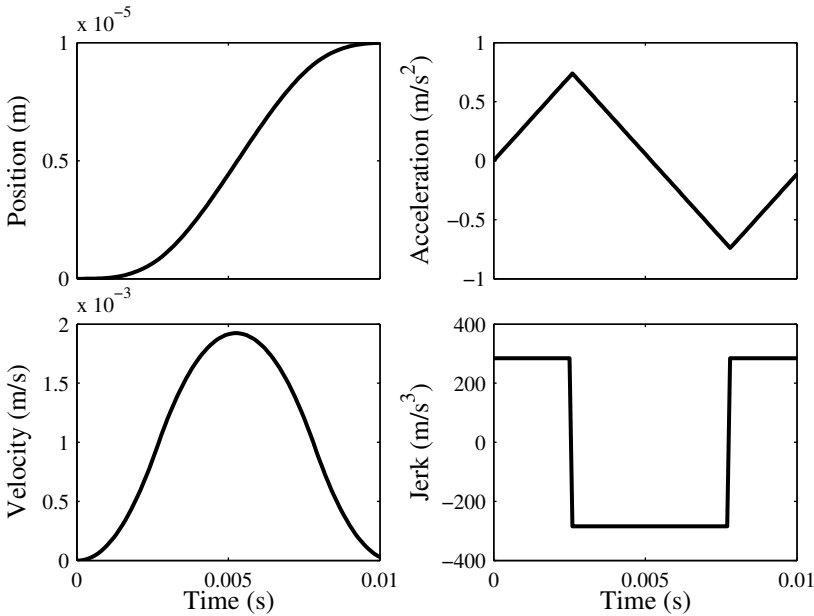


Figure 5.4: Setpoint trajectory for the z -direction.

5.5.6 Data-based design

For the experiments the cost-criterion (5.10) has been modified, such that it only contains the out-of-plane directions., i.e.

$$e_{m,l} = \begin{bmatrix} e_{z,l} \\ e_{R_x,l} \\ e_{R_y,l} \\ e_{\text{torsion}} \end{bmatrix}, \quad (5.22)$$

where $e_{\text{torsion}} = 0 - \text{torsion}$, is the error in the torsion coordinate, which is defined in (5.20). Furthermore, initial experiments were performed with $\bar{\gamma}_i = 1, \forall i$, i.e. all motion directions are considered equally important. However, in the experiments the error e_{R_y} was relatively large due to the combination of imperfect rigid-body decoupling and the setpoint trajectory in z -direction. Furthermore, the vibrations in e_{torsion} were not weighted sufficiently to have an influence on the solution. Therefore, $\bar{\gamma}_1 = 1$, $\bar{\gamma}_2 = 2$, $\bar{\gamma}_3 = 0.1$, $\bar{\gamma}_4 = 3$, are chosen.

Due to the fact that only motion in z -direction is required, the number of design parameters can be reduced. This also limits the number of perturbation experiments to obtain the gradients of the error and the objective function.

Construction of the optimization space and gradients

Using B_b from (D.1), the free directions for the optimization can be identified as (5.4). With the body-mode directions and the free $n_s = 6$ directions, the total parametrization of the feedforward controller in (5.8) can be constructed.

In Chapter 4, a model of the system in Fig. 4.3 was presented, which can be employed for model-based gradient estimation. However, estimation of parameters by experiments is inexpensive and typically results in more accurate estimates. Therefore, the parameter perturbation method from Section 5.4.3 has been employed to construct the gradients. Eight experiments have been performed, i.e. one nominal experiment and seven perturbation experiments. The resulting gradient is calculated using (5.19). The gradient for the perturbation of θ_2 , is shown in Fig. 5.5. The perturbation sizes, defined by (5.19), are chosen equal to 0.5 for the free directions. For the mass-parameter, the perturbation size was equal to 1.

5.5.7 Results

In this section the experimental results of data-based spatial feedforward are presented. The setpoint trajectory is only non-zero in the z -direction, therefore the optimization as presented in Section 5.4 is limited to the out-of-plane directions as in (5.22).

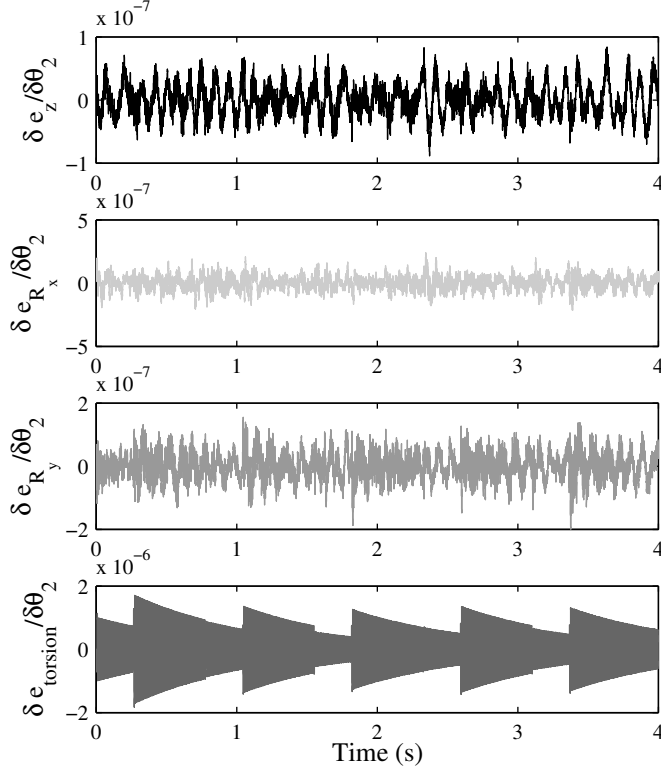


Figure 5.5: Measured gradient ∇e_m using a parameter perturbation method. The different subplots show the elements of ∇e_m for the perturbation of θ_2 , which consist of the stacked tracking errors. The different components of the tracking errors in the gradient are $\frac{\delta e_z}{\delta \theta_2}$ (—), $\frac{\delta e_{R_x}}{\delta \theta_2}$ (—), $\frac{\delta e_{R_y}}{\delta \theta_2}$ (—), $\frac{\delta e_{\text{torsion}}}{\delta \theta_2}$ (—). This shows that the error indeed can be modified by changing the parameters.

Convergence and parameters

The objective function (5.10) for the experimental results, is shown in Fig. 5.6a. In this figure, it can be seen that the data-based spatial feedforward has converged after 2 task trials. The changes after task trial 2 are mainly due to trial varying disturbances and noise. The value of the objective function at first task trial is determined by the feedback controller and the accuracy of the initial mass estimate. The change in the cost-function V is small since the initial estimate is quite close to the optimal value. The change in the perceived mass between the first and final task trial is approximately 3.1% of the parameter value, see Fig. 5.6b.

Remark 5.14. The convergence of the objective function is non-monotonic. This effect is due to trial-varying disturbances and noise. However, convergence properties are outside the scope of this chapter and subject of future research.

The convergence of the perceived mass parameters is shown in Fig. 5.6b. The perceived mass is approx. 10.7% larger than the actual system mass, which can be explained by the non-ideal gravity compensators and/or the lack of higher order basis functions. Furthermore, the convergence of this parameter shows that the amount of force on the system in z -direction remains approximately constant for a fixed setpoint trajectory.

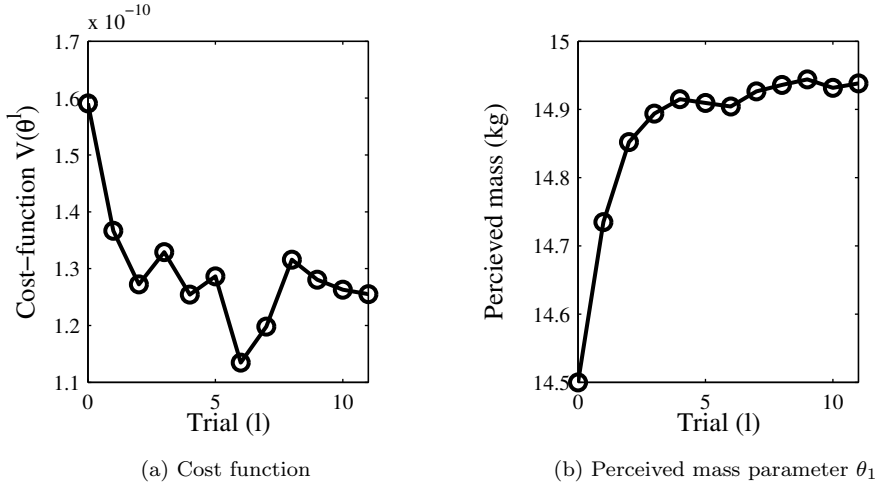


Figure 5.6: Cost function and perceived mass parameter θ_1 as a function of task trials.

Feedforward controller

The feedforward controller at the first task trial with $\bar{\theta}_0 = 0$ and the initial mass estimate is given by,

$$K_{ff,z}^0(\bar{\theta}_0) = 1.6111 \cdot [1 \ 1 \ 1 \ 1 \ 1 \ 1 \ 1 \ 1 \ 1]^T, \quad (5.23)$$

where the elements of the initial feedforward controller (5.23) exactly sum up to the initial estimate of the perceived mass, i.e. $\hat{m} = 14.5$. This feedforward controller is equal to a standard body-mode decoupling and diagonal feedforward control, i.e. all actuators generate an equal amount of force to realize the displacement of the stage.

The feedforward controller at the final task trial is given by,

$$K_{ff,z}^{11}(\bar{\theta}_{11}) = \begin{bmatrix} 1.8206 \\ 1.4734 \\ 1.8597 \\ 1.9629 \\ 1.1965 \\ 1.7077 \\ 2.0945 \\ 1.1791 \\ 1.6440 \end{bmatrix}. \quad (5.24)$$

Again, the elements sum up to the new estimated mass. However, the ratio between the actuator forces completely changed. If all actuators are equal by design, this imposes a limit on the achievable acceleration of the system, i.e. the acceleration is limited by the maximum element from (5.24) and the maximum allowed input.

Tracking errors

The experimental tracking errors of e_z and e_{R_x} using the feedforward controller in (5.23) and (5.24) are shown for $t \in [0, 0.1]$ in Figs. 5.7 and 5.8, respectively. In these figures the result of the first and final task trial are shown. The time plot of the tracking error e_{R_y} is not shown, due to the fact that the errors are very similar for both the first and final task trial. For e_z , e_{R_x} and e_{R_y} it holds that the peak error of the final task trial is smaller than the peak value for the first trial. The reduction of the peak error can be explained as the compensation of the limited stiffness of the stage using additional actuators, i.e. over-actuation.

The cumulative power spectrum (CPSD) of e_z , e_{R_x} and e_{R_y} calculated from $t \in [0, 1]$ are shown in Fig. 5.9. Here, it can be observed that for e_z the power for the final task trial is lower than for the first task trial. For e_{R_x} and e_{R_y} the power of the tracking error at the final task trial is slightly worse. Furthermore, the flexible modes are not visible in the cumulative power spectrum, except for the small bump around 500 Hz in e_{R_x} .

The error in the torsion direction e_{torsion} and its cumulative power spectral density are shown in Figs. 5.10 and 5.11, respectively. From Fig. 5.10 it is clear that the initial feedforward controller excites the torsion mode at 143 Hz. This additional motion direction allows to observe the deformation of the stage, which can be used to optimize the performance. The peak error at the final task trial is reduced by approximately a factor 1.4 with respect to the first trial. In the cumulative power spectrum in Fig. 5.11 it becomes clear that the torsion mode, which is excited at the first task trial, has almost disappeared in the final task trial. Here, the excitation of a flexible mode is prevented by a data-based optimization in the free direction which does not affect the body-mode behaviour.

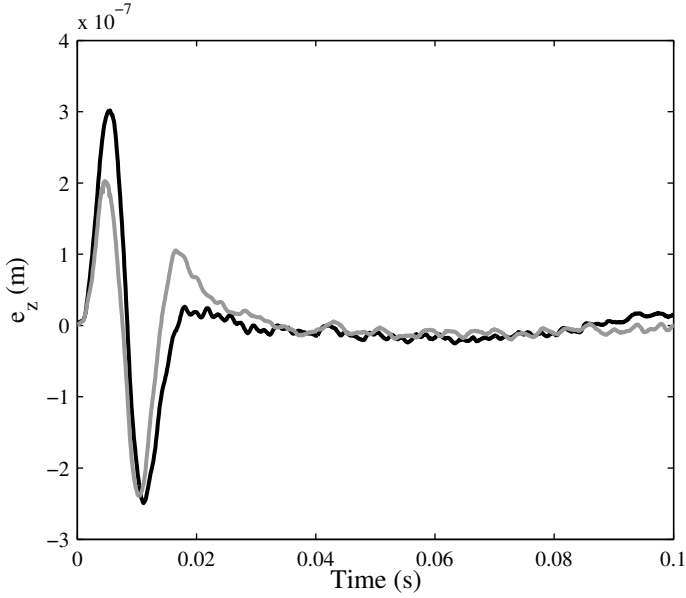


Figure 5.7: Servo-error e_z , first (—) and final (—) iteration.

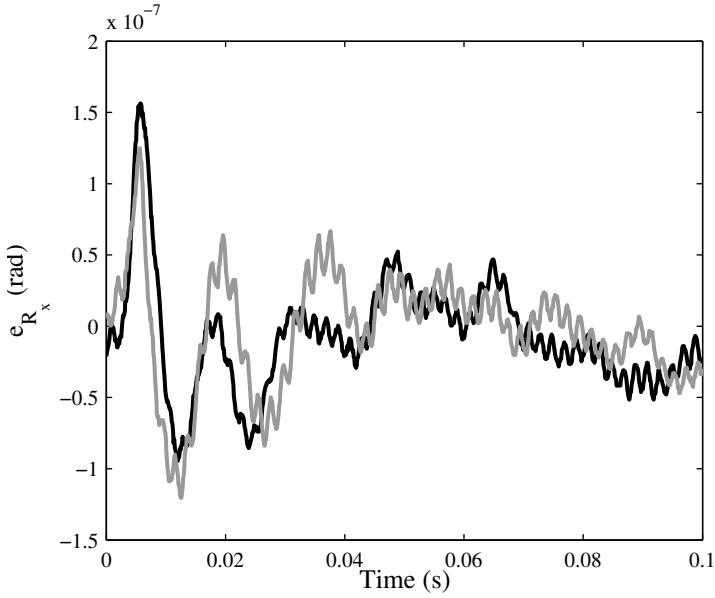


Figure 5.8: Servo-error e_{R_x} , first (—) and final (—) iteration.

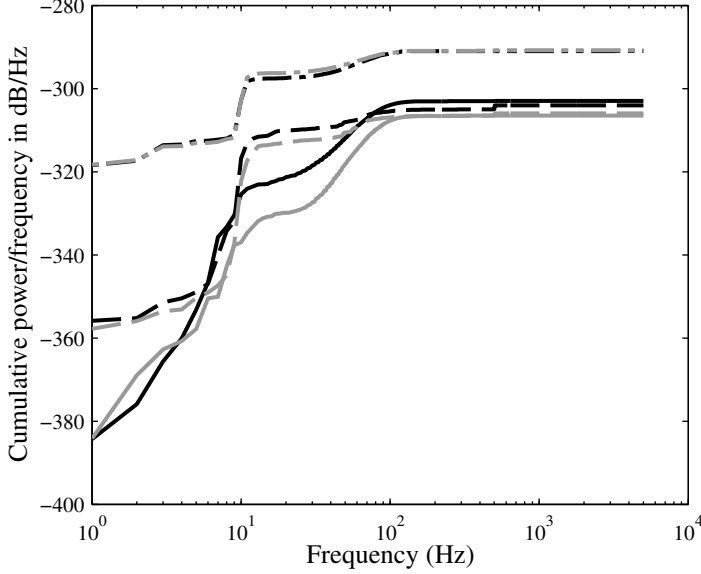


Figure 5.9: CPSD of the servo-error e_z , e_{R_x} , e_{R_y} (solid, dashed, dash-dotted), first (—) and final (—) iteration.

A different approach to prevent the excitation would be to apply input shaping. However, input shaping modifies the setpoint trajectory, which is typically undesired as the setpoint trajectory is dictated by the given application. The properties of input shaping and (model-based) spatial feedforward are compared in Chapter 4 and Ronde et al. (2013b).

Additionally, a piezo strain sensor is present to measure the internal deformations of the stage. The time plot and its cumulative power spectrum are presented in Figs. 5.12 and 5.13 respectively. From Fig. 5.12 the difference is not well observable except for a smaller peak value at the final task trial. In Fig. 5.13 it can be observed that the mode at 143 Hz, which was present during the first task trial has disappeared at the final task trial. The jump in the CPSD at the final task trial indicates that the higher order modes around 500 Hz are more severely excited at the final task trial. However, the total energy in the strain signal has been reduced at the final task trial.

5.6 Conclusions

This chapter presents a data-based optimization for spatial feedforward. To apply the presented method it is required that the system approximately satisfies a modal structure. Therefore, non-linearities, actuator constraints, external disturbances and time-varying dynamics may hamper the application of the method. Moreover, the identification of a parametric MIMO model is replaced by a dedicated parameter identification experiment. More specifically only the input matrix with respect to the rigid-body modes is required. Additionally, the gradient with respect to the parameters has to be identified to apply this method. The additional advantage is that the selection of the modes to be suppressed is automatically determined based on the objective function provided this is chosen well, i.e. the data-based method results in optimal controller parameters with respect to the actual plant.

The resulting feedforward controller designed using the method proposed in this chapter is setpoint trajectory invariant in contrast to many data-based methods. Moreover, the proposed method does not modify the setpoint trajectory in contrast to input shaping. However, both methods can prevent the excitation of flexible modes, i.e. the performance can be improved over the complete structure.

In this chapter it is shown that vibrations, which are introduced by the feedforward signal, can be prevented using over-actuation. Using additional sensors, i.e. over-sensing, it is possible to suppress the observed vibrations by changing the direction of the input. This new input direction does not deteriorate the performance in the motion direction. Because the limited stiffness of the stage is compensated by the additional actuators, the performance shows a slight improvement in the motion directions as well. Furthermore, using an additional piezo strain sensor it is verified that the torsion mode (143 Hz) included in the optimization indeed is not visible at other locations on the stage, i.e. the mode is not excited by applying the proposed feedforward method.

For systems with as many flexible modes as the degree of over-actuation, i.e. $n_s = n_r$, the data-based solution converges to the model-based spatial solution. However, for practical systems having less actuators than the number of flexible modes, i.e. $n_s < n_r$, the data-based optimum is a combination of suppression of the vibrations and compensating the limited stiffness of the higher order modes.

The framework in this chapter relies on the diagonal structure of the feedforward controller, which assumes perfect body-mode decoupling. As shown in the experiments, there is cross talk present between the different axes. Therefore, the framework could be extended such that compensation of cross-talk due to imperfect decoupling would be possible. Moreover, the data-based optimum is dependent on the frequency content of the setpoint trajectory. Therefore, the criterion could be extended such that multiple setpoint trajectories are included to have a good overall performance.

Furthermore, the framework could be extended with additional basis functions,

e.g. higher order derivatives of the setpoint trajectory, to improve the performance at the sensors. Moreover, it is possible to extend the parametrization of the feedforward, such that the delay in the system can be compensated for (Van der Meulen et al., 2008).

In the next chapter the conclusions of this thesis are presented. Moreover, recommendations for future research are motivated.

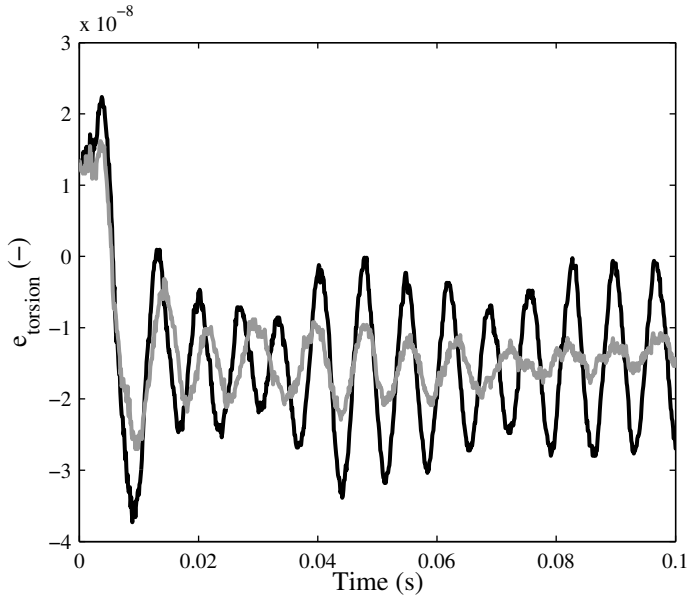


Figure 5.10: Servo-error e_{torsion} , first (—) and final (---) iteration.

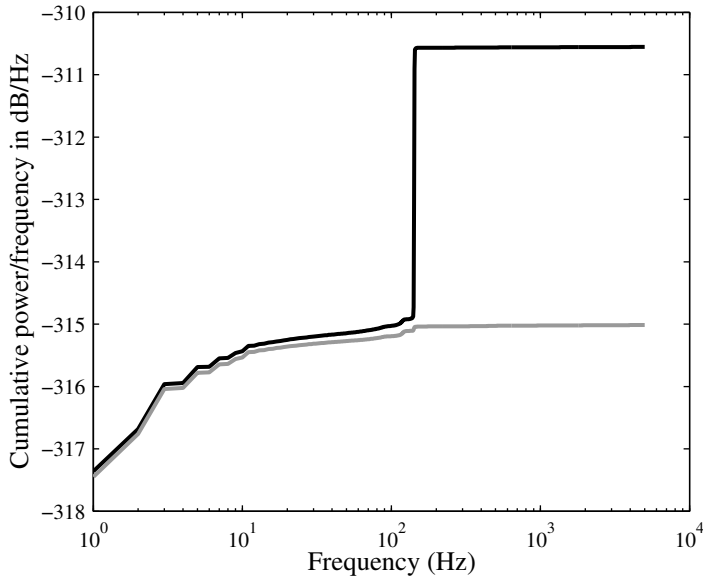


Figure 5.11: CPSD of the servo-error e_{torsion} , first (—) and final (---) iteration.

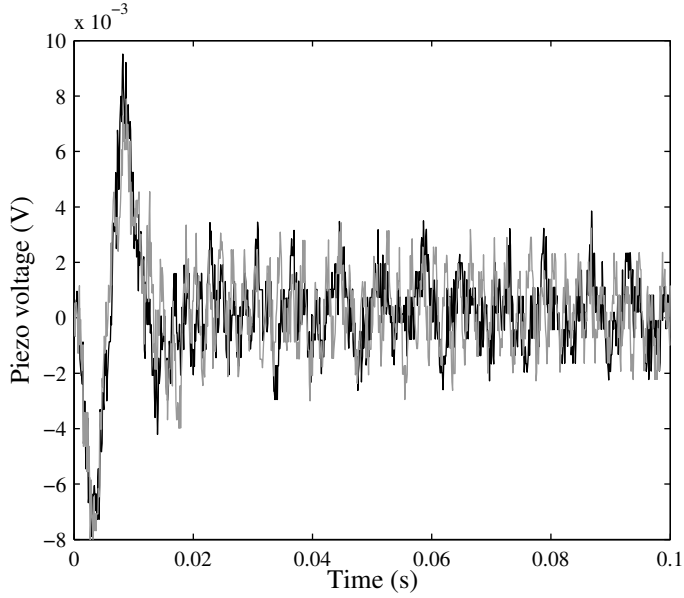


Figure 5.12: Piezo strain sensor, first (—) and final (—) iteration.

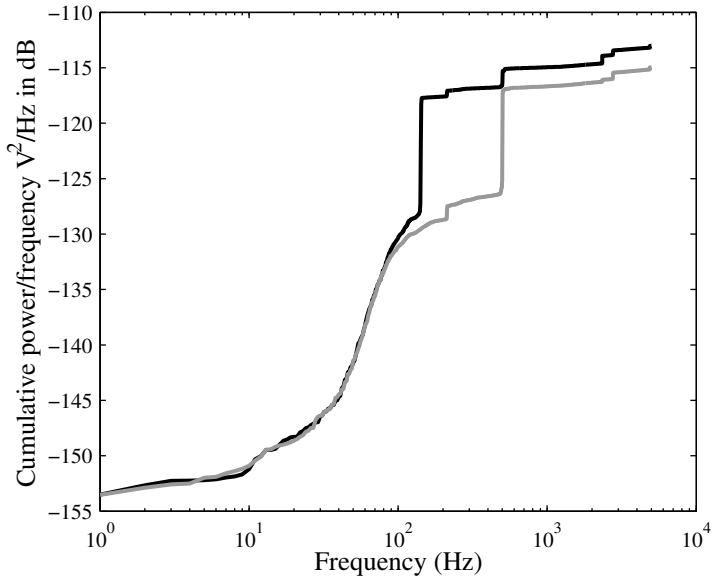


Figure 5.13: CPSD of the piezo strain sensor, first (—) and final (—) iteration.

Chapter 6

Conclusions and recommendations

IN this chapter the main results of this thesis are presented, and recommendations for future research on feedforward control for lightweight motion systems are given.

6.1 Conclusions

In this thesis, feedforward control of lightweight motion systems has been considered. To enable a higher production throughput, more aggressive setpoint trajectories or larger wafer sizes are required. In the rigid-body design paradigm, which aims at designs with a very high stiffness, this leads in an evolutionary way to systems with an increasing moving mass. Such systems require more and more power, such that this paradigm rapidly approaches the boundary of its scalability due to thermal constraints. Therefore, lightweight motion systems are designed with a reduced moving mass compared to rigid-body designed systems. As a consequence mechanical resonances appear in the frequency region of interest, which poses several challenges for control design. First of all, the attainable bandwidth is limited compared to rigid-body design. Secondly, the setpoint trajectory excites the flexible dynamics, which results in performance deterioration. In a typical production process the sensors are located at different physical locations as where the actual processing takes place. Moreover, due to flexibilities between the measurement- and performance location the performance cannot be evaluated or controlled using the sensors and the use of simple geometrical coordinate transformations. For lightweight motion systems two different subclasses can be distinguished: traditional and over-actuated systems. In traditional systems, the amount of actuators

equals the amount of rigid-body modes, in contrast to over-actuated motion systems, which contain more actuators than rigid-body modes.

For traditional actuated motion systems, a framework to design feedforward controllers for lightweight motion systems with physically non-collocated sensor- and performance locations was presented in Chapter 2. This framework can deal with inferential motion systems (measurement location is not equal to the performance location), which are possibly non-square due to over-actuation and/or an unequal number of measurement and performance variables. The method allows for a feedforward control design, which is independent of the feedback controller and setpoint trajectory, in contrast to existing methods. Moreover, simultaneous design of the feedback- and feedforward controller is not required in contrast to existing solutions for inferential control. Furthermore, it is shown that a different setpoint for the feedback- and feedforward control are required to avoid conflicting control goals. Moreover, the method proposed in this chapter has been validated on a prototype lightweight motion system.

To apply this method, a performance model is required, which is typically obtained using an identification procedure. Therefore, sensor(s) at the performance location are required during the modeling phase. However, these sensors are not required during operation. The attainable performance improvement is limited by the quality of the parametric model and the amount of truncated singular values, i.e. the accuracy of the inversion.

For systems with a time-varying performance location an exploratory study was presented in Chapter 3. In this chapter it is shown that direct application of the framework from Chapter 2 leads to infeasible feedforward signals. By incorporating a weighting filter, which penalizes undesired frequency contents, feasible feedforward signals can be obtained. The proposed method has been validated by experiments with a lightweight motion system, which shows that it is possible to design a feedforward controller for a system with a time-varying performance location.

To apply this method, a time-varying performance model is required, which might be hard to obtain in actual production machines. Moreover, the weighting on the input signal does not result in hard constraints, but in an iterative design procedure. Furthermore, once the feedforward controller has been designed, the time-varying performance model is fixed. Therefore, the feedforward controller is only valid for this specific predetermined performance model. In practice, this means that the feedforward controller only works for slight variations of the setpoint trajectory. The step from the presented simple motion system towards industrial motion systems is still challenging. Although the performance location in industrial applications changes more gradually, similar changes in performance dynamics are also expected. Moreover, changes in performance dynamics will occur more often than the presented application due to the presence of multiple relevant modes.

The second subclass of lightweight motion systems which are investigated in this thesis are over-actuated motion systems, which are considered in Chapters 4 and 5. These systems have additional design freedom compared to traditionally actuated systems, which is explored and characterized in Chapter 4. This resulted in a control framework with different input decoupling transformations in the feedback- and feedforward-path to reflect the different goals of the feedback- and feedforward controller. For feedforward it is desirable to make the flexible modes uncontrollable, such that the flexible modes are not excited. However, for feedback control this might not be beneficial as disturbances might be present which excite the flexible modes. The proposed method, called *model-based spatial feedforward*, exploits the number of extra actuators to render equally many flexible modes of the moving structure uncontrollable from the feedforward input. Also, explicit conditions have been formulated for the existence of such solutions. Moreover, the proposed method is experimentally validated on an industrial prototype motion system and is compared to both standard mass feedforward and input shaping methods. The experiments show that it is indeed possible to avoid excitation of the flexible dynamics by applying over-actuation. Also, the approach does not suffer from the typical drawbacks of input shaping, i.e. there are no delays introduced and there is no filtering applied to the setpoint trajectory and feedforward input.

The application of model-based spatial feedforward is limited to over-actuated motion systems, which can be modeled in modal form. In industrial motion systems, extra dynamics due to sensors and actuator might be present in the frequency range of interest. In such cases, these dynamics must be compensated for. However, these dynamics are ideally prevented by the integrated design of the actuators, sensors and mechanics of the system. Moreover, the model-based spatial feedforward solution relies on the input matrix of the system, which basically contains the mode-shapes of the system. The exactness of these modes shapes determines how well the excitation of flexible modes is prevented. Furthermore, the required forces are determined by the fixed actuator locations and the flexible modes which should not be excited. The unequal force distribution among the actuators resulting from the spatial decoupling might violate the input constraints. In such cases, the acceleration should be limited to reduce the amount of force required within the attainable limits.

To compute the optimal decoupling and feedforward controller for the true machine, a data-based solution is presented in Chapter 5. A model of the rigid-body behavior is employed to identify the available design freedom. Subsequently, this design freedom is used in a data-based optimization, which employs the servo-errors of a previous experiment to improve the performance. Moreover, in this framework additional signals representing elastic deformations in the system can be employed to reduce the elastic deformations during motion. The data-based spatial feedforward is experimentally validated on an industrial prototype motion system. In these experiments it is shown that it is possible to suppress these

vibrations. Furthermore, it is shown that this method is effective for the complete structure, i.e. the vibrations which were present disappeared on the additional sensor after application of the data-based optimization. The additional sensors were not collocated with the other sensors or used in the optimization. The data-based method can be regarded as a dedicated system identification experiment, which results in a model with the required parametrization.

The limitations of data-based spatial feedforward are similar to those of model-based spatial feedforward, which both require over-actuation and a modal structure of the model. Although the parameters are identified in a data-based optimization approach, the method still relies on a rigid-body model to construct the optimization space and to obtain the rigid-body decoupling. Also, the optimization is unconstrained, which can result in inputs which are unattainable by the system.

6.2 Recommendations for future research

6.2.1 General recommendations

- The improvement which can be obtained by feedforward control depends on the uncertainty associated with the model (Devasia, 2002). Therefore, improvement of model quality has a direct impact on the attainable performance of model-based feedforward. For systems with intrinsically multi-variable behavior and a large number of in- and outputs the complexity of obtaining parametric models increases rapidly (Van Herpen, 2014). Moreover, it should be investigated how model uncertainty affects the attainable performance using feedforward at the performance location.
- In this thesis, only feedforward control of the setpoint trajectory is considered. However, in typical applications the setpoint trajectory is not the only relevant disturbance. Therefore, the combination of over-actuated feedforward solutions with an over-actuated feedback controller in the framework of Fig. 1.3 should be investigated. To this end, decoupling approaches for over-actuated and over-sensed systems can be applied to create additional feedback loops for the flexible modes, which is for instance explored in Rampadarath (2010); Durango Galvan et al. (2012). Additionally, model-based approaches which provide extra damping (Boeren et al., 2013) or enhance the stiffness (Van Herpen, 2014, Chapter 6) due to active control of the flexible dynamical behavior should be investigated.
- A system design with a reduced moving mass leads to increased sensitivity to force disturbances. Therefore, it is expected that the present disturbances become increasingly important, such that explicit characterization and compensation is required. Furthermore, it must be investigated how these disturbances affect the performance location. To this end, the control structure from Fig. 1.3 must be extended with disturbance models as for ex-

ample shown in Gawronski (2004, Section 3.5). Moreover, these disturbance models must be employed in the control design to improve the performance at the performance location.

6.2.2 Recommendations for traditionally actuated systems

- In this thesis, a feedforward design method for non-square inferential motion systems is presented in Chapter 2. However, several questions still remain. First of all, the method heavily relies on the quality of the model. Secondly, the generated setpoint trajectory is computed based on model information only, i.e. errors in this model directly affect the performance. Moreover, the presented feedforward design results in a convolution-based feedforward controller, i.e. the resulting approach is setpoint-trajectory-invariant. However, the complete setpoint trajectory needs to be known in advance in order to compute the feedforward. Therefore, it is desirable to investigate the design of an causal feedforward controller or a feedforward controller with a limited number of preview samples of the setpoint trajectory.
- The feedforward design methods for systems with time-varying performance locations, as presented in Chapter 3, pose additional research challenges. In lithographic systems, the performance location is varying due to the production process, which leads to position-dependent (zero) dynamics. It must be investigated how to identify such models. Additionally, it is desirable to explore how to reduce the number of identification experiments to obtain such models. For lightweight motion systems, which can be modeled in a modal framework, initial estimates from FEM can be used to speed up this process, i.e. the modeshapes can be used to interpolate between different locations.
- Moreover, once the feedforward controller has been designed using the method of Chapter 3 with a predetermined performance definition and thus the setpoint trajectory is fixed. Therefore, methods to design feedforward controllers for position-varying performance locations should be investigated.

6.2.3 Recommendations for over-actuated systems

- The model- and data-based spatial feedforward solution depends on the modeshapes of the system. This determines the required force distribution over the actuators to prevent the excitation of flexible modes. However, in this thesis, the actuator locations are considered to be fixed. By removing this constraint, i.e. by placement of the actuators, the amount of energy consumed could possibly be reduced, which is relevant in view of thermal constraints. Demands for increased production throughput together with thermal constraints are the reason to consider the design of lightweight systems in the first place. For feedforward control the placement of actuators

on the nodes of the relevant modes is desirable. However, in practice this is hard to achieve, since any model is inaccurate. Moreover, the actuator typically adds mass, which influences the modeshape and thus the location of the nodes. For feedback control, this will not lead to the desired result, because the corresponding mode will be uncontrollable and any disturbance in this direction cannot be dealt with. Further investigation is required to determine an optimal actuator placement for feedforward control in conjunction with feedback control for over-actuated systems.

- The question which mode is important depends, among others, on the performance location, i.e. at or near the nodal lines the resonant dynamics of a mode is typically less pronounced. However, near the anti-node these resonant dynamics mode may be very relevant. Also compliant dynamics should be taken into account. Therefore, the performance location should be taken into account explicitly by combining spatial feedforward with inferential control. Also it must be investigated if it is possible to schedule the feedforward decoupling matrix according to the performance location. Moreover, it is the question how to divide the scheduling regions of the performance locations, such that the method is applicable for different setpoint trajectories. First of all, it is not desirable to switch between different feedforward decoupling matrices during the exposure of the chips. Secondly, a smooth transition of the feedforward inputs is required, such that the flexible modes are not excited more severely. Thirdly, it may not be possible to make the desired flexible model uncontrollable due to actuator placement. Finally, high accuracy models are required for final implementation.
- Planar motors, such as presented in Jansen (2007); van Lierop (2008); Rovers (2013), typically contain much more active actuators than rigid-body degrees of freedom. Therefore, a large degree of over-actuation is present. However, due to the position-dependent and non-linear nature of these planar motors it is the question whether the assumptions to apply spatial feedforward hold. For example, the quality of the position-dependent decoupling determines the linearity of the system to be controlled, which is one of the requirements for spatial feedforward. If the assumptions for spatial feedforward control do not hold, it should be explored if and how these assumptions can be relaxed such that the additional design freedom present can still be exploited.

Recommendations for model-based spatial feedforward

- In this thesis it is shown that the application of model-based spatial feedforward improves the performance of the system by designing an input transformation such that selected flexible modes become uncontrollable. However, application of this method is still challenging. First of all, obtaining the required multivariable model is a complex and tedious task. Secondly, since the method is based on a multivariable model, manual (re)tuning is not ob-

vious, i.e. small changes in system dynamics may require the identification of a new model. Finally, in case the amount of over-actuation is less than the number of relevant modes, the selection of the modes to be suppressed is not obvious. This depends, among others, on the performance location, system dynamics and setpoint trajectory. Therefore, the robustness of the solution against plant variations must be investigated and possibly improved.

Recommendations for data-based spatial feedforward

- In Chapter 5 data-based spatial feedforward is presented, which optimizes the input transformation and feedforward controller to suppress vibrations. However, some challenges are still remaining. The design freedom for over-actuation and the decoupling of the rigid-body modes still originates from a model, i.e. any errors in this model cannot be compensated for. Moreover, the basis functions are limited to the acceleration, such that higher order dynamics cannot be compensated for. Extensions of the basis functions to higher order terms allow to compensate for these dynamics at the sensor locations. However, it should be investigated what the effect is for the complete system, i.e. what are the consequences at the performance location.
- Data-based spatial feedforward employs a Gauss-Newton method to compute the optimal parameters for the spatial feedforward. This leads to non-ideal convergence and sensitivity to noise. Therefore, alternative optimization and/or parameter identification methods, such as instrumental variable methods (Söderström and Stoica, 1983) should be investigated.
- Data-based spatial feedforward clearly benefits from the application of over-sensing due to the fact that individual modes are separated in individual output channels. Therefore, from a control perspective the ideal solution would be to apply as many sensors as the number of relevant modes. However, from a systems engineering perspective this solution is not feasible for two reasons: i) costs, and ii) geometric constraints of the construction. Therefore, it should be investigated whether estimation of the system state by an observer can be used in conjunction with data-based spatial feedforward. Furthermore, extensions towards systems with position-dependent dynamics are relevant for future applications.
- The solution of the data-based optimization approach can result in input signals beyond the attainable limits due to input saturation. In case input saturation occurs, the linearity of the system is compromised. Therefore, constraints on the inputs can be added to the data-based method to prevent such situations.

Bibliography

- Achterberg, J., van Lierop, C. M. M., and van den Bosch, P. P. J. (2010). Active reduction of a static deformation in a moving magnet planar actuator. In *Proceedings of the 25th Annual Meeting of the American Society for Precision Engineering (ASPE 2010)*, Atlanta, Georgia, USA.
- Ahn, H.-S., Chen, Y., and Moore, K. (2007). Iterative learning control: Brief survey and categorization. *IEEE Transactions on Systems, Man, and Cybernetics, Part C: Applications and Reviews*, 37(6):1099–1121.
- Antsaklis, P. and Michel, A. (2006). *Linear Systems*. Birkhauser Verlag, Boston, MA.
- Arnold, B. (2009). Shrinking possibilities. *IEEE Spectrum*, 46(4):26–28, 50–56.
- Aström, K. J., Hagander, P., and Sternby, J. (1984). Zeros of sampled systems. *Automatica*, 20(1):31–38.
- Avrachenkov, K. E. and Longman, R. W. (2003). Iterative learning control for over-determined, under-determined, and illconditioned systems. *International Journal of Applied Mathematics and Computer Science*, 13(1):113–122.
- Baggen, M., Heertjes, M., and Kamidi, R. (2008). Data-based feed-forward control in MIMO motion systems. In *American Control Conference*, pages 3011–3016.
- Bamieh, B., Pearson, J., Francis, B. A., and Tannenbaum, A. (1991). A lifting technique for linear periodic systems with applications to sampled-data control. *Systems & Control Letters*, 17(2):79–88.
- Baumgart, M. D. and Pao, L. Y. (2007). Discrete time-optimal command shaping. *Automatica*, 43(8):1403–1409.
- Ben-Israel, A. and Greville, T. N. E. (2003). *Generalized Inverses, Theory and Applications*. Springer, second edition.

- Bernstein, D. S. (2009). *Matrix Mathematics*. Princeton University Press, second edition.
- de Best, J., van de Molengraft, R., and Steinbuch, M. (2012). High speed visual motion control applied to products with repetitive structures. *IEEE Transactions on Control Systems Technology*, 20(6):1450–1460.
- de Best, J. J. T. H. (2011). *Feature-based motion control for near-repetitive structures*. PhD thesis, Eindhoven University of Technology.
- de Boeij, J. (2009). *Multi-Level Contactless Motion System*. PhD thesis, Eindhoven University of Technology.
- Boeren, F., van Herpen, R., Oomen, T., van de Wal, M., and Bosgra, O. (2013). Enhancing performance through multivariable weighting function design in \mathcal{H}_∞ loop-shaping: With application to a motion system. In *American Control Conference*, pages 6051–6056.
- Boerlage, M. (2006). MIMO jerk derivative feedforward for motion systems. In *American Control Conference*, pages 3892–3897.
- Boerlage, M., Steinbuch, M., Lambrechts, P., and van de Wal, M. (2003). Model-based feedforward for motion systems. In *IEEE conf. on Control Applications*, volume 2, pages 1158–1163.
- Boerlage, M. L. G., Tousain, R. L., and Steinbuch, M. (2004). Jerk derivative feedforward control for motion systems. In *American Control Conference*, pages 4843–4848.
- Boyd, S. and Vandenberghe, L. (2004). *Convex Optimization*. Cambridge University Press.
- Brinkerhoff, R. and Devasia, S. (2000). Output tracking for actuator deficient/redundant systems: Multiple piezoactuator example. *AIAA Journal of Guidance, Control and Dynamics*, 23(2):370–373.
- Bristow, D., Tharayil, M., and Alleyne, A. (2006). A survey of iterative learning control. *IEEE Control Systems Magazine*, 26(3):96–114.
- Brosilow, C. and Tong, M. (1978). Inferential control of processes: Part ii. the structure and dynamics of inferential control systems. *AIChE Journal*, 24(3):492–500.
- Bruijnen, D. and van Dijk, N. (2012). Combined input shaping and feedforward control for flexible motion systems. In *American Control Conference*, pages 2473–2478.

- Butler, H. (2011). Position control in lithographic equipment. *IEEE Control Systems Magazine*, 31(5):28–47.
- Butler, H. (2013). Adaptive feedforward for a wafer stage in a lithographic tool. *IEEE Transactions on Control Systems Technology*, 21(3):875–881.
- Butterworth, J. A., Pao, L. Y., and Abramovitch, D. Y. (2009). A comparison of control architectures for atomic force microscopes. *Asian Journal of Control*, 11(2):175–181.
- de Caigny, J., Demeulenaere, B., Swevers, J., and De Schutter, J. (2007). Optimal design of spline-based feedforward for trajectory tracking. In *American Control Conference*, pages 4524–4529.
- Clayton, G. M., Tien, S., Leang, K. K., Zou, Q., and Devasia, S. (2009). A review of feedforward control approaches in nanopositioning for high-speed SPM. *Journal of Dynamic Systems, Measurement, and Control*, 131(6):061101–19.
- Cutforth, C. F. and Pao, L. Y. (2004). Adaptive input shaping for maneuvering flexible structures. *Automatica*, 40(4):685–693.
- Devasia, S. (2002). Should model-based inverse inputs be used as feedforward under plant uncertainty? *IEEE Transactions on Automatic Control*, 47(11):1865–1871.
- Devasia, S., Chen, D., and Paden, B. (1996). Nonlinear inversion-based output tracking. *IEEE Transactions on Automatic Control*, 41(7):930–942.
- Dijkstra, B. G. (2004). *Iterative Learning Control with applications to a wafer stage*. PhD thesis, Technische Universiteit Delft.
- Doyle, F. J. (1998). Nonlinear inferential control for process applications. *Journal of Process Control*, 8(5-6):339–353.
- Durango Galvan, S., Heertjes, M., and Dunand, R. (2012). Plant enhancements in motion systems by modal control. In *American Control Conference*, pages 5348 – 5353.
- Fleming, A. J. and Wills, A. G. (2009). Optimal periodic trajectories for band-limited systems. *IEEE Transactions on Control Systems Technology*, 17(3):552–562.
- Fliess, M., Lévine, J., Martin, P., and Rouchon, P. (1995). Flatness and defect of non-linear systems: introductory theory and examples. *International Journal of Control*, 61(6):1327–1631.
- Francis, B. and Wonham, W. (1975). The internal model principle for linear multivariable regulators. *Applied mathematics & optimization*, 2(2):170–194.

- Franklin, G. F., Powel, J. D., and Emani-Naeini, A. (2005). *Feedback control of dynamic systems*. Prentice Hall, 5th edition.
- Freudenberg, J. and Looze, D. (1985). Right half plane poles and zeros and design tradeoffs in feedback systems. *IEEE Transactions on Automatic Control*, 30(6):555–565.
- Gawronski, W. K. (2004). *Advanced structural dynamics and active control of structures*. Mechanical Engineering Series. Springer-Verlag, New York.
- de Gelder, E., van de Wal, M., Scherer, C., Hol, C., and Bosgra, O. (2006). Nominal and robust feedforward design with time domain constraints applied to a wafer stage. *Journal of Dynamic Systems, Measurement, and Control*, 128(2):204–215.
- Gevers, M. (2002). A decade of progress in iterative process control design: from theory to practice. *Journal of Process Control*, 12(4):519–531.
- Grosdidier, P. and Morari, M. (1986). Interaction measures for systems under decentralized control. *Automatica*, 22(3):309–319.
- Gunnarsson, S., Collignon, V., and Rousseaux, O. (2003). Tuning of a decoupling controller for a 2×2 system using iterative feedback tuning. *Control Engineering Practice*, 11(9):1035–1041.
- Hara, S., Yamamoto, Y., Omata, T., and Nakano, M. (1988). Repetitive control system: a new type servo system for periodic exogenous signals. *IEEE Transactions on Automatic Control*, 33(7):659–668.
- Hashemi, S. and Hammond, J. K. (1996). The interpretation of singular values in the inversion of minimum and non-minimum phase systems. *Mechanical Systems and Signal Processing*, 10(3):225–240.
- Heath, M. T. (2002). *Scientific computing, An Introductory Survey*. McGraw-Hill, New York, second edition.
- Heertjes, M., Hennekens, D., and Steinbuch, M. (2010). MIMO feed-forward design in waferscanners using a gradient approximation-based algorithm. *Control Engineering Practice*, 18(5):495–506.
- Heertjes, M. F. and van de Molengraft, R. M. J. G. (2009). Set-point variation in learning schemes with applications to wafer scanners. *Control Engineering Practice*, 17(3):345–356.
- van Herpen, R. M. A. (2014). *Identification for Control of Complex Motion Systems, Optimal Numerical Conditioning using Data-Dependent Polynomial Bases*. PhD thesis, Eindhoven University of Technology.

-
- Hjalmarsson, H. (2002). Iterative feedback tuning - an overview. *Int. J. Adapt. Control Signal Process.*, 16(5):373–395.
- Hjalmarsson, H., Gevers, M., Gunnarsson, S., and Lequin, O. (1998). Iterative feedback tuning: theory and applications. *IEEE Control Systems Magazine*, 18(4):26–41.
- Hoagg, J. B. and Bernstein, D. S. (2007). Nonminimum-phase zeros - much to do about nothing - classical control - revisited part II. *IEEE Control Systems Magazine*, 27(3):45–57.
- Hughes, P. (1987). Space structure vibration modes: How many exist? which ones are important? *IEEE Control Systems Magazine*, 7(1):22–28.
- Hunt, L., Meyer, G., and Su, R. (1996). Noncausal inverses for linear systems. *IEEE Transactions on Automatic Control*, 41(4):608–611.
- Jansen, J. W. (2007). *Magnetically levitated planar actuator with moving magnets: Electromechanical analysis and design*. PhD thesis, Eindhoven University of Technology.
- Kailath, T. (1980). *Linear Systems*. Prentice-Hall Information and System Science Series. Prentice Hall.
- Katalenic, A. (2013). *Control of reluctance actuators for high-precision positioning*. PhD thesis, Eindhoven University of Technology.
- Lambrechts, P., Boerlage, M., and Steinbuch, M. (2005). Trajectory planning and feedforward design for electromechanical motion system. *Control Engineering Practice*, 13(2):145–157.
- Lau, M. A. and Pao, L. Y. (2003). Input shaping and time-optimal control of flexible structures. *Automatica*, 39(5):893–900.
- Levinson, H. J. (2011). *Principles of Lithography*, volume PM198. SPIE Press Monograph, third edition.
- van Lierop, C. M. M. (2008). *Magnetically levitated planar actuator with moving magnets: Dynamics, commutation and control design*. PhD thesis, Eindhoven University of Technology.
- Lomonova, E. A. (2010). Advanced actuation systems - state of the art : fundamental and applied research. In *International Conference on Electrical Machines and Systems (ICEMS)*.
- Longman, R. W. (2000). Iterative learning control and repetitive control for engineering practice. *International Journal of Control*, 73(10):930 – 954.

- van Loock, W., Pipeleers, G., and Swevers, J. (2013). Time-optimal path planning for flat systems with application to a wheeled mobile robot. In *Workshop on Robot Motion and Control (RoMoCo)*, pages 192–196.
- Maciejowski, J. M. (1989). *Multivariable feedback design*. Electronic systems engineering series. Addison-Wesley Publishers Ltd.
- Mack, C. (2007). *Fundamental Principles of Optical Lithography: The Science of Microfabrication*. Wiley.
- Mack, C. (2012). Why 450-mm wafers? <http://www.lithoguru.com/scientist/essays/why450.html>.
- Mack, C. A. (2011). Fifty years of moore’s law. *IEEE Transactions on Semiconductor Manufacturing*, 24(2):202–207.
- Makarovic, J. (2006). *Lightweight positioning: Design and optimization of an actuator with two controlled degrees of freedom*. PhD thesis, Eindhoven University of Technology.
- Makarovic, J., Schneiders, M., van der Wielen, A. M., Lomonova, E., van de Molengraft, M. J. G., Druten, R. M. v., Compter, J. C., Steinbuch, M., and Schellekens, P. H. J. (2004). Integrated design of a lightweight positioning system. In *7th International Conference on Motion and Vibration Control*, St. Louis.
- Merry, R., Uyanik, M., Koops, R., Molengraft, R. v. d., Veghel, M. v., and Steinbuch, M. (2009). Identification, control and hysteresis compensation of a 3DOF metrological AFM. *Asian Journal of Control*, 11(2):130–143.
- Merry, R. J. E. (2009). *Performance-driven control of nano-motion system*. PhD thesis, Eindhoven University of Technology.
- Merry, R. J. E., Ronde, M. J. C., van de Molengraft, M. J. G., and Steinbuch, M. (2011). Directional repetitive control of a metrological AFM. *IEEE Transactions on Control Systems Technology*, 19(6):1622–1629.
- van der Meulen, S., Tousain, R., and Bosgra, O. (2007). Fixed structure feed-forward controller tuning exploiting iterative trials, applied to a high-precision electromechanical servo system. In *American Control Conference*, pages 4033–4039.
- van der Meulen, S., Tousain, R., and Bosgra, O. (2008). Fixed structure feedforward controller design exploiting iterative trials: Application to a wafer stage and a desktop printer. *Journal of Dynamic Systems, Measurement, and Control*, 130:0510061–05100616.

- Meyer, C. (2000). *Matrix Analysis and Applied Linear Algebra*. SIAM.
- Mišković, L., Karimi, A., Bonvin, D., and Gevers, M. (2007). Correlation-based tuning of decoupling multivariable controllers. *Automatica*, 43(9):1481–1494.
- Moore, G. E. (1965). Cramming more components on integrated circuits. *Electronics*, 38(8):114–117.
- Moore, G. E. (1975). Progress in digital integrated electronics. In *International Electron Devices Meeting*, volume 21, pages 11–13.
- Moore, K. L. (1998). Iterative learning control - an expository overview. *Applied Comput. Contr. Signal Processing, Circuits*, 1(1):151–214.
- Munnig Schmidt, R., Schitter, G., and van Eijk, J. (2011). *The Design of High Performance Mechatronics*. IOS Press.
- Olsson, H., Aström, K. J., Canudas de Wit, C., Gäfvert, M., and Lischinsky, P. (1998). Friction models and friction compensation. *European Journal of Control*, 4(3):176–195.
- Oomen, T., Bosgra, O., and van de Wal, M. (2009). Identification for robust inferential control. In *IEEE conf. on Decision and Control*, pages 2581–2586.
- Oomen, T., Grassens, E., Hendriks, F., Herpen, R. v., and Bosgra, O. (2011). Inferential motion control: Identification and robust control with unmeasured performance variables. In *IEEE conf. on Decision and Control*, pages 964–969.
- Oomen, T., van Herpen, R., Quist, S., van de Wal, M., Bosgra, O., and Steinbuch, M. (2013). Connecting system identification and robust control for next-generation motion control of a wafer stage. *IEEE Transactions on Control Systems Technology*, pages 1–17. <http://dx.doi.org/10.1109/TCST.2013.2245668>.
- Oomen, T. A. E. (2010). *System Identification for Robust and Inferential Control, with Applications to ILC and Precision Motion Systems*. PhD thesis, Eindhoven University of Technology.
- Owens, D. H. and Feng, K. (2003). Parameter optimization in iterative learning control. *International Journal of Control*, 76(11):1059–1069.
- Pao, L. Y. (1999). Multi-input shaping design for vibration reduction. *Automatica*, 35(1):81–89.
- Parrish, J. and Brosilow, C. (1985). Inferential control applications. *Automatica*, 21(5):527–538.

- Pintelon, R. and Schoukens, J. (2001). *System identification : a frequency domain approach*. IEEE, New York.
- Prempain, E. and Postlethwaite, I. (2008). A feedforward control synthesis approach for LPV systems. In *American Control Conference*, pages 3589–3594.
- Rampadarath, B. R. (2010). Over-actuation of a lightweight prototype motion system. Master’s thesis, Eindhoven University of Technology.
- Rijlaarsdam, D., Nuij, P., Schoukens, J., and Steinbuch, M. (2012). Frequency domain based nonlinear feed forward control design for friction compensation. *Mechanical Systems and Signal Processing*, 27(0):551–562.
- Rijlaarsdam, D. J. (2012). *Frequency Domain Based Performance Optimization of Systems with Static Nonlinearities*. PhD thesis, Eindhoven University of Technology.
- Ronde, M. J. C., van den Bulk, J. D. J. M., van de Molengraft, M. J. G., and Steinbuch, M. (2013a). Feedforward for flexible systems with time-varying performance locations. In *American Control Conference*, pages 6045 – 6050, Washington, DC, USA.
- Ronde, M. J. C., van de Molengraft, M. J. G., and Steinbuch, M. (2012a). Model-based feedforward for inferential motion systems, with application to a prototype lightweight motion system. In *American Control Conference*, pages 5324–5329, Montréal, Canada.
- Ronde, M. J. C., Schneiders, M. G. E., Kikken, E. J. G. J., van de Molengraft, M. J. G., and Steinbuch, M. (2013b). Model-based spatial feedforward for over-actuated motion systems. *Mechatronics*, pages 1–11. <http://dx.doi.org/10.1016/j.mechatronics.2013.09.010>.
- Ronde, M. J. C., Schneiders, M. G. E., van de Molengraft, M. J. G., de Haas, D., and Steinbuch, M. (2012b). Spatial feedforward for over-actuated flexible motion systems. In Scheidl, R. and Jakoby, B., editors, *The 13th Mechatronics Forum International Conference*, volume 1/3, pages 254–260, Linz. Trauner-Verlag.
- de Roover, D. and Bosgra, O. H. (2000). Synthesis of robust multivariable iterative learning controllers with application to a wafer stage motion system. *International Journal of Control*, 73(10):968 – 979.
- Rovers, J. M. M. (2013). *Multiphysical Modeling of High-Precision Electomechanical Devices, towards nanometer-accurate planar actuators*. PhD thesis, Eindhoven University of Technology.

- Rovers, J. M. M., Achterberg, J., Ronde, M. J. C., Jansen, J. W., Compter, J. C., Lomonova, E., van Lierop, C. M. M., and Molengraft, M. J. G. v. d. (2013). The deformation of a moving magnet plate of a commutated magnetically levitated planar actuator. *Mechatronics*, 23(2):233–239.
- Rovers, J. M. M., Jansen, J. W., Lomonova, E. A., and Ronde, M. J. C. (2009). Calculation of the static forces among the permanent magnets in a halbach array. *IEEE Transactions on Magnetics*, 45(10):4372–4375.
- Ruszczynski, A. (2006). *Nonlinear Optimization*. Princeton University Press.
- Sato, M. (2003). Gain-scheduled inverse system and filtering system without derivatives of scheduling parameters. In *American Control Conference*, volume 5, pages 4173–4178.
- Sato, M. (2005). Robust performance analysis of linear time-invariant parameter-dependent systems using higher-order lyapunov functions. In *American Control Conference*, pages 615–620.
- Sato, M. (2008). Inverse system design for LPV systems using parameter-dependent Lyapunov functions. *Automatica*, 44(4):1072–1077.
- Schneiders, M., Makarovic, J., van de Molengraft, M. J. G., and Steinbuch, M. (2005). Design considerations for electromechanical actuation in precision motion systems. In *IFAC World Congress*, pages 139–144, Prague, Czech Republic.
- Schneiders, M. G. E., van de Molengraft, M. J. G., and Steinbuch, M. (2003). Introduction to an integrated design for motion systems using over-actuation. In *European Control Conference*, pages cd-rom.
- Schneiders, M. G. E., van de Molengraft, M. J. G., and Steinbuch, M. (2004a). Benefits of over-actuation in motion systems. In *American Control Conference*, volume 1, pages 505–510.
- Schneiders, M. G. E., van de Molengraft, M. J. G., and Steinbuch, M. (2004b). Modal framework for closed-loop analysis of over-actuated motion systems. In *ASME International Mechanical Engineering Congress and Exposition*, pages 1–6, Anaheim, California.
- Silverman, L. (1969). Inversion of multivariable linear systems. *IEEE Transactions on Automatic Control*, 14(3):270–276.
- Singer, N. and Seering, W. (1990). Preshaping command input to reduce system vibration. *Journal of Dynamic Systems, Measurement, and Control*, 112:76–82.
- Singer, N., Singhose, W., and Seering, W. (1999). Comparison of filtering methods for reducing residual vibration. *European Journal of Control*, 5:208–218.

- Singh, T. (2008). Minimax input shaper design using linear programming. *Journal of Dynamic Systems, Measurement, and Control*, 130(5):051010–9.
- Singh, T. (2010). *Optimal Reference Shaping for Dynamical Systems, Theory and Applications*. CRC Press. ISBN: 978-1-4398-0562-6.
- Singh, T. and Singhose, W. (2002). Tutorial on input shaping/time delay control of maneuvering flexible structures. In *American Control Conference*, pages 1717–1731.
- Singhose, W., Singer, N., and Seering, W. (1995). Comparison of command shaping methods for reducing residual vibration. In *European Control Conference*.
- Singhose, W. E. (1997). *Command Generation for Flexible Systems*. PhD thesis, Massachusetts Institute of Technology.
- Skogestad, S. and Postlethwaite, I. (2005). *Multivariable Feedback Control, Analysis and Design*. John Wiley & Sons, second edition. ISBN: 0-470-01168-8.
- Söderström, T. and Stoica, P. G. (1983). *Instrumental Variable Methods for System Identification*, volume 57 of *Lecture Notes in Control and Information Sciences*. Springer-Verlag, Berlin Heidelberg New York Tokyo.
- Soemers, H. (2010). *Design Principles for precision mechanisms*. T-Pointprint.
- Soemers, H. M. J. R. (2001). The design of high performance manipulators. In *IEEE/ASME conf. on Advanced Intelligent Mechatronics*, volume 1, pages 26–31.
- Sogo, T. (2008). Inversion of sampled-data system approximates the continuous-time counterpart in a noncausal framework. *Automatica*, 44(3):823–829.
- Sogo, T. (2010). On the equivalence between stable inversion for nonminimum phase systems and reciprocal transfer functions defined by the two-sided laplace transform. *Automatica*, 46(1):122–126.
- Spall, J. C. (1992). Multivariate stochastic approximation using a simultaneous perturbation gradient approximation. *IEEE Transactions on Automatic Control*, 37(3):332–341.
- Spall, J. C. (1997). A one-measurement form of simultaneous perturbation stochastic approximation. *Automatica*, 33(1):109–112.
- Steinbuch, M. (2002). Repetitive control for systems with uncertain period-time. *Automatica*, 38(12):2103–2109.

- Steinbuch, M., Merry, R. J. E., Boerlage, M. L. G., Ronde, M. J. C., and van de Molengraft, M. J. G. (2010). Advanced motion control design. In Levine, W. S., editor, *The Control Handbook, Control System Applications*, chapter 27, pages 1–25. CRC Press, second edition. ISBN: 978-1-4200-7360-7.
- Steinbuch, M. and Norg, M. L. (1998). Advanced motion control: An industrial perspective. *European Journal of Control*, 4(4):278–293.
- Steinbuch, M., Weiland, S., and Singh, T. (2007). Design of noise and period-time robust high-order repetitive control, with application to optical storage. *Automatica*, 43(12):2086–2095.
- Suzuki, K. and Smith, B. W., editors (2007). *Microlithography: science and technology*. CRC Press.
- Tallents, G., Wagenaars, E., and Pert, G. (2010). Lithography at EUV wavelengths. *Nature Photonics*, 4:809–811.
- Tomizuka, M. (1987). Zero phase error tracking algorithm for digital control. *Journal of Dynamic Systems, Measurement, and Control*, 19:65–68.
- Torfs, D., De Schutter, J., and Swevers, J. (1992). Extended bandwidth zero phase error tracking control of nonminimal phase systems. *Journal of Dynamic Systems, Measurement, and Control*, 114(3):347–351.
- Tousain, R. and van der Meulen, S. (2009). *Model-Based Control: Bridging Rigorous Theory and Advanced Technology*, chapter Advances in Data-driven Optimization of Parametric and Non-parametric Feedforward Control Designs with Industrial Applications, pages 167–184. Springer.
- Vaes, D. (2005). *Optimal static decoupling for multivariable control design*. PhD thesis, Katholieke Universiteit Leuven.
- Vaes, D., Souverijns, W., De Cuyper, J., Swevers, J., and Sas, P. (2003). Optimal decoupling for improved multivariable controller design, applied on an automotive vibration test rig. In *American Control Conference*, volume 1, pages 785–790.
- Wagner, C. and Harned, N. (2010). Lithography gets extreme. *Nature Photonics*, 4:24–26.
- van der Wielen, A. M. (2009). *Positioning system mass reduction due to exchange of structural stiffness by additional actuators*. PhD thesis, Eindhoven University of Technology.
- van de Wijdeven, J. and Bosgra, O. H. (2007). Hankel iterative learning control for residual vibration suppression with MIMO flexible structure experiments. In *American Control Conference*, pages 4993–4998.

- van de Wijdeven, J. and Bosgra, O. H. (2008). Residual vibration suppression using hankel iterative learning control. *International Journal of Robust and Nonlinear Control*, 18(10):1034–1051.
- van de Wijdeven, J. and Bosgra, O. H. (2010). Using basis functions in iterative learning control: analysis and design theory. *International Journal of Control*, 83(4):661–675.
- van de Wijdeven, J. J. M. (2008). *Iterative Learning Control design for uncertain and time-windowed systems*. PhD thesis, Eindhoven University of Technology.
- Wu, B. and Kumar, A. (2009). Extreme ultraviolet lithography: Towards the next generation of integrated circuits. *Optics & Photonics Focus*, 7(4).
- Zhang, J. and Agustriyanto, R. (2003). Multivariable inferential feed-forward control. *Ind. Eng. Chem. Res.*, 42:4186–4197.
- Zhong, H. and Pao, L. Y. (2013). h_2 model matching feedforward control for tape head positioning servo systems. In *American Control Conference*, pages 4511–4516.
- Zou, Q. and Devasia, S. (1999). Preview-based stable-inversion for output tracking of linear systems. *Journal of Dynamic Systems, Measurement, and Control*, 121(4):625–630.
- Zou, Q. and Devasia, S. (2004). Preview-based optimal inversion for output tracking: Application to scanning tunneling microscopy. *IEEE Transactions on Control Systems Technology*, 12(3):375–386.

Appendix A

Inferential feedforward

A.1 SVD truncation

The system J_z can be represented as,

$$\begin{aligned} J_z &= U \Sigma V^T, \\ &= \begin{bmatrix} U_1 & | & U_2 \end{bmatrix} \begin{bmatrix} \Sigma_1 & | & 0 \\ 0 & | & \Sigma_2 \end{bmatrix} \begin{bmatrix} V_1^T \\ V_2^T \end{bmatrix}, \end{aligned}$$

Combining (2.2), (2.9) and Proposition 2.10 results in,

$$\begin{aligned} e_z &= r_z - z, \\ &= (I - J_z J_z^\dagger) r_z, \\ &= \left(I - \begin{bmatrix} U_1 & | & U_2 \end{bmatrix} \begin{bmatrix} \Sigma_1 & | & 0 \\ 0 & | & \Sigma_2 \end{bmatrix} \begin{bmatrix} V_1^T \\ V_2^T \end{bmatrix} V_1 \Sigma_1^{-1} U_1^T \right) r_z, \\ &= (I - U_1 U_1^T) r_z, \\ &= U_2 U_2^T r_z. \end{aligned}$$

A.2 Equivalence of control structures

The feedforward controllers and prefilters from Chapters 2 and 3 are given in Table A.1.

Chapter	F	K_{ff}
2	$G_y K_{ff}$	G_z^\dagger
3	I	$(G_z S_i)^\dagger - K_{fb}$

Table A.1: Feedforward controller and prefilters from Chapters 2 and 3.

Consider the feedforward controllers and possible prefilters from Chapter 2 and 3 in the general 2DOF control structure,

$$u = \begin{bmatrix} K_{fb}F + K_{ff} & K_{fb} \end{bmatrix} \begin{bmatrix} r_z \\ -y \end{bmatrix}.$$

For the feedforward controller and prefilter of Chapter 2 this results in,

$$u = \begin{bmatrix} (I + K_{fb}G_y) G_z^\dagger & K_{fb} \end{bmatrix} \begin{bmatrix} r_z \\ -y \end{bmatrix}. \quad (\text{A.1})$$

For the feedforward controller and prefilter of Chapter 3 this results in,

$$\begin{aligned} u &= \begin{bmatrix} K_{fb} + (G_z S_i)^\dagger - K_{fb} & K_{fb} \end{bmatrix} \begin{bmatrix} r_z \\ -y \end{bmatrix}, \\ &= \begin{bmatrix} (G_z S_i)^\dagger & K_{fb} \end{bmatrix} \begin{bmatrix} r_z \\ -y \end{bmatrix}. \end{aligned} \quad (\text{A.2})$$

The 2DOF control structures of (A.1) and (A.2) are equivalent if and only if,

$$n_z = n_y = n_u.$$

In case all dimensions are equal, the pseudo-inverse may be replaced by a normal inverse. Therefore, the following holds,

$$(G_z S_i)^{-1} = S_i^{-1} G_z^{-1},$$

where $S_i^{-1} = (I + K_{fb}G_y)$ by definition. This renders both controllers (A.1) and (A.2) equivalent.

A.3 Parametric beam model

The parametric model from Section 2.5.4 in modal form is given by,

$$G : \begin{cases} \dot{x}(t) &= Ax(t) + Bu(t), & x(0) = x_0 \\ y(t) &= Cx(t) + Du(t) \end{cases},$$

where,

$$A = \text{diag}(A_1, \dots, A_7),$$

and,

$$\begin{aligned} A_1 &= \begin{bmatrix} 0 & 1 \\ -513.4 & -9.5 \end{bmatrix}, & A_2 &= \begin{bmatrix} 0 & 1 \\ -1447.3 & -10.7 \end{bmatrix}, \\ A_3 &= \begin{bmatrix} 0 & 1 \\ -43954.1 & -8.3 \end{bmatrix}, & A_4 &= \begin{bmatrix} 0 & 1 \\ -375432.6 & -19.2 \end{bmatrix}, \\ A_5 &= \begin{bmatrix} 0 & 1 \\ -1270020.5 & -9.1 \end{bmatrix}, & A_6 &= \begin{bmatrix} 0 & 1 \\ -3233164.0 & -36.1 \end{bmatrix}, \\ A_7 &= \begin{bmatrix} 0 & 1 \\ -7625745.1 & -12.0 \end{bmatrix}, \\ B &= \begin{bmatrix} 0 & 0 & 0 \\ -35.7 & -47.8 & -54.0 \\ 0 & 0 & 0 \\ -48.7 & -6.7 & 35.6 \\ 0 & 0 & 0 \\ -44.5 & 60.5 & -36.0 \\ 0 & 0 & 0 \\ -8.4 & 6.9 & -3.5 \\ 0 & 0 & 0 \\ -21.2 & 62.0 & -24.1 \\ 0 & 0 & 0 \\ -9.6 & -0.2 & 8.3 \\ 0 & 0 & 0 \\ 37.4 & 36.6 & 38.9 \end{bmatrix}, & C^T &= \begin{bmatrix} -51.4 & -78.1 & -88.7 \\ 0 & 0 & 0 \\ -152.4 & -26.6 & 111.4 \\ 0 & 0 & 0 \\ -73.9 & 83.5 & -42.7 \\ 0 & 0 & 0 \\ -11.0 & 6.2 & -7.1 \\ 0 & 0 & 0 \\ -5.3 & 67.5 & -43.1 \\ 0 & 0 & 0 \\ -34.9 & 8.1 & 75.4 \\ 0 & 0 & 0 \\ -50.4 & -67.9 & -78.1 \\ 0 & 0 & 0 \end{bmatrix}, \\ D &= \begin{bmatrix} 0.0042 & 0.0002 & 0.0002 \\ -0.0003 & 0.0043 & 0.0010 \\ -0.0001 & 0.0004 & 0.0049 \end{bmatrix}. \end{aligned}$$

Appendix B

Zero-Vibration Input Shaper

This appendix presents a similar derivation of a zero-vibration input shaper as presented in Singer and Seering (1990); Singh and Singhose (2002). The response to N impulses of a second-order with underdamped poles is given by

$$\begin{aligned} y(t) &= \sum_{i=0}^{N-1} a_i \frac{\omega}{\sqrt{1-\zeta^2}} e^{-\zeta\omega(t-t_i)} \sin\left(\omega\sqrt{1-\zeta^2}(t-t_i)\right), \\ &= e^{-\zeta\omega t} \frac{\omega}{\sqrt{1-\zeta^2}} \sum_{i=0}^{N-1} a_i e^{\zeta\omega t_i} \sin\left(\omega\sqrt{1-\zeta^2}(t-t_i)\right), \end{aligned}$$

where a_i and t_i are the amplitude and time of the i^{th} impulse input. Furthermore, ω is the undamped eigenfrequency, ζ the damping ratio and t is the time. The damped eigenfrequency is defined by

$$\omega_d = \omega\sqrt{1-\zeta^2}.$$

The sum of two sinusoids with the same frequency can be computed with the trigonometric identity,

$$\begin{aligned} b_0 \sin(\omega_d t + \phi_0) + b_1 \sin(\omega_d t + \phi_1) &= A_{amp} \sin(\omega_d t + \psi), \\ \phi_i &= -\omega_d t_i, \end{aligned}$$

where

$$\begin{aligned} A_{amp} &= \sqrt{(b_0 \cos \phi_0 + b_1 \cos \phi_1)^2 + (b_0 \sin \phi_0 + b_1 \sin \phi_1)^2}, \\ \psi &= \tan^{-1} \left(\frac{b_0 \cos \phi_0 + b_1 \cos \phi_1}{b_0 \sin \phi_0 + b_1 \sin \phi_1} \right). \end{aligned}$$

For N impulses this results in,

$$V(\omega, \zeta) = e^{-\zeta\omega t} \sqrt{C(\omega, \zeta)^2 + S(\omega, \zeta)^2},$$

where

$$C(\omega, \zeta) = \sum_{i=0}^{N-1} a_i e^{\zeta\omega t_i} \cos(\omega_d t_i),$$

$$S(\omega, \zeta) = \sum_{i=0}^{N-1} a_i e^{\zeta\omega t_i} \sin(\omega_d t_i)$$

Solving for $V(\omega, \zeta) = 0$ for $N = 2$ leads to,

$$a_0 e^{\zeta\omega t_0} \cos(\omega_d t_0) + a_1 e^{\zeta\omega t_1} \cos(\omega_d t_1) = 0,$$

$$a_0 e^{\zeta\omega t_0} \sin(\omega_d t_0) + a_1 e^{\zeta\omega t_1} \sin(\omega_d t_1) = 0.$$

To avoid trivial solutions and to obtain bounded solution, the following constraints are added (Singh and Singhose, 2002),

$$\sum_{i=0}^{N-1} a_i = 1, \tag{B.1}$$

$$a_i > 0, \quad \forall i.$$

Without loss of generality $t_0 = 0$ can be chosen, which results is,

$$a_0 + a_1 e^{\zeta\omega t_1} \cos(\omega_d t_1) = 0, \tag{B.2}$$

$$a_1 e^{\zeta\omega t_1} \sin(\omega_d t_1) = 0. \tag{B.3}$$

Equation (B.3) is zero in a nontrivial manner when $\sin(\omega_d t_1) = 0$. Therefore it follows that,

$$\omega_d t_1 = n\pi, \quad n \in \mathbb{N}^+.$$

To construct the shortest input shaper, $n = 1$ is chosen, which results in,

$$t_1 = \frac{\pi}{\omega_d} = \frac{T_d}{2}, \tag{B.4}$$

where T_d is the period of the damped vibration. Applying the constraint in (B.1) to (B.2) with t_1 from (B.4) results in,

$$a_0 - (1 - a_0) e^{\frac{\zeta\pi}{\sqrt{1-\zeta^2}}} = 0.$$

Rearranging,

$$a_0 \left(1 + e^{\frac{\zeta \pi}{\sqrt{1-\zeta^2}}} \right) - e^{\frac{\zeta \pi}{\sqrt{1-\zeta^2}}} = 0,$$

and solving for the coefficients using (B.1) results in,

$$a_0 = \frac{e^{\frac{\zeta \pi}{\sqrt{1-\zeta^2}}}}{1 + e^{\frac{\zeta \pi}{\sqrt{1-\zeta^2}}}},$$
$$a_1 = \frac{1}{1 + e^{\frac{\zeta \pi}{\sqrt{1-\zeta^2}}}}.$$

Appendix C

Model-based spatial feedforward

C.1 Rigid-body feedforward design

$$T_{b,1} = \begin{bmatrix} 0.2500 & 1.1374 & -1.1492 \\ 0.2500 & 1.1374 & 1.1492 \\ 0.2500 & -1.1374 & 1.1256 \\ 0.2500 & -1.1375 & -1.1256 \\ 0 & 0 & 0 \\ 0 & 0 & 0 \end{bmatrix}. \quad (\text{C.1})$$

C.2 Spatial feedforward design

The body-mode $T_{b,2}$ matrix for the extended actuator configuration of six actuators is computed similarly to $T_{b,1}$ and is given by,

$$T_{b,2} = \begin{bmatrix} 0.2069 & 1.0972 & -1.1364 \\ 0.2069 & 1.0972 & 1.1364 \\ 0.1379 & -0.7837 & 1.1364 \\ 0.1379 & -0.7837 & -1.1364 \\ 0.1724 & 0.1567 & 0.0000 \\ 0.1379 & -0.7837 & 0.0000 \end{bmatrix}.$$

The spatial feedforward $T_{u,ff}$ is given by,

$$T_{u,ff} = \begin{bmatrix} 0.1632 & 0.7882 & -356.1909 \\ 0.1768 & 1.0010 & 356.2118 \\ 0.1634 & -0.4074 & -353.9162 \\ 0.1770 & -0.1946 & 353.9411 \\ 0.3201 & 0.9670 & -0.0419 \\ -0.0004 & -2.1543 & -0.0040 \end{bmatrix}$$

where $T_{u,ff}$ is designed such that the internal modes 3, 4 and 5 are uncontrollable according to Theorem 4.10. By applying these input transformations to the B-matrix we get,

$$BT_{b,1} = \left[\begin{array}{ccc|ccc} 0.2695 & -0.0000 & 0.0000 & 0.0000 & -0.0001 & 0.0000 \\ -0.0000 & 1.4704 & -0.0000 & 0.0001 & -0.0027 & 0.0002 \\ -0.0000 & 0.0000 & 1.4704 & -0.0009 & 0.3452 & 1.1245 \\ \hline 0.0000 & -0.0001 & 0.0000 & 0.0084 & -1.1262 & 0.3445 \\ 0.0001 & -0.0027 & 0.0002 & 0.2472 & 0.0392 & -0.0075 \\ -0.0009 & 0.3452 & 1.1245 & & & \end{array} \right], \quad (C.2)$$

$$BT_{u,ff} = \left[\begin{array}{ccc|ccc} 0.2695 & 0.0000 & 0.0000 & -0.0127 & -0.1994 & -662.3603 \\ 0.0000 & 1.4690 & 0.0000 & -0.0003 & -0.6315 & 0.4729 \\ -0.0000 & -0.0000 & 1.4690 & -0.0000 & -0.0000 & 0.0000 \\ \hline -0.0127 & -0.1994 & -662.3603 & 0.0000 & 0.0000 & -0.0000 \\ -0.0003 & -0.6315 & 0.4729 & -0.0000 & 0.0000 & -0.0000 \\ -0.0000 & -0.0000 & 0.0000 & & & \end{array} \right]. \quad (C.3)$$

Appendix D

Data-based spatial feedforward

D.1 Relation between the data-based feedforward controller and a diagonal feedforward controller and feedforward decoupling

In Chapter 5, the feedforward controller is parameterized as,

$$K_{ff}(\theta) = \Psi_0 \overline{K_{ff}} + \sum_{j=0}^{n_s} \Psi_j \Theta_j.$$

Apply factorization to collect the common factor Ψ_0 as,

$$K_{ff}(\theta) = \Psi_0 (\overline{K_{ff}} + \Theta_0) + \sum_{j=1}^{n_s} \Psi_j \Theta_j,$$

Define the feedforward controller estimated from data as,

$$\hat{K}_{ff} := (\overline{K_{ff}} + \Theta_0),$$

i.e. the initial estimate plus the adaptation by the parameters. The resulting matrix in the null-space of B_b is defined as,

$$T_s := \sum_{j=1}^{n_s} \Psi_j \Theta_j.$$

With the definition of $\Psi_0 = T_b$ we get,

$$K_{ff}(\theta) = T_b \hat{K}_{ff} + T_s, = \left(T_b + T_s \hat{K}_{ff}^{-1} \right) \hat{K}_{ff},$$

which has the same form as the feedforward controller and feedforward decoupling in Chapter 4 and Ronde et al. (2013b).

D.2 Convexity of the objective function

Theorem D.1. *The objective function $V(\bar{\theta}_l)$ in (5.10) is convex in $\bar{\theta}_l$ if:*

1. *the tracking error $e_m(t)$ is affine in $\bar{\theta}_l$, and*
2. *the matrix $\Gamma \succ 0$.*

Proof: The tracking error $e_m(t)$ for the l -th task trial is given by,

$$\begin{aligned} e_{m,l}(\bar{\theta}_l) &= S_{o,d} \left(I - T_y G K_{ff}(\theta_l) s^2 \right) r_m, \\ &= S_{o,d} \left(I - T_y G (\Psi_0 \overline{K_{ff}} + \sum_{j=0}^{n_s} \Psi_j \Theta_j s^2) \right) r_m, \end{aligned}$$

i.e. due to the structure of the feedforward controller all parameters in the tracking error $e_m(\bar{\theta}_l)$ appear linear in $\bar{\theta}_l$. Hence, the tracking error $e_m(t)$ is affine in $\bar{\theta}_l$.

The objective function $V(\bar{\theta}_l)$ is convex if and only if the Hessian in (5.12) is positive semidefinite for all controller parameters. The Hessian in (5.12) is approximated by (5.14). The approximated Hessian is positive definite if and only if $\Gamma \succ 0 \Leftrightarrow \bar{\gamma}_i > 0$ and $\nabla e_{m,l} \neq 0$. In case $\nabla e_{m,l} = 0$, this renders the approximated Hessian positive semidefinite.

$$\nabla^2 V(0) \succeq 0 \iff 2\nabla e_{m,l}^T(0) \Gamma \nabla e_{m,l}(0) \succeq 0,$$

since $\Gamma = \Gamma^T$ and diagonal, define $\bar{\Gamma} = \sqrt{\Gamma}$.

$$2\nabla e_{m,l}^T(0) \Gamma \nabla e_{m,l}(0) \succeq 0 \iff 2\nabla e_{m,l}^T(0) \bar{\Gamma}^T \bar{\Gamma} \nabla e_{m,l}(0) \succeq 0.$$

Now define $A := \bar{\Gamma} \nabla e_{m,l}(0)$ and rewrite

$$2\nabla e_{m,l}^T(0) \bar{\Gamma}^T \bar{\Gamma} \nabla e_{m,l}(0) \succeq 0 \iff 2A^T A \succeq 0,$$

which is known to be positive semidefinite for any real A . ■

D.3 Selection of Λ

Lemma D.2. $\Lambda = I$ in (5.3) can be selected without loss of generality.

Proof: The reference sensitivity for the control structure of Fig. 5.1 is given by,

$$\begin{aligned} e_m &= (I - T_y G T_{u,fb} K_{fb})^{-1} (I - T_y G K_{ff}(\theta) s^2) r_m, \\ &= (I - T_y G T_{u,fb} K_{fb})^{-1} (I - T_y G T_{u,ff}(\theta) \overline{K_{ff} s^2}) r_m. \end{aligned}$$

Inserting the definition of G from (5.1), while ignoring the internal dynamics results in,

$$e_m = (I - T_y G T_{u,fb} K_{fb})^{-1} (I - T_y C_b \Theta^{(b)}(s) B_b T_{u,ff}(\theta) \overline{K_{ff} s^2}) r_m.$$

Selecting $B_b T_{u,ff}(\theta) = \Lambda$ results in,

$$e_m = (I - T_y G T_{u,fb} K_{fb})^{-1} (I - T_y C_b \Theta^{(b)}(s) \Lambda \overline{K_{ff} s^2}) r_m.$$

Selecting $B_b T_{u,ff}(\theta) = I$ results in,

$$\begin{aligned} e_m &= (I - T_y G T_{u,fb} K_{fb})^{-1} (I - T_y C_b \Theta^{(b)}(s) I \overline{K_{ff} s^2}) r_m, \\ &= (I - T_y G T_{u,fb} K_{fb})^{-1} (I - T_y C_b \Theta^{(b)}(s) \Lambda \Lambda^{-1} \overline{K_{ff} s^2}) r_m, \end{aligned}$$

i.e. selecting $B_b T_{u,ff}(\theta) = I$ results in a scaling of $\overline{K_{ff}}$ by Λ^{-1} . ■

D.4 Input matrix

$$B_b^T = \begin{bmatrix} 0.2695 & 0.3232 & -0.3232 \\ 0.2695 & 0.3232 & 0.3232 \\ 0.2695 & -0.3232 & 0.3232 \\ 0.2695 & -0.3232 & -0.3232 \\ 0.2695 & 0.0000 & -0.0000 \\ 0.2695 & 0.3232 & -0.0000 \\ 0.2695 & 0.0000 & 0.3232 \\ 0.2695 & -0.3232 & -0.0000 \\ 0.2695 & 0.0000 & -0.3232 \end{bmatrix}, \quad (\text{D.1})$$

Appendix E

List of symbols

Roman uppercase

Symbol	Description	Unit
A	State matrix	
B	Input matrix	
C	Output matrix	
D	Direct feedthrough matrix	
	Damping matrix	
E	Output multiplicative error	
F	Setpoint trajectory prefilter	
G	Plant	
H	General input shaper	
I	Identity matrix	
J	Convolution matrix	
K	Stiffness matrix	
	Controller	
K_{fb}	Feedback controller	
K_{ff}	Feedforward controller	
$K_{ff}(\theta)$	Parametric feedforward controller	
L	Length	m
	Open-loop	
M	Mass matrix	
R	Rotation	rad
$T_{u,fb}$	Feedback input decoupling transformation	
$T_{u,ff}$	Feedforward input decoupling transformation	
T_y	Output transformation to motion coordinates	

S	Sensitivity	
S_d	Diagonal sensitivity	
S_i	Input sensitivity	
T	Torque	Nm
T_d	Diagonal complementary sensitivity	
U	Output singular vectors	
\mathcal{U}	Input space	
V	Input singular vectors	
	Objective function	
\mathcal{V}	Input space (free directions)	
W	Weighting filter	
\mathcal{W}	Input space (body mode directions)	
Z	Damping matrix	-

Roman lowercase

Symbol	Description	Unit
a	Impulse response parameters	
	Acceleration setpoint	m/s^2
a, b, c	Polynomials	
d	Damping	Ns/m
e	Error	
f	Force	N
	Frequency	Hz
h	Impulse response	
k	Stiffness	N/m
m	Motion coordinates	
r	Setpoint trajectory	
s	Laplace variable ($s = j\omega$)	rad/s
t	Time	s
t_s	Sample time	s
u	Input	
w	Free direction	
x	State vector	
y	Sensor outputs	
z	Performance outputs	
	z -transform variable ($z = e^{j\omega}$)	rad/s

Greek

Symbol	Description	Unit
Γ	Weighting matrix	
Λ	Diagonal matrix	
Ω	Eigenfrequency matrix	rad/s
Ψ	Basis of free directions	
Σ	Singular values	
Θ	Modal transfer functions	
	Diagonal parameter matrix	
α	Weighting filter gain	
μ	Structured singular value	
ω	Frequency	rad/s
σ	Singular values	
θ	Optimization parameters	
ζ	Damping	-

Subscripts, superscripts and indices

Symbol	Description
b	body-mode
d	diagonal
dec	decoupled
fb	feedback
ff	feedforward
int	internal mode
i	index
j	index
k	discrete time index
l	trial index
m	representation in motion coordinates
	modal form
nd	non-diagonal
n_b	number of body-modes
n_u	number of inputs
n_m	number of modes to be controlled
n_r	number of modes
n_s	Degree of over-actuation
n_y	number of sensor outputs
n_z	number of performance outputs

r	index
N	number of samples
y	representation in sensor coordinates y -direction
z	representation in performance coordinates

Special symbols and operators

Symbol	Description
$ \cdot $	Absolute value
$\angle \cdot$	Angle
ceil	Ceiling operation
dim	Dimension
ker	Kernel
$(\cdot)^\dagger$	Moore-Penrose pseudo-inverse
$\overline{(\cdot)}$	Model
$\max(\cdot)$	Maximum
$\ \cdot\ _p$	p-norm
$\tilde{\cdot}$	Partial selection of a matrix
Im	Image of a matrix
rank	Rank of a matrix
$(\cdot)^T$	Transpose

Acronyms and initialisms

Symbol	Description
COG	Center Of Gravity
CPSD	Cumulative Power Spectral Density
DOF	Degree of Freedom
EBZPETC	Extended Bandwidth Zero Phase Error Tracking Controller
FEM	Finite Element Method
FIR	Finite Impulse Response
FRF	Frequency Response Function
IC	Integrated Circuit
IFT	Iterative Feedback Tuning
ILC	Iterative Learning Control
LTI	Linear Time Invariant
LPV	Linear Parameter Varying
LTV	Linear Time Variant

MIMO	Multi Input Multi Output
NMP	Non-Minimum Phase
NST	Nearest Sample Time
OA	Over-Actuated
OS	Over-Sensed
PSD	Power Spectral Density
RC	Repetitive Control
RGA	Relative Gain Array
RMS	Root Mean Square
SIMO	Single Input Multi Output
SISO	Single Input Single Output
ZPETC	Zero Phase Error Tracking Controller
ZV	Zero-Vibration

Summary

Feedforward Control for Lightweight Motion Systems

Feedforward control is a common method to compensate for tracking errors due to known and measurable disturbances. In motion systems these disturbances are mainly introduced by the setpoint trajectory. Typically these setpoint trajectories are point-to-point motions, which might be changing due to the production process. The tracking errors during motion and the residual vibrations determine both the achievable production speed and production quality, which can be enhanced by proper feedforward control design.

This thesis addresses feedforward control design for lightweight electromechanical motion systems. Lightweight systems pose several challenges for feedforward control design: i) flexible modes in the frequency region of interest: the setpoint trajectory excites the resonant dynamics of the flexible modes, and ii) the relation between the measured variables and the performance variables can not be described by a static relation. The second item implies that the performance can not be calculated or controlled using simple geometrical transformations. Such a control problem is known as inferential control.

The first part of the thesis deals with feedforward control design for systems with inferential performance locations. An inferential performance location is the actual location where performance is required, i.e. the area to be illuminated or component to be placed. Typically, there are no sensors available at such locations and accurate control is not possible due to flexibilities. It is shown that different setpoint trajectories are required for the performance- and sensor location to avoid conflicting control requirements. For traditionally actuated systems, a feedforward control design framework is proposed which improves the performance the inferential performance location. These results are experimentally validated on a multivariable flexible structure.

Moreover, an exploratory study towards motion systems with time-varying inferential performance locations is presented. The problem of time-varying performance location occurs naturally in many manufacturing systems, such as wafer-

stages and pick-and-place machines. In these machines the location where the tool operates, i.e. the area to be exposed or the location of the component to be placed, is constantly varying. To this end, the feedforward control design framework is extended towards time-varying performance locations. However, direct application of this framework leads to infeasible feedforward signal. To this end, an input weighting is added to the design procedure. Experimental validation on a two-mass system with flexible shaft shows that the proposed framework is able to deal with time-varying performance locations.

The research on feedforward control design methods for over-actuated systems is divided in two parts. In the first part, the presented method provides guaranteed performance over the complete structure, similar to input shaping. However, the presented method does not modify the setpoint trajectory, thereby overcoming one of the main drawbacks of input shaping. To this end, a novel feedforward control design framework is introduced, which employs a different decoupling in the feedforward path. Using a model-based design strategy, the excitation of internal modes can be avoided, which provides performance improvement over the complete structure. The theoretical results are supported by experimental results on an industrial over-actuated lightweight motion system.

In the second part, a data-based method is presented for over-actuated systems in absence of a detailed model. The presented method optimizes the feedforward decoupling and - controller based on measured data in one simultaneous optimization using a similar parametrization as the model-based method. The data-based method aims at minimizing the tracking errors instead of preventing the excitation of flexible modes. Therefore, the data-based also takes the compliance effects of higher order flexible modes into account. These results are supported by experimental validation on an industrial over-actuated lightweight motion system. The data-based method shows an improvement with respect to the model-based method, which can be accounted to model inaccuracies.

Dankwoord

Met het schrijven van dit dankwoord komt het einde van mijn promotie en een lange periode op de TU/e in zicht. Een periode waar ik met veel plezier op terugkijk. Hierbij wil ik dan ook graag een aantal mensen in het bijzonder bedanken voor hun bijdrage aan het tot stand komen van dit proefschrift.

Allereerst wil ik Maarten bedanken voor de kans en het vertrouwen om aan dit promotieonderzoek te beginnen. Voor jouw inspirerende coaching en enthousiasme tijdens de IWO's, maar ook voor je oprechte interesse op persoonlijk vlak wil ik je graag bedanken. Voor de dagelijkse begeleiding wil ik René bedanken. Jouw kritische vragen, vermogen om verbanden te leggen, maar ook het afstand nemen van het werk heeft bijgedragen aan de kwaliteit van dit proefschrift. Daarnaast wil ik je bedanken voor de diverse onderwijstaken, die naast het onderzoek, voor een leuke en leerzame afwisseling zorgden.

I would also like to thank all the members of the committee: Georg Schitter, Jan Swevers, Hans Butler, Elena Lomonova and Marcel Heertjes for reading my thesis and providing valuable input.

Mijn collegae promovendi binnen het project, Hans, Jaron en later ook Koen wil ik bedanken voor de prettige samenwerking. Daarnaast wil ik alle mensen van het Equipment and Prototype Center en de project partners ASML, Prodrive, Tecnotion en VDL ETG bedanken voor hun inzet en expertise.

Marc ben ik dankbaar voor het lezen van mijn proefschrift en het mogelijk maken van de experimenten bij ASML. George en Edward wil ik bedanken voor de assistentie bij het experimenteren, jullie kennis van de opstelling maakte het mogelijk om op een efficiënte manier experimenten te doen.

De studenten die ik heb mogen begeleiden bij hun (afstudeer)opdrachten hebben allemaal op hun eigen manier bijgedragen aan het schrijven van dit proefschrift: Randjanie, Roel, Ezequiel, John en Daniël bedankt hiervoor.

Alle collega's van de DCT sectie wil ik bedanken voor de gezelligheid in de koffiepauzes en bij de verschillende conferenties, cursussen en uitjes. In het bijzonder wil ik mijn kamergenoten Robbert en Irmak bedanken voor de vele discussies over de meest uiteenlopende onderwerpen. Ook wil ik jullie bedanken voor alle gezelligheid, bij onder andere de verschillende roomie events. De gesprekken tij-

dens het dagelijkse rondje over de campus waren een prettige onderbreking van het schrijfproces. Ook een goede start van de dag met koffie in het DCT lab mocht hierbij niet ontbreken. Daarnaast wil ik alle mensen van Tech United bedanken voor de onvergetelijke toernooien en de unieke sfeer binnen het team.

Verder wil ik mijn familie en vrienden bedanken voor jullie interesse. In het bijzonder wil ik mijn ouders bedanken voor alle kansen en steun die jullie mij hebben gegeven. Tenslotte, gaat mijn grootste dank uit naar Lisa voor je interesse in mijn werk, voor alle steun en geduld tijdens de drukke periodes in mijn promotie traject en voor alle liefde in de afgelopen jaren.

Michael Ronde,
December 2013

Curriculum Vitae

Michael Ronde was born on January 1, 1984 in Dordrecht, the Netherlands.

- | | |
|-----------|--|
| 1996-2002 | Pre-university education, Stedelijk Dalton Lyceum, Dordrecht. |
| 2003-2005 | Bachelor of Engineering, Mechanical Engineering, Hogeschool Rotterdam. |
| 2005-2009 | Master of Science, Systems and Control, Eindhoven University of Technology, graduated <i>with great appreciation</i> , including: |
| 2008-2009 | Graduation research, NMI Van Swinden Laboratory, Research and Development,

<i>MIMO and repetitive control of a calibration Atomic Force Microscope.</i> |
| 2009-2014 | PhD candidate at Eindhoven University of Technology, department of Mechanical Engineering, Control Systems Technology group. |

